Title
Very High Resolution Photofragmentation-translational Spectroscopy

Author
Wodtke, A.M.

Publication Date
1986-11-01

Lawrence Berkeley Laboratory
UNIVERSITY OF CALIFORNIA

Materials & Molecular Research Division

VERY HIGH RESOLUTION
PHOTOFRAGMENTATION-TRANSLATIONAL SPECTROSCOPY

A.M. Wodtke
(Ph.D. Thesis)

November 1986

Prepared for the U.S. Department of Energy under Contract DE-AC03-76SF00098

DISCLAIMER

LBL-22619

VERY HIGH RESOLUTION PHOTOFRAGMENTATION-TRANSLATIONAL SPECTROSCOPY

Alec M. Wodtke

Ph. D. Thesis

Lawrence Berkeley Laboratory
University of California
Berkeley, California 94720

This work was supported by the Director, Office of Energy Research, Office of Basic Energy Sciences, Chemical Sciences Division of the U.S. Department of Energy under Contract No. DE-AC03-76SF00098 and the Office of Naval Research under Contract No. N00014-83-K-0069.

Very High Resolution Photofragmentation-Translational Spectroscopy

by

Alec M. Wodtke

ABSTRACT

We have designed and constructed a new higher resolution molecular beam apparatus, specifically for studying laser induced dissociation under collision free conditions. By measuring the translational energy distributions of products from single UV photon induced dissociation important thermochemical data have been derived and from infra-red multiphoton dissociation (IRMPD) studies, new insights into unimolecular thermal decomposition have been obtained.

Specifically, the photochemistry of acetylene at 193 nm has been studied. By finding the maximum release of translational energy of the products C_2H and H, $D_0(C_2H\text{-}H)$ was derived with high accuracy and precision. Resolved structure in the product's translational energy distribution sheds light on the vibronic properties of the C_2H radical.

The heat of formation of the vinyl radical was determined by studying the photodissociation of vinylbromide at 193 nm. The observation of metastable C_2H_3 was thought to be due to formation

of the first excited doublet state of the vinyl radical and a value for $T_{oo}(\tilde{A} \leftarrow \tilde{X})$ was suggested.

The collision free unimolecular decomposition of three nitroalkanes: nitromethane, nitroethane and 2-nitropropane, was investigated using IRMPD. The isomerization of CH_3NO_2 to CH_3ONO was observed for the first time and raises interesting questions about the primary decomposition pathways of other nitro-containing molecules. Through a novel application of RRKM theory, the barrier height to isomerization was found to be ~5 kcal/mol lower than the C-N bond energy in nitromethane. This RRKM method was tested by finding the barrier heights for HONO elimination from nitroethane and 2-nitropropane. The results are in very good agreement with known activation energies. It was also found that HONO elimination in these two molecules is accompanied by, on the average, ~1 eV of translational energy release.

TABLE OF CONTENTS

CHAPTER III cont'd

LIST OF TABLES

LIST OF FIGURES

CHAPTER III cont'd

CHAPTER IV cont'd

CHAPTER V: The Infrared Multiphoton Dissociation of Three Nitroalkanes

CHAPTER V cont'd

ACKNOWLEDGEMENTS

Graduate school is a difficult time in most peoples lives and for me it has been no exception. This thesis along with a handful of publications is what I have to show for it. But the important part does not appear in print. The relationships and interactions that come as a result of a mutual interest in nature are the highest rewards in science. Therefore, I mention those people who played a role in my stay at Berkeley. Above all others my wife Natasha Aristov has provided me with the loving and stable emotional environment so necessary to intense and concentrated work. She has also taught me to pick up my dirty socks for which my mother is forever in awe. My dear friends Jeff Brown and Debbi Jo Friedman have made my life joyous, the spirit within which good scientific work can and should be done. I do not see how I can ever replace them.

Of course, Yuan Lee is the chief instigator of whatever success I have achieved. The words from the acknowledgements of so many doctoral dissertations do no justice to reality. I will not even try, but to say: If you should ever have a chance to work with this man on some scientific project, DO IT !!!

There are several people who graduated ahead of me with which it was my pleasure to come into contact and they deserve special mention. Bob Baseman taught me how to use the 35" machine. Dan Neumark and I learned together how to find reaction resonances in

$F+H_2$ and he had the most direct "on hands" impact on my experimental education. Just don't break my legs, Dan, o.k.. Despite all attempts to the contrary on his part, I must say that I admire Doug Krajnovich as a scientist as much or more than any other graduate student I have known. His willingness to work hard and be thorough, his persistent skepticism and broad scientific knowledge was inspiring to me. Doug was actually responsible for much of the design and construction of the rotating source machine and deserves much more credit for this than he is ever going to get. I did have the opportunity to work with Laurie Butler and discovered that, yes, competition between the sexes is alive and well no matter how enlightened you think you are.

The technical staff of LBL and the chemistry department continue to be the unsung heroes of Berkeley's dominance in the field of chemistry. From the determined ingenuity of Fred Wolff, the guarded generosity of Ed Voronin, and the ebulient optimism of Tony Moscarelli, to the "shaky hands" of Charlie Taylor[1], the overloaded schedule of Fred Vogelsberg[2] and the grandfatherly confidence of Ed Arnold, all have made a personal contribution to making Berkeley a place where research gets done substantially faster than anywhere else.

When we got the rotating source machine up and running, there was a flood of talented people that I had a chance to work with. John Somarjai helped on some of the early vinylbromide experiments. Jeremy Frey discovered some unexpected aspects of CS_2 photochemistry. Isabelle Dubourg learned a great deal about the photochemistry of

ethylene in a very short time which is to her credit. Zhao Xinsheng, who really is a "little Yuan", was a true joy to work with. Finally, great thanks and appreciation go to Eric Hintsa who will carry on the work. His mind cannot be poisoned!

A word about Ann Weightman to the younger students of the group. Although she will never publicly admit it, she is a softy. The secret's out. Don't let that tough, skeptical exterior fool you. That's just there so she can better fight through the bureaucracy, frequently on your behalf. Thankyou Ann for all the headaches you have allowed me not to have.

Cultural enlightment was obtained from many sources in the Lee group. Special thanks go to: Tim Minton for tongue muscle weight training, Matt Vernon for better ways to argue through opera and other forms of vocal exercise, Gary Robinson for settling the question: is it better to argue over middle east policy or kill yourself.[3] Rick Brudzinski wins the Moose Stubing third base coach of the year award of which I will never let him forget.

There are those who will not find there names here. Take solace in the words of a wise man who once said: "...Your good works are remembered by your Father who loves you." I also love you.

REFERENCES TO ACKNOWLEDGEMENTS

1. Those shaky hands could by the way do precision machining within ±0.0002".
2. If I don't get to it by the end of the acknowledgements remind me to say how many times Fred helped get my electronics back in working order.
3. Kill yourself is the correct answer.

CHAPTER I: An Introduction to Photofragmentation Translational Spectroscopy

The advancement of lasers in combination with the molecular beams technique has made a great impact on our understanding of primary photophysical and photochemical proccesses in the past twenty years. The ever increasing spectral and time resolution, in addition to the power and range of wavelengths available, have made it possible to excite molecules selectively and with high efficiency, to study their time evolution and to carry out state specific detection of dissociation products. The supersonic molecular beam source, which provides large densities of molecules with translational and rotational temperatures below a few degrees Kelvin, has provided a way to study photochemical processes under isolated conditions.

While a number of photodissociation studies measure properties in transition between excitation and dissociation,[1] the vast majority determine so-called asymptotic properties of the dissociation process, either measuring product quantum state distributions or velocity and angular distributions of the products. For state specific detection of smaller fragments, especially diatomics, laser induced fluoresence (LIF), multiphoton ionization (MPI) and coherent raman scattering (CRS) have provided extremely detailed information on the dynamics of photodissociation.[2] Unfortunately, the vast majority of photochemically interesting product molecules can either not be detected by these methods or it is impractical to derive useful information from their spectra. The reasons for this are manifold. Consider LIF for example, where in order to determine product state distributions, quite a number of requirements must be satisfied. First, one must have a good knowledge of the identities of all the products of the photolysis. Second, these molecules must have optical transitions that can be efficiently probed. Third, their line strengths and transition frequencies must be well characterized. Finally, the excited state produced by the probe laser must have a fairly large quantum yield for emmision of a photon as opposed to dissociation or some other dissipation process.

For most polyatomic radicals, one or more of these conditions cannot be satisfied. Even when they are, because of the large excess energy disposed into the products, one may need to know a great deal more than what is provided by conventional room-temperature

spectroscopy. In addition for highly internally excited molecules, the inverse density of states may be much smaller than the laser bandwidth, preventing resolution and identification of the state distribution of interest.

The detection of primary dissociation products using mass spectromers with electron impact ionization has the advantage of very high sensitivity, <1 molecule/cc, and universal detection ability. In the past the dissociation inherent to the ionization process has made it difficult to experimentally distinguish between daughter ions from electron-impact-induced dissociative ionization and photon-induced fragmentation and has limited the usefulness of mass spectrometry in the identification of primary photoproducts. An example of this can be found in the infrared multiphoton dissociation (IRMPD) of 2-nitropropane.[3]

In this system there are two possible dissociation pathways.:

$$C_3H_7NO_2 \xrightarrow{nh\nu} [C_3H_7NO_2]^{\ddagger} \longrightarrow C_3H_7 + NO_2 \qquad (I)$$

$$C_3H_7NO_2 \xrightarrow{nh\nu} [C_3H_7NO_2]^{\ddagger} \longrightarrow C_3H_6 + HONO \qquad (II)$$

Mass spectrometric detection of laser dependent signal at m/e=46, NO_2^+, and m/e=43, $C_3H_7^+$, would be a good indication of the presence of channel I; unfortunately, because of the presence of C_3H_7 which also gives $C_3H_6^+$ daughter ion, the detection of m/e=42 would not necessarily mean that process II were present. Additionally, because HONO appears only as NO^+ at m/e=30, a strong peak in the mass spectrum of NO_2, it would be indistinguishable by

simple mass spectrometric methods. In order to determine whether the observation of a low m/e signal is due to a neutral fragment of that mass number or merely the ionizer induced ionic fragment of a heavier neutral component, analytical chemists tackling the problem of complex mixture analysis, often have to use a hybrid technique combining gas chromatography with mass spectrometry (GC/MS), for example.

It is a general feature of photodissociation that products from different decomposition pathways appear with different recoil velocities, governed not only by the interaction potential and the propensity of the system to channel energy into translation, but dependent also upon the relative masses of the recoiling fragments. Therefore, if one performs high resolution measurements of the product velocity distribution, in combination with mass spectrometric detection, it is not at all essential that the photoproducts appear at their parent m/e's. This is like GC/MS on the μsec time scale using vaccuum as the chromatography column!

In practical terms, we accomplish this by producing a molecular beam, in which all of the molecules of interest have approximately the same direction and velocity. By firing a pulsed laser at the beam, only dissociation products, which can recoil away from the beam direction, are observed in the mass spectrometric detector, which is facing the beam/laser intersection region but is situated away from the beam direction. By measuring the arrival time distribution of the neutral photoproducts over a calibrated flight length as a function of

detector angle away from the beam direction, the translational energy distribution and angular distribution of the products can be obtained.

In the IRMPD of nitropropane mentioned earlier, because of a substantial activation barrier to molecular elimination and the particular dynamics of this molecule, HONO is produced with much more translational energy than NO_2 and can be clearly resolved in the "GC/MS", monitoring NO^+ at m/e=30, shown in fig. 1d. By resolving the two components, it is possible to quantitatively determine the relative probabilities of reactions I and II.

The sensitivity and resolution of the molecular beam photofragmentation translational spectroscopic method, originally introduced by Wilson and coworkers,[4] has been improved immensly using second generation molecular beam machines in our laboratory over the last ten years. The determination of collision-free dissociation pathways and their relative probabilities even for quite large polyatomic molecules with complex sequential decomposition processes is a standard capability of this technique.[5] This was a critical feature of recent experiments that demonstrated bond selective photochemistry.[6] Secondary photodissociation of primary free radical photoproducts can also be resolved by this method and can yield interesting information on free radical photochemistry as will be discussed in chapter III.[7]

Additionally because of total energy conservation, the translational energy distribution gives the product internal energy distribution directly. For example in the photodissociation of

Fig. 1. TOF Spectra for the IRMPD of 2-nitropropane: The lab angle is 10° from the molecular beam. The arrows indicate the beam arrival if it were to appear at this angle. The dash-dotted line is from molecular elimination while the dashed line is from simple-bond rupture. a) m/e=46, NO_2^+ from NO_2. b) m/e=43, $C_3H_7^+$ from C_3H_7. c) m/e=42, $C_3H_6^+$ from C_3H_7 and C_3H_6. d) m/e=30, NO^+ from HONO and from NO_2

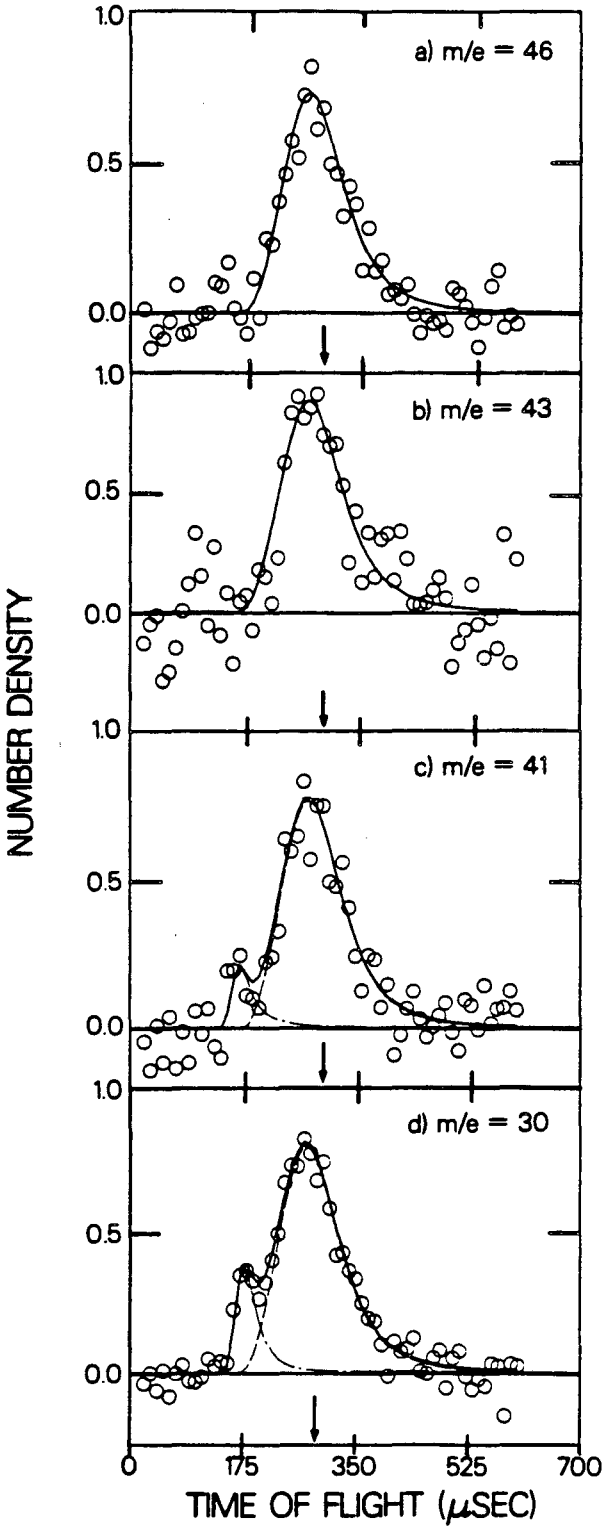

XBL 8512-5048

O_3[8] and CH_3I[9], the vibrational population distribution of $O_2(^1\Delta)$ and the CH_3 umbrella mode vibrational distribution, respectively, have been determined.

The high resolution available also makes the determination of very accurate thermochemical data possible.[10] The small or non-existent absorption cross-sections at the energy threshold for dissociation of most molecules and the substantial barriers to dissociation in many molecules make it impossible to measure dissociation energies by observing the photodissociation yield as a fuction of wavelength. However, by photodissociating molecules well above the dissociation threshold, where the absorption cross section is substantial and by measuring the maximum release of translational energy of the products, i.e. the translational energy corresponding to production of ground state products, the heats of formation of important free radicals can be obtained. Although the resolution of the translational energy measurement is limited to ~1 kcal/mol, it avoids the complications of using large thermochemical cycles typical of photoionization threshold approaches which can introduce large systematic uncertainties. High resolution TOF measurements can also yield thermochemical data on excited electronic states of free radicals which are commonly formed in photodissociation. Fig. 2 shows the way in which the singlet-triplet splitting of methylene was determined from the photodissociation of ketene.[11]

One very exciting additional fact is that the translational energy distribution reflects the forces present <u>during</u> dissociation

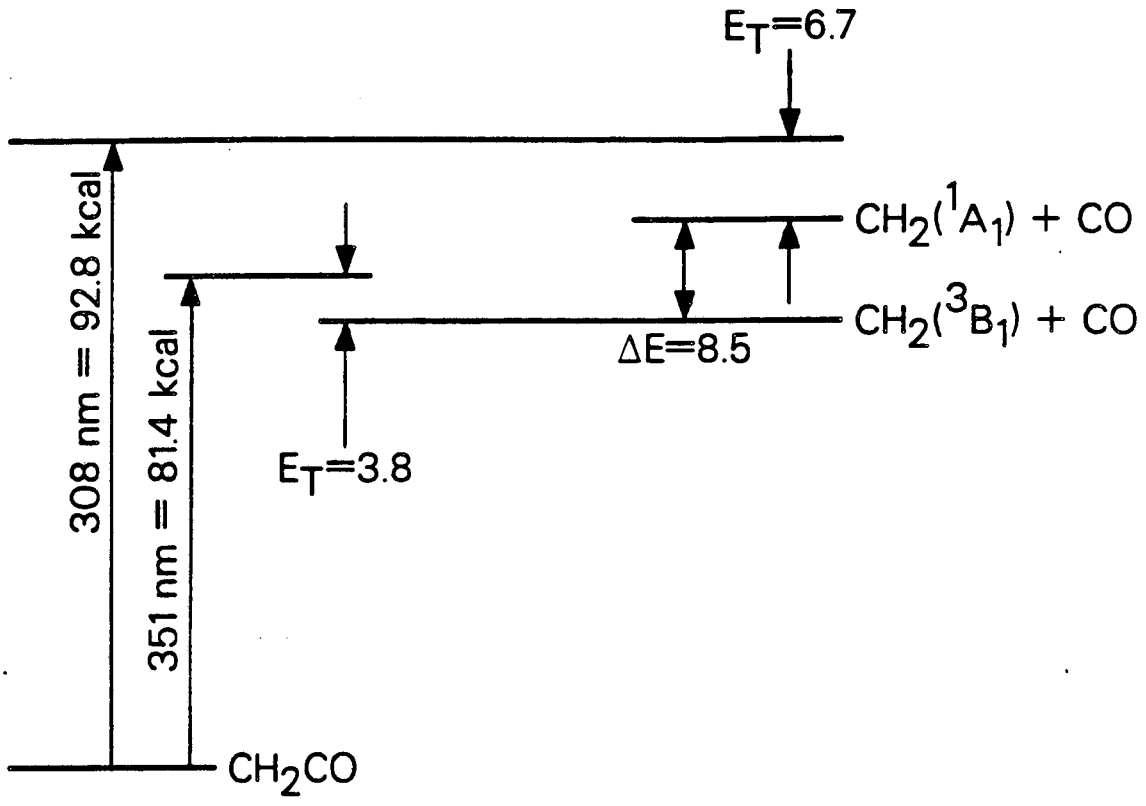

XBL 869-3248

Fig. 2. The Singlet-Triplet Splitting in Methylene: Two experiments at different photon energies were performed. The two values of the maximum release of translational energy were measured, marked E_T. ΔE is the derived singlet-triplet splitting.

and as such can be used to glean very clear information on the nature of the potential energy surface (PES). For instance molecular elimination from formaldehyde channels a large amount of the available energy into translation, whereas simple bond rupture to form HCO + H does not. This is due to a large barrier in the exit channel of the PES which efficiently channels energy into translation through a strong repulsion between the newly formed closed-shell products.

The unimolecular decomposition of vibrationally excited molecules is another problem ideally suited to study by photofragmentation translational spectroscopy. Initial experiments on thermal decomposition were by necessity done under collisional conditions since collisions were the pumping mechanism. As a result, it has always been a very difficult task to be sure that the conclusions of such experiments were not derived from collisional artifacts such as secondary reactions. Today, it is possible to study pyrolysis under collision free conditions since, due to the fact that IVR is much faster than infrared photon absorption or the rate of dissociation of molecules near their dissociation energies, a CO_2 laser can be used to create essentially thermal vibrational population distributions under collision free conditions. Simple bond rupture reactions,[12] three and four center elimination reactions,[13] as well as concerted elimination reactions that proceed through five and six membered rings have been systematically studied.

In the past two years, we have constructed a new, third generation molecular beam apparatus specifically designed and

optimized for the study of photodissociation and IRMPD. This apparatus is configured with a rotating source and a fixed detector and incorporates many new ideas for background reduction and resolution enhancement. The greatly increased resolution and reduced background have enhanced our ability to study many of the questions to which we have already alluded. A few of the most recent examples will be presented in this thesis in order to give the reader a flavor for what is possible with the most advanced high resolution photofragmentation translational spectroscopy now available.

Specifically, chapter II is an experimental section describing the new "rotating source machine" we have constructed. The new background reduction techniques we have used are included here. Chapter III describes the photodissociation of acetylene at 193 nm, in which we were able to make the most direct measurement of the C-H bond energy to date. In addition the nascent population distribution of the C_2H radical was resolved and preliminary information on its photochemistry was obtained. Chapter IV is on the photodissociation of vinylbromide at 193 nm where we went after the heat of formation of another important free radical, C_2H_3. We were able to evaluate the assumptions that govern the validity of the maximum release of translational energy method for determining thermochemical data. In addition, the metastable first excited electronic state of C_2H_3 was observed and its adiabtic excitation energy was measured. Chapter V descibes the IRMPD of three nitroalkanes: nitromethane, nitroethane and 2-nitropropane. In nitromethane, the collision free isomerization

to CH_3ONO was observed for the first time and by a novel application of RRKM theory, the barrier height to this process was determined. This technique was tested on the molecular elimination channels occuring in nitroethane and 2-nitropropane and found to give very reliable results.

REFERENCES

1. D. Imre, J.L. Kinsey, A. Sinha, J. Krenos, J. Phys. Chem., 1984, 88, 3956

2. (a) M.A.A. Clyne and I.S. McDermid, Adv. Chem. Phys., 1982, 50, 1; (b) S.R. Leone, Adv. Chem. Phys., 1982, 50, 255; (c) J.J. Valentini, Spectrometric Techniques, 1985, v. 4, p. 2, Academic Press, London; (d) D. Debarre, M. Lefebvre, M. Pealet, J.-P.E. Taran, D.J. Bamford, C.B. Moore, J. Chem. Phys., 1985, 83, 4476; (e) C.B. Moore, J.C. Weisshaar, Ann. Rev. Phys. Chem., 1983, 34, 525; (f) D.J. Bamford, S.V. Filseth, M.F. Foltz, J.W. Hepburn, C.B. Moore, J. Chem. Phys., 1985, 82, 3032; (g) P. Andresen, G.S. Ondrey, B. Titze, E.W. Rothe, J. Chem. Phys., 1984, 80, 2548

3. A.M. Wodtke, E.J. Hintsa, Y.T. Lee, J. Phys. Chem., 1986, 90, 3549

4. S.J. Riley, K.R. Wilson, Faraday Disc. of the Chem. Soc., 1972, 53, 132

5. The most complex example of this is the unimolecular decomposition of $(CH_2NNO_2)_3$ known as RDX, a test explosive used by the military. This molecule has three primary decomposition channels, the products of which each have numerous secondary and tertiary decomposition pathways! X. Zhao, E.J. Hintsa, Y.T. Lee, to be published.

6. L.J. Butler, E.J. Hintsa and Y.T. Lee, J. CHem. Phys., 1986, 84, 4104

7. A.M. Wodtke, Y.T. Lee, J. Chem. Phys, 89, 4744

8. R.K. Sparks, L.R. Carlson, K. Shobatake, M.L. Kowalczyk, Y.T. Lee, J. Chem. Phys., 1980, 72, 1401

9. R.K. Sparks, K. Shobatake, L.R. Carlson, Y.T. Lee, J. Chem. Phys., 1981, 75, 3838

10. The importance of accurate thermochemical data to kinetics has been demonstrated convincingly. S.W. Benson, Thermochemical Kinetics, 1976, John Wiley and Sons, New York

11. C.C. Hayden, D.M. Neumark, K. Shobatake, R.K. Sparks, Y.T. Lee, J. Chem. Phys., 1982, 76, 3607

12. Aa.S. Sudbo, P.A. Schultz, E.R. Grant, Y.R. Shen, Y.T. Lee, J. Chem. Phys., 1979, 79, 912

13. Aa.S. Sudbo, P.A. Schultz, Y.R. Shen, Y.T. Lee, J. Chem. Phys., 69, 2312 (1978)

CHAPTER II: Experimental Descriptions and Considerations

A. Experimental Apparatus.- Fig. 1 shows a detailed scaled drawing of the instrument used in all of the experiments to be described. A continuous molecular beam is produced at 1 by expanding the molecule of interest, diluted in rare gas and typically at a total pressure of 200–500 torr, through a 125 μm nozzle. The nozzle can be heated with coaxial heating wire, shown at 2, to increase the beam velocity and/or to remove clusters that can form due to the low internal temperature of the molecules produced by the expansion. The pressure in the molecular beam source chamber is ordinarily ~10^{-4} torr when the beam is running and is pumped by two 6" diffusion pumps, one of which is shown at 10, providing 5000 L/s pumping speed. A Leybold-Heraeus-360

Fig. 1 The Rotating Source Machine: 1, molecular beam source. 2, heating wire. 3, background "gobbler". 4, focussing lens for laser. 5, molecular/laser beam crossing region. 6, liquid nitrogen cooled panels. 7, gate valve assembly for detector. 8, retractable slotted chopping wheel. 9, main chamber diffusion pump. 10, source chamber diffusion pump. 11, brink's-type electron-impact ionizer. 12, quadrupole mass filter. 13, magnetically suspended turbomolecular pump for ionization region. 14, exit ion optics. 15, ion target. 16, scintillator. 17, grease-sealed turbomolecular pumps for differential pumping of detector. 18, photomultiplier tube. 19, liquid nitrogen reservoirs.

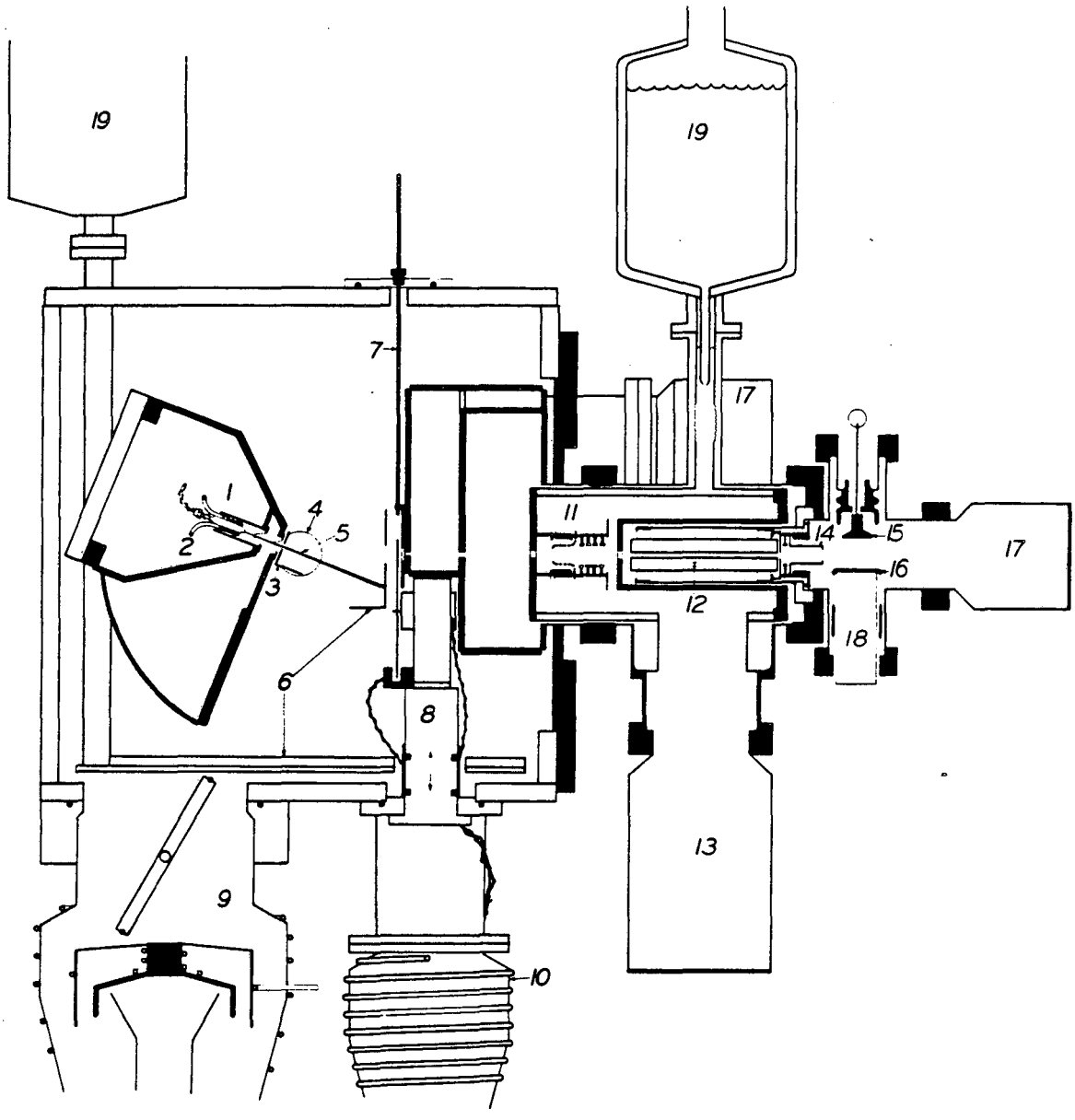

XBL 862-713

turbomolecular pump is used to differentially pump a chamber between the source and the main chamber. This helps to carry away the large gas load of the molecular beam and maintains the operating main chamber pressure at ~10^{-7} torr. The pumping system in the main chamber consists of a 10" Edwards Diffstack, 9, and several large liquid nitrogen cooled copper panels, 6.

The source and differential pumping chambers are welded to a vacuum seal which rotates in the plane of the figure about point 5, where the molecular and laser beams cross. The velocity of the parent molecular beam can be measured with the retractable slotted chopping wheel shown at 8. This entire assembly can slide downward, out of the way, without breaking vacuum when the photodissociation experiment is to be performed. The laser, either a Lambda-Physics EMG103MSC excimer or a GENTEC TEA CO_2, is focussed by the lens at 4 and propogates along the beam source rotation axis.

The pulse of light intersects the molecular beam at 5 and induces dissociation. A small angular fraction of the photoproducts travels through the acceptance apertures of the detector, traversing a 36.75 cm flight path through two ultrahigh vacuum differential pumping chambers. The ionization chamber is equipped with a very fast time response electron impact Brink's ionizer, 11, with an ionization length of 5 mm.[1] This makes our apparatus the highest resolution ($L/\Delta L = 36.75/0.5 = 74$) photofragmentation spectrometer in the world, although one has a longer flight length.[2] The ionizer is contained within a liquid nitrogen cooled dewar. Due to the very high

sensitivity of the detector, this is essential. The ions formed at 11 are mass analyzed by an electric quadrupole MS at 12, and counted by a Daly-type ion counter, 15, 16, 18. The differential pumping chambers of the detector are pumped by Leybold-Heraeus-360 grease-sealed turbomolecular pumps, 17, and the ionization chamber is pumped by a magnetically suspended 500 L/s turbomolecular pump, 13.

The detector can be sealed off with the gate valve assembly, 7, when the main chamber needs to be vented. The entire detector is mounted with ball bearing rollers on two stainless steel rods and can be removed from the main chamber while under vacuum for intense baking out.

The TOF spectrum is recorded by triggering a multichannel scaler with the laser and recording the ion counts at each m/e as a function of time after the laser pulse. Our typical scaler time resolution element is 1-2 μs although we have the ability to go down to 150 ns when signal allows. The data acquisition is overseen and directed by a macro program running on a DEC LSI-11 lab computer.

B. Background Reduction Techniques.- B.1. Cryogenic Methods.- The holes in the detector walls between 3 and 7 in Fig. 1 are precision machined and define the viewing window of the detector. These are placed so that, regardless of the source angle, the detector sees all parts of the interaction volume at 3. One might think that the background in the detector that is created by the operation of the molecular beam could be calculated from the conductance of the

defining slits and the pumping speeds of the pumps on each region of differential pumping according to the following equation.

$$P_{Detector} = P_{Main\ Chamber} \frac{C_1}{S_1} \frac{C_2}{S_2} \frac{C_3}{S_3}$$

Where

$P_{Detector}$ = partial pressure in the detector

$P_{Main\ Chamber}$ = partial pressure in the main chamber

C_i = Conductance of each differential pumping aperture

S_i = Pumping speed of each pump on each differential pumping region

However, for those molecules that travel straight through all of the differential pumping apertures, the above equation will not apply. This direct-through background cannot be decreased by any number of differential pumping regions. This effect is the reason that the above equation almost always calculates a background level much lower than that which is experimentally observed. Since the pressure in the main chamber is $\sim 10^{-7}$ torr, the mean free path is much larger than the dimensions of the chamber itself. For this reason direct-through background can only be formed by first bouncing off of surfaces within the viewing window of the detector. To combat this effect, a closed cycle refrigerator is used to cool a copper collimation slit to 30°K at 3 in Fig. 1. This ensures that all surfaces within the detector's viewing window will be below 30°K. This lowers the background originating from the main chamber typically by a factor of ten.

We have also placed liquid nitrogen cooled copper panels, shown at 6, so that the molecular beam is terminated on a 77°K surface. For condensible gasses this is a very effective beam catcher. In addition, these cooled panels are designed to surround the collimation slit and therefore limit the sources of thermal radiation in the main chamber and allow the collimation slit to attain its lowest possible temperature.

B.2. Optimized Detector Pumping System.- The heart of the molecular beam machine is a very high sensitivity electron-impact Brinks-type ionizer. The details of ionization efficiency calculations have recently been described in ref 3. Briefly, given a typical electron flux of 10 mamps/cm^2 or $6x10^{16}$ $e^-cm^{-2}s^{-1}$, and an ionization cross-section of 10^{-16} cm^2, the rate of ionization will be six molecules per second. However, if the molecules travel through a .5 cm ionizer at a speed of 10^5cm/sec their residence time is only 5 μs. So, the probability that a molecule will be ionized in this situation is only $3x10^{-5}$. That is, if $3x10^4$ molecules/s pass through the 1 cm^2 area of the ionizer, this will give an ion count rate of 1 Hz, the nominal detection limit of the apparatus under typical conditions of background. If one converts the flux, $3x10^4cm^{-2}s^{-1}$, to number density using the velocity, 10^5cm/s, one obtains a detection limit of 0.3 molecules/cc. In other words a number density of 0.3 molecules/cc will give a signal count rate of 1 Hz.

With this sensitivity, one of the major objectives in the design of the detector is to achieve an extremely clean ultra-high vacuum. In the past, ion pumps have been used extensively, due to their relatively low price and unsurpassable reliabilty. However, because they depend upon a large surface-sticking coefficient for the molecule to be pumped, they are terrible for pumping rare gasses. This is particularly inconvenient for molecular beam experiments since it is extremely common to use a rare gas in the molecular beam itself. If one needs to look for signal at the rare gas masses, m/e=4, 20, or 40, one will really be in trouble with ion pumps. There is a related problem of more experimental significance. It has often been said that "ion pumps are great as long as you don't have to pump anything". That is, they give a terrific ultimate pressure, but if you have a significant gas load, difficulties may arise. For instance, a large gas load can induce molecules to be emitted that have been trapped in the pump from previous use. This can give rise to background at unexpected masses depending upon what has been pumped in the past. This problem can be overcome by sandblasting the insides of the pumps.

The most severe problem with ion pumps is that they actually have a negative pumping speed for hydrocarbons. This is a result of electron impact induced cracking of hydrocarbons by the plasma in the ion pump. Large hydrocarbons give numerous molecules of small hydrocarbons.

For these reasons we have redesigned this detector with turbomolecular pumps. Turbopumps are actually the simplest form of

momentum transfer pumps. They consist of a very high speed rotor and a stator that act like a fan, literally blowing the molecules out of the chamber. They have comparable or better pumping speeds as ion pumps for everything except H_2. They are much better at pumping rare gasses and hydrocarbons and transfer the molecules physically out of the chamber in contrast to ion pumps. They have very low ultimate pressures and are reasonably reliable. For the ionization region of the detector we have used a magnetically suspended turbopump that has a very low ultimate pressure since there is no lubricating fluid for the magnetic bearing.

This overall detector design is especially effective for low hydrocarbon background. A partial pressure for CH_4 of 10^{-13} torr is easily obtained in our apparatus.

C. Data Analysis Methods.- Data analysis consists of finding the center-of-mass frame translational energy distribution function, $P(E_T)$, from the observed laboratory frame TOF spectra. For the analysis of primary dissociation processes we use the "forward convolution" method. We guess at a trial $P(E_T)$ and calculate what our data should look like, taking into consideration several instrumental averaging factors including: beam velocity and angular dispersion, ionizer length, detector angular resolution and multichannel scaler channel width. We then alter the $P(E_T)$ until the calculated TOF fits the data.

For secondary dissociation, we use a similar program which performs much more averaging. In a sense looking at secondary dissociation is like looking at a primary process with a very poorly defined molecular beam. In this forward convolution program, the entire primary dissociation flux map in the three dimensional laboratory frame is calculated. This flux map is converted to number density and used to characterize the angular and velocity distributions of the "molecular beam" to which the primary process gives rise.

The program ANALMAX is included in this thesis as an appendix. It includes polarization dependent simulations for the geometry of the rotating source machine and has the capacity for secondary dissociation simulations.

REFERENCES

1. This was determined by measuring the TOF spectrum of H atoms recoiling from the photochemical reaction:

$$HI \xrightarrow{248\ nm} H + I$$

The width of the TOF spectrum is entirely due to the finite size of the ionizer and the interaction volume. The size of the interaction region was measured to be 3mm and this gave rise to the 5mm value for the ionizer length.

2. M.D. Barry, P.A. Gorey, Mol. Phys., 1984, 52, 461. His machine has a 50 cm flight length.

3. Y.T. Lee, "Reactive Scattering: Non-Optical Techniques", Atomic and Molecular Beam Methods, Eds. G. Scoles, U. Buck, Oxford University Press, New York, New York, 1986

CHAPTER III: The Photodissociation of Acetylene at 193 nm

A. Introduction.- The photodissociation of hydrocarbons and molecules that give hydrocarbon products has traditionally been a problem for the photofragmentation translation technique. The two main reasons for this are the high detector background at hydrocarbon masses found in most mass spectrometers and the lack of intense UV light sources needed to excite enough molecules to make the experiment possible. Calvert and Pitts[1] have a good summary of hydrocarbon UV absorption spectra illustrating this aspect of the problem. In general absorption at long wavelengths increases with the size of the molecule and with the degree of unsaturation. Ethylene for example, has an absorption cross-section of $\sim 2 \times 10^{-20}$ cm^{-2} at 193.5 nm while

saturated hydrocarbons do not absorb at all at wavelengths longer than 165 nm even up to the butanes.

Although the availability of UV lasers is limited, the ArF laser is a standout both in terms of spectral brightness and reliability. Lasing occurs at 193.3 nm with a full bandwidth of 0.8 nm. The wavelength resolved output is characteristically spiked, due to intracavity absorption of trace O_2.[2] These lasers typically produce 10^{17} photons/pulse at a repetition rate of 100 Hz. Despite the small absorption cross-section, the photodissociation of acetylene was quite easy with our new machine and a Lambda-Physics excimer laser.

In our new apparatus, we have succeeded in lowering the detector's hydrocarbon background principally through the use of turbomolecular pumps. A methane partial pressure of $\sim 10^{-13}$ torr can be easily obtained. See chapter II for a more detailed discussion of the experimental apparatus and the background reduction techniques employed. This has even allowed us to investigate the photodissociation of ethylene at 193 nm with the use of a pulsed molecular beam.

Acetylene was a good choice for one of the first studies of hydrocarbon photochemistry since, because of its importance in combustion, there is already a lot of information available. The ultraviolet spectrum in the 200 nm range has been analyzed and found to be due to absorption to a trans-bent ^1A_u excited state.[3,4] Electron energy loss spectroscopy was used to place the approximate energy of two low lying triplet states.[5] Irion and Kompa[6]

have used an unfocused ArF laser to dissociate acetylene in a gas cell, analyzing the collisionally quenched, stable products with TOF mass spectrometry. They concluded that C-H bond rupture is the primary dissociation pathway.

$$C_2H_2 \xrightarrow{193\ nm} C_2H + H \qquad (I)$$

McDonald, Baranovski, and Donnelly[7] and more recently Okabe, Cody, and Allen[8] have used a focused ArF laser (3×10^{26} photons/cm^2 second) to photolyze acetylene. They observed two and three photon absorption processes to form C_2 and CH in excited electronic states which were observed by dispersed fluorescence spectroscopy. Again, using a strongly focused ArF laser, emission from electronically excited C atom was observed by Miziolek, et al.[9]

Despite the large amount of effort, one fundamental structural aspect of this molecule which is still quite uncertain is the C-H bond energy, $D_o(C_2H\text{-}H)$. The lowest dissociative ionization threshold, producing $C_2H^+ + H + e^-$, was measured to be 17.365 eV by Dibeler, Walker and McCulloh[10] (DWM) and more recently in a molecular beam by Ono and Ng[11] (ON) to be 16.79 eV. Combining the ionization potential (IP) of C_2H radical[12,13] with these thresholds, $D_o(C_2H\text{-}H)$ can be derived. In an analogous way the electron affinity of C_2H[14] was combined in a thermochemical cycle with the acidity of C_2H_2[15] and the IP of H to give $D_o(C_2H\text{-}H)$. Unfortunately, due to the systematic deviations

between experiments, the uncertainty in the determination of $D_0(C_2H-H)$ has not been smaller than 0.5 eV.

Additionally, the role of other primary photodissociation pathways, for instance loss of H_2, remains unknown and essentially nothing is known about the dynamics of the UV photodissociation of acetylene. Does acetylene undergo internal conversion before dissociation like formaldehyde? How is the energy partitioned in the products? We already know that multiphoton absorption is occuring.[7,8,9] What is the mechanism for these proccesses? Does the parent acetylene molecule absorb many photons before dissociating or do the products of primary dissociation absorb the secondary photons? Is it possible to obtain detailed information on the photochemistry of free-radicals? In order to answer these and related questions and in an effort to nail down $D_0(C_2H-H)$ in acetylene, we performed molecular beam experiments designed to measure the translational energy release of fragments from the photolysis of acetylene at 193.3 nm under collision free conditions.

B. Experimental Supplement.- The details of the apparatus have already been described in chapter II and what follows are only the experimental details peculiar to this experiment. A continuous molecular beam was formed by passing 250 torr of a 15 percent mixture of acetylene in neon through a dry ice ethanol trap to remove acetone and expanding it through a 0.125 mm nozzle into the source region. Experiments were done at two nozzle temperatures to observe the

influence of unrelaxed bending vibrations in acetylene and also a neat beam of acetylene was used for low laser power experiments. Table I gives the beam characteristics used in all of the experiments.

The laser was a Lambda-Physik EMG 103 MSC Excimer laser and was run with ArF. Typially, 100 mJ/pulse at 150 Hz was obtained and focused to a 1 mm x 3 mm rectangular spot.

In order to obtain information on the lifetime of the excited acetylene molecule, we polarized the excimer laser output for some of the experiments. This was accomplished by passing the 193 nm light through a MgF_2 prism. MgF_2 is ideal for transmitting 193 nm light and its birefringence is substantial enough to separate the vertical from the horizontal polarization by ~3°. Typically we could achieve 30 mJ/pulse of vertically polarized light and 20 mJ/pulse of horizontally polarized light. Because the vertically polarized light passed through our optics at or near Brewster's angle, it was significantly more intense than the horizontally polarized component, which passed though all of the optics at 0° angular incidence. By mounting the MgF_2 prism in a micrometer driven rotation stage, it was easy to change the polarization of the light used to produce the TOF spectra. By comparison of the TOF spectra produced by the two polarizations, it was possible to determine the polarization effect.

C. Results and Analysis.- Laser photolysis gives signal at m/e's of 25, 24, 13, and 12 amu. From a comparison of the TOF spectra, we know that the signal at m/e=13 and 12 comes from electron-impact induced

Table I

Expansion Conditions	$\Delta V/V$	Most Probable Velocity	ΔE_T^{LAB}
Seeded 300°K	12	7.9×10^4 cm/s	1 kcal/mole
Seeded 530°K	12	10.8×10^4 cm/s	1 kcal/mole
Neat 300°K	25	8.4×10^4 cm/s	2 kcal/mole

Table I: Conditions and Characteristics of the Molecular Beams used in this Experiment

dissociative ionization of neutral products of masses 25 and 24. The TOF spectra at 20° for m/e=25 and 24 are shown in fig. 1. The m/e=25 signal can only come from C_2H radical produced in the photolysis process. C_2H^+ ion formed in the ionizer can easily fragment to C_2^+ and gives rise to some of the signal at m/e=24. If C_2H were the only neutral product the m/e=25 and 24 spectra would be identical, apart from a very small difference in the flight time of the ions. The m/e=24 spectrum shows a substantial amount of signal arriving at significantly shorter arrival times (higher translational energies) than the C_2H product. As will be shown in the next section from the laser power dependence of the dissociation signal, processes I and II which involve sequential photolysis of C_2H product during the laser pulse are responsible for the observed data.

$$C_2H_2 \xrightarrow{193\ nm} C_2H + H \qquad (I)$$

$$C_2H \xrightarrow{193\ nm} C_2 + H \qquad (II)$$

The determination of $D_o(C_2H\text{-}H)$ in acetylene relies on the principle of conservation of energy. When acetylene absorbs a photon at 193.3 nm it has 148 kcal/mol of energy at its disposal. We assume that the C_2H radical appearing with maximum translational energy corresponds to the ground state fragment. The difference between the photon energy and the maximum translational energy release then is $D_o(C_2H\text{-}H)$. The validity of the ground state fragment assumption will be discussed in relation to the photodissociation of vinyl bromide in chapter IV. Although we can neglect any rotational energy

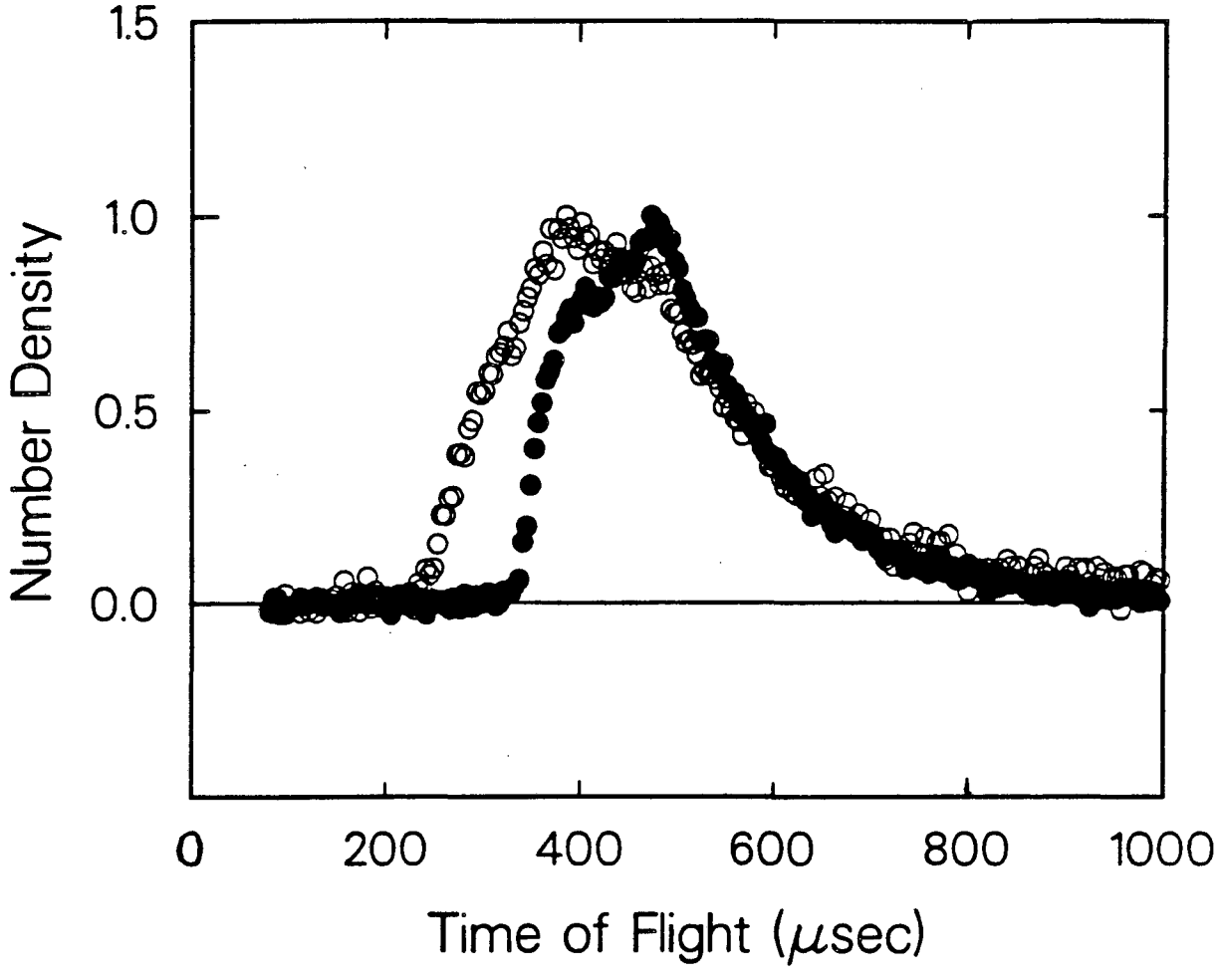

XBL 868-3123

Fig. 1. Mass 25 and 24 Time of Flight Spectra: The open circles are m/e=24, the closed circles are m/e=25. Signal was observed at an angle of 20° away from the parent molecular beam.

of the parent acetylene which is well relaxed during the supersonic expansion, we cannot ignore unrelaxed vibrational energy in the two, doubly degenerate bending modes which can contribute to the translational energy of the products. The harmonic frequencies of these two vibrations are 611 cm^{-1} and 729 cm^{-1} which correspond to about 3kT at room temperature. These will not be cooled efficiently in the supersonic expansion. In principle, one could remove these "hot bands" by cooling the nozzle, but in practice it is necessary to avoid cluster formation at low temperatures by heating the nozzle and identifying the contribution from the bending modes by observing a temperature dependent increase in the fastest products. By carefully characterizing the temperature dependence of the product appearing with the maximum translational energy, a very accurate determination of the C-H bond energy in acetylene was possible.

C.1. Time-of-Flight Spectra of C_2H at 300°K Nozzle Temperature.- Fig. 2 shows the Newton diagram for process I using the 15 percent acetylene seeded neon beam at a nozzle temperature at 300°K. The purpose of a Newton diagram is to clarify the relationship between the lab frame of reference and the center-of-mass frame of reference. The bold arrow represents the molecular beam velocity in the lab frame. The center-of-mass of the dissociation system travels inertially along this vector. Vectorially adding the beam velocity vector to any center-of-mass frame vector yields the corresponding laboratory frame vector. The circles which are drawn centered on the tip of the beam

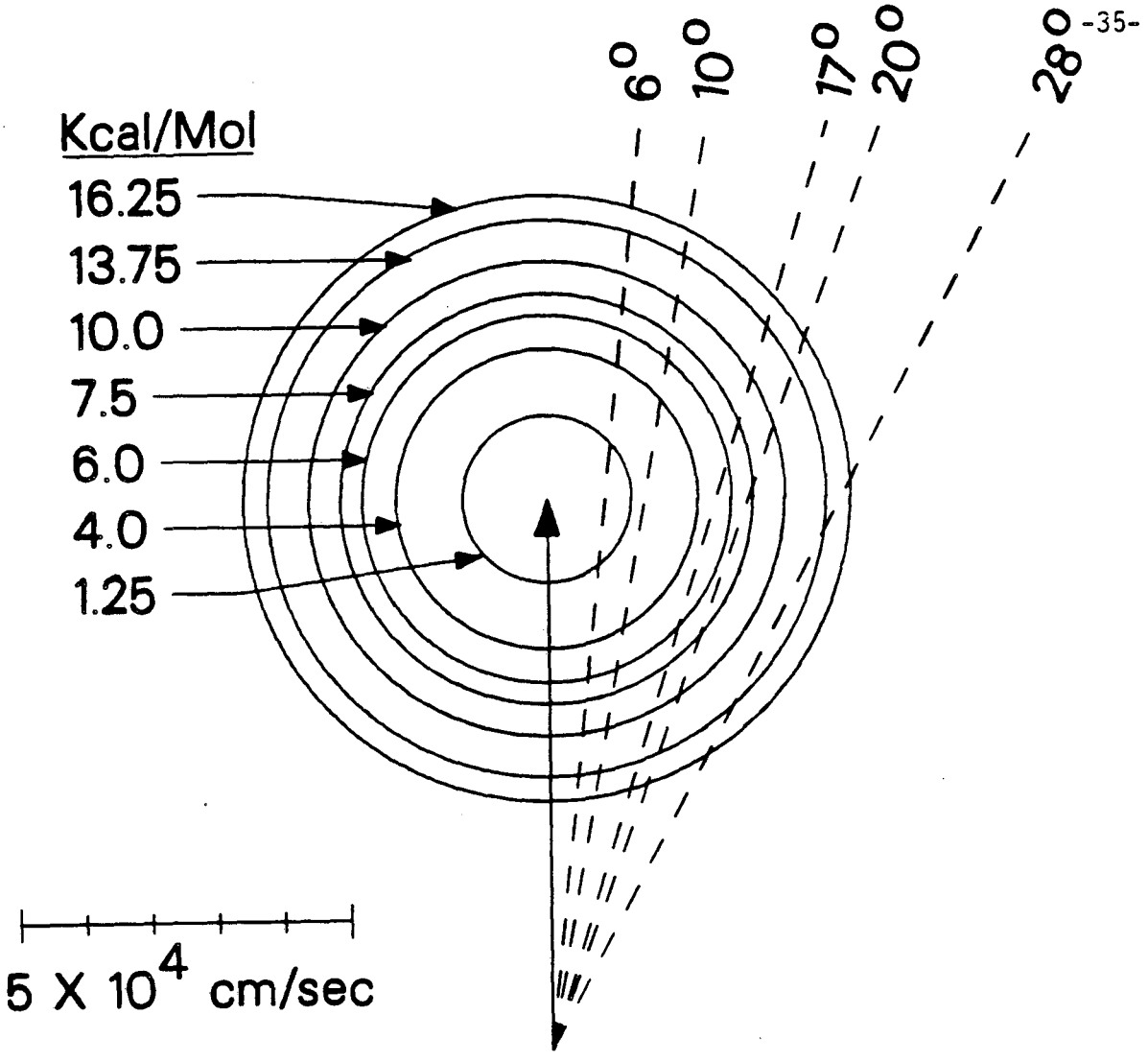

XBL 855-2463

Fig. 2. Newton Diagram for Seeded Beam at 300°K: The angles shown are where data was taken. The circles represent the velocities of the C_2H radical produced in process I and the corresponding center-of-mass, relative, kinetic energies.

vector indicate various recoil speeds in the center-of-mass frame of reference for the C_2H fragment. That is, all lab velocities observed on a given circle are from the same center-of-mass recoil speed of the dissociating fragment. Fig. 2 indicates the relative translational energy release to which these C_2H fragment speeds correspond. One can see that molecules with a large amount of internal excitation and hence low center-of-mass translational energies will not be scattered far from the beam. It is therefore necessary to look as close as 6° from the beam to see the most internally excited products. A more subtle experimental consideration comes from the fact that the resolution of the measurement of the laboratory velocity is limited by the ratio of the length of the ionizer to the total flight length, according to the following relationships.

$$\frac{\Delta V_{LAB}}{V_{LAB}} = \frac{\Delta t}{t} = \frac{\Delta L}{L} = \frac{0.5\ cm}{37\ cm} \simeq 0.014 \qquad (1)$$

where

ΔL = ionizer length (0.5 cm)

L = flight length (37 cm)

ΔV_{LAB} = lab velocity resolution element

V_{LAB} = lab velocity

Δt = arrival time resolution element

t = arrival time

From equation (1) one can see that at high lab velocities a certain

velocity difference will be spread out in time to a lesser extent than at low lab velocities. At large laboratory angles, the lab velocity for a given Newton circle is smaller. In addition, the separation between a pair of Newton circles in laboratory velocity space is larger. Therefore, it is always better to look at large angles to get better resolution of the fast products.

Fig.'s 3a-e show the data obtained at 28°, 20°, 17°, 10°, and 6° and fig. 4 shows the center-of-mass translational energy probability distribution, $P(E_T)$, used to fit the data. In fig.'s 3a-e the circles are the data and the solid lines are the fit to the data. The structure that is being partially resolved is due to the internal state population distribution of the nacent C_2H radical. The peaks in the $P(E_T)$, Fig. 4, have been labeled with arbitrary symbols and correspond to the like labeled bumps and shoulders in the TOF spectra. Experimentally, the peaks marked 1 and 2 are the least well determined. The $P(E_T)$ shown has the minimum structure necessary to fit the data. A discussion of the assignment of the features in this $P(E_T)$ can be found in section D.2..

C.2. Time of Flight Spectra of C_2H at 530°K Nozzle Temperature.- In order to determine the effect of unrelaxed bending vibrations in C_2H_2 on the determination of the maximum release of translational energy, the nozzle was heated to 530°K, about tripling, in comparison to the 300°K experiment, the number of parent acetylene molecules not in the ground vibrational state. The TOF spectrum at 21° is shown in

Fig. 3. Time of Flight Spectra of m/e=25: The data was obtained at various angles away from the parent molecular beam. The open circles are the data and the solid lines are the best fit to the data based on the center-of-mass translational energy distribution shown in fig. 4. The symbols refer to fig. 4. (a) 28°, (b) 20°, (c) 17°, (d) 10°, (e) 6°

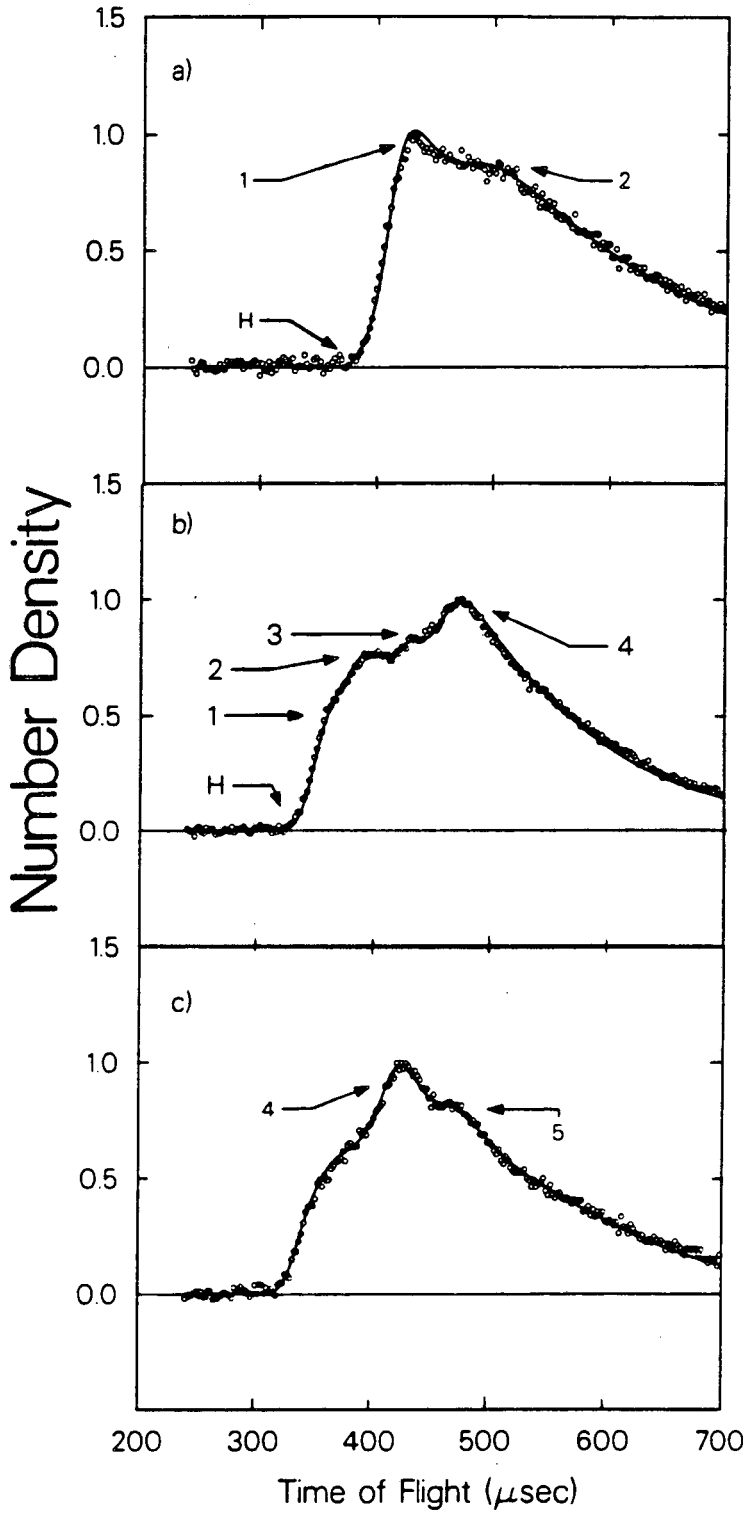
a)
b)
c)
1
2
H
3
4
5
Number Density
Time of Flight (μsec)
1.5
1.0
0.5
0.0
200
300
400
500
600
700

XBL 868-3126

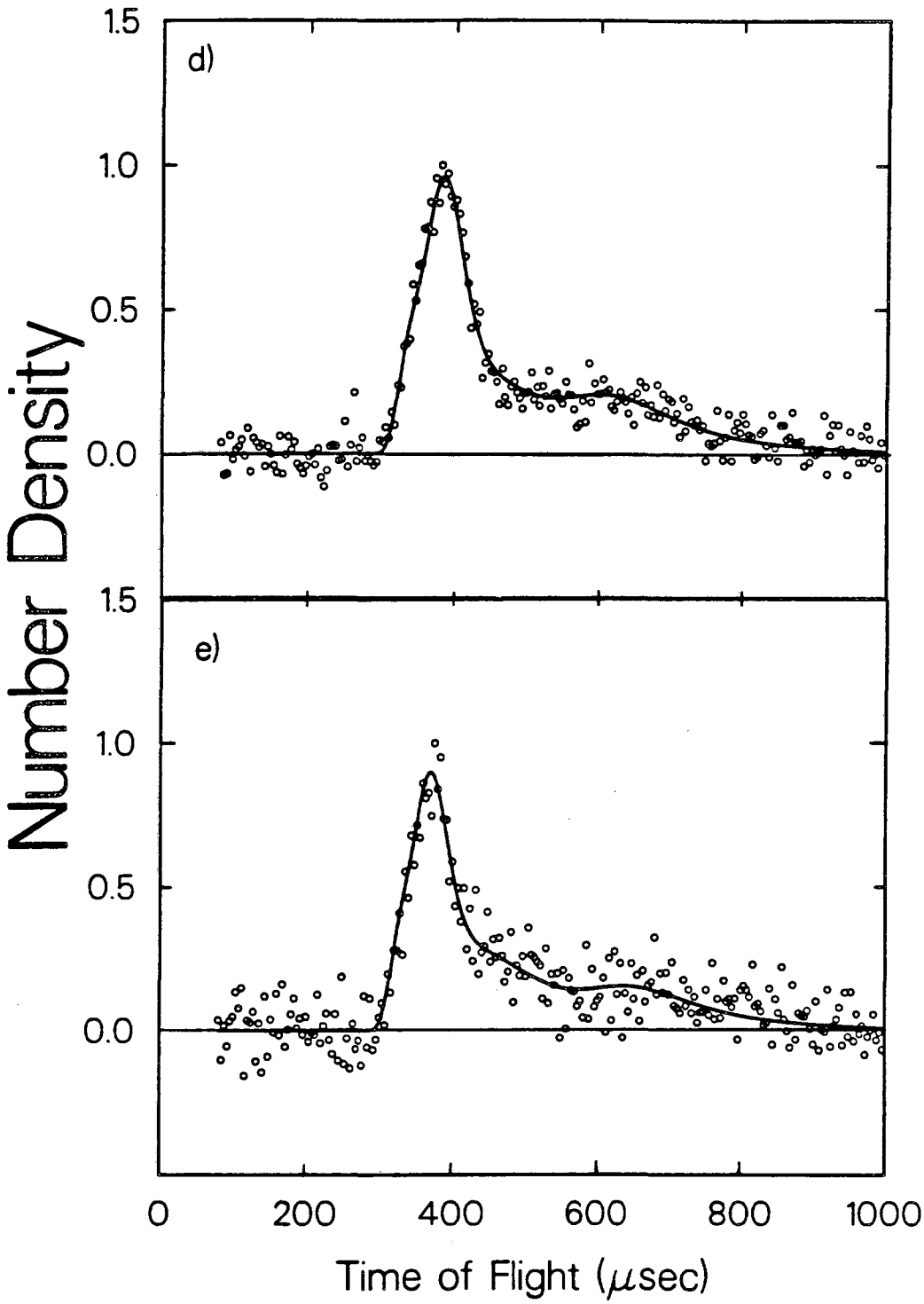
d)
e)
1.5
1.0
0.5
0.0
Number Density
0
200
400
600
800
1000
Time of Flight (μsec)

XBL 868-3127

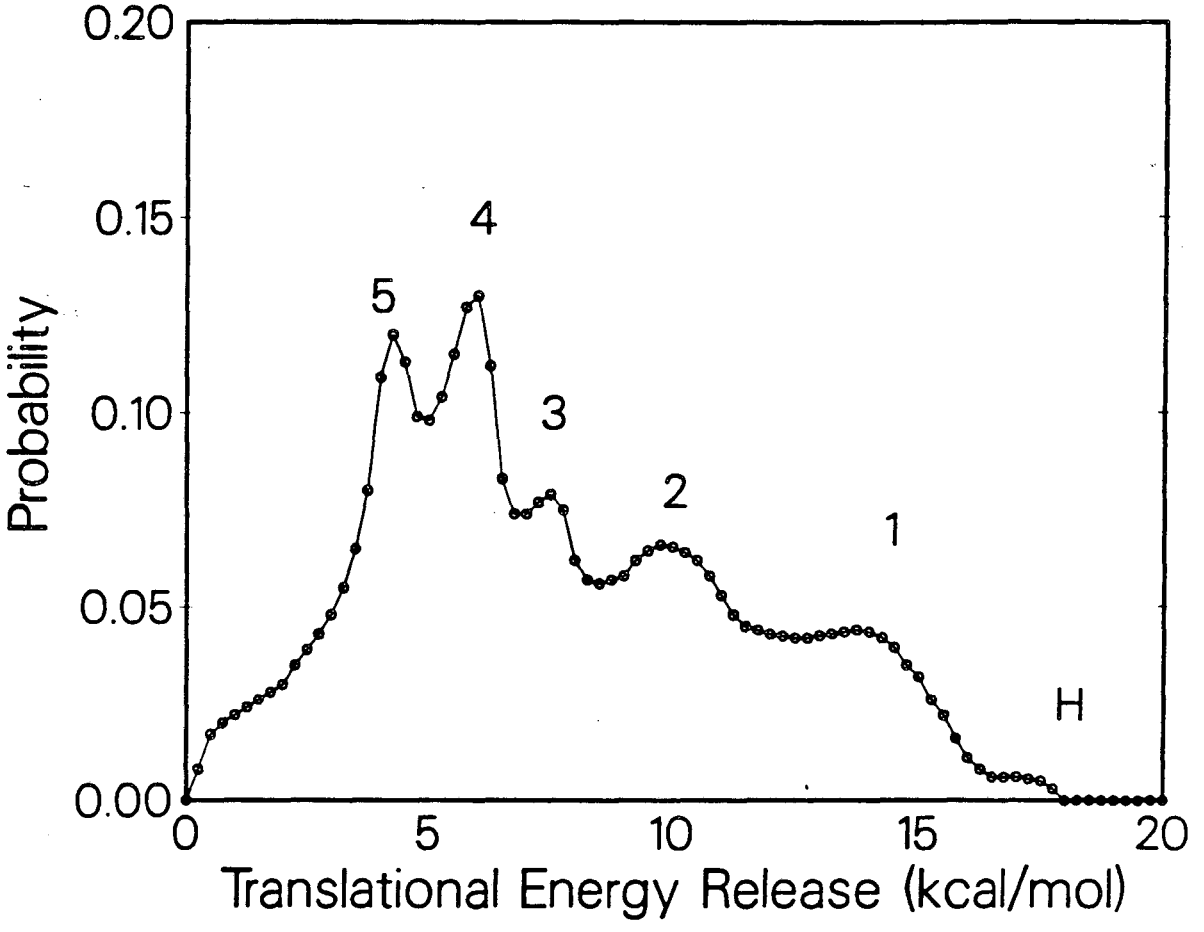

XBL 868-3124

Fig. 4. Translational Energy Probability Distribution Used to Fit Data in Fig. 3: The small open circles are separated by 0.25 kcal/mol.

Fig. 5. The $P(E_T)$ in fig. 4 does not fit this data at all well; however, the fit shown in fig. 5 is obtained by simply increasing the peak labelled "H" by a factor of three. We therefore conclude that the peak labelled "H" is due to vibrationally unrelaxed parent C_2H_2 present in the beam and that the maximum release of translational energy occurs not at 18 kcal/mol but at slightly more than 16 kcal/mole, giving a $D_0(C_2H-H)$ of 132 kcal/mole.

C.3. Secondary Dissociation.- Fig.'s 6 and 7 show the m/e=24 (C_2^+) TOF spectrum and the $P(E_T)$ used to fit the secondary process II. A special program was written to analyse secondary dissociation and is described in appendix 1. Although there is considerably less detail in this $P(E_T)$, the qualitative features are still apparent. The $P(E_T)$ appears to have two components. One is a sharp peak at about 10 kcal/mol and the other is a broad hump extending out to the maximum allowed translational energy. The maximum release of translational energy indicates that C_2H has absorbed only one photon.

Fig. 8 shows the results of the m/e=25 power dependence experiment that was performed in order to clarify the mechanism of the secondary photodissociation. These spectra were taken with a neat acetylene beam for maximum signal. It has close to the same velocity as the neon seeded beam but the velocity distribution is nearly twice as broad. See table I. The asymptotically low power TOF spectrum for m/e=25 at 20° was obtained by photodissociating a neat beam of

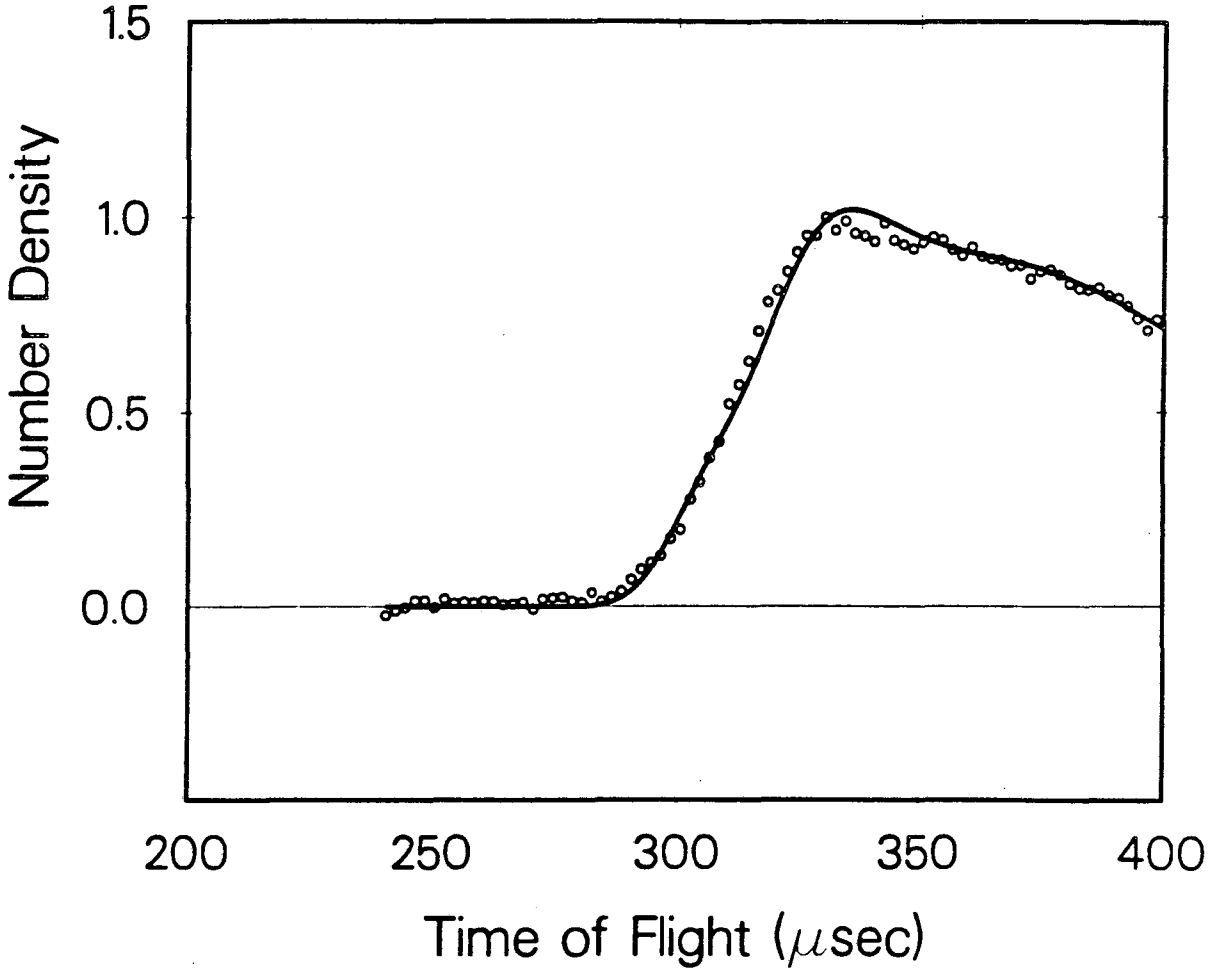

Fig. 5. Time of Flight Spectrum for a Nozzle Temperature of 530°K: m/e=25, 21°.

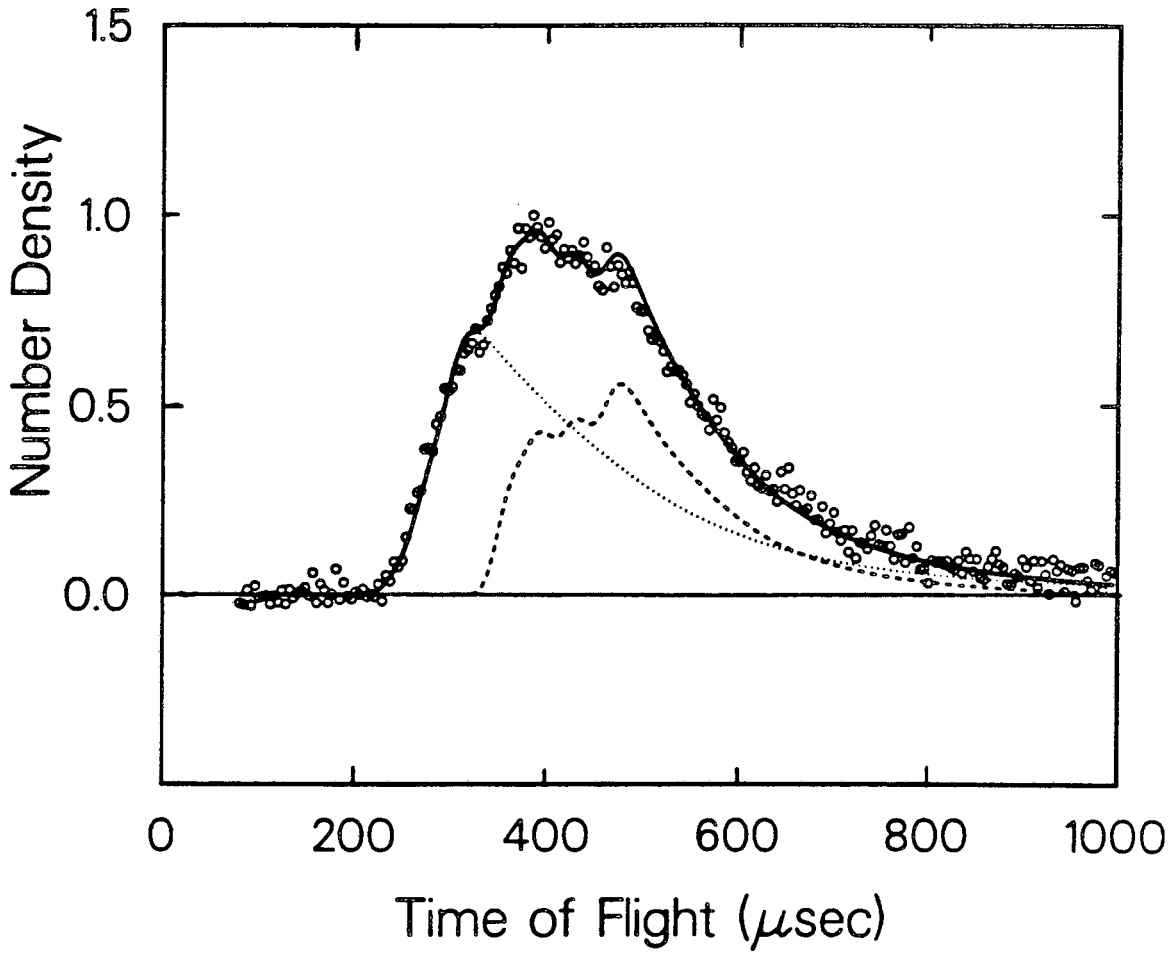

XBL 868-3133

Fig. 6. Time of Flight Spectrum of m/e=24: The laboratory angle is 20°. The solid line is the total calculated TOF, the dashed line is the contribution from C_2H and the dotted line is the contribution from C_2.

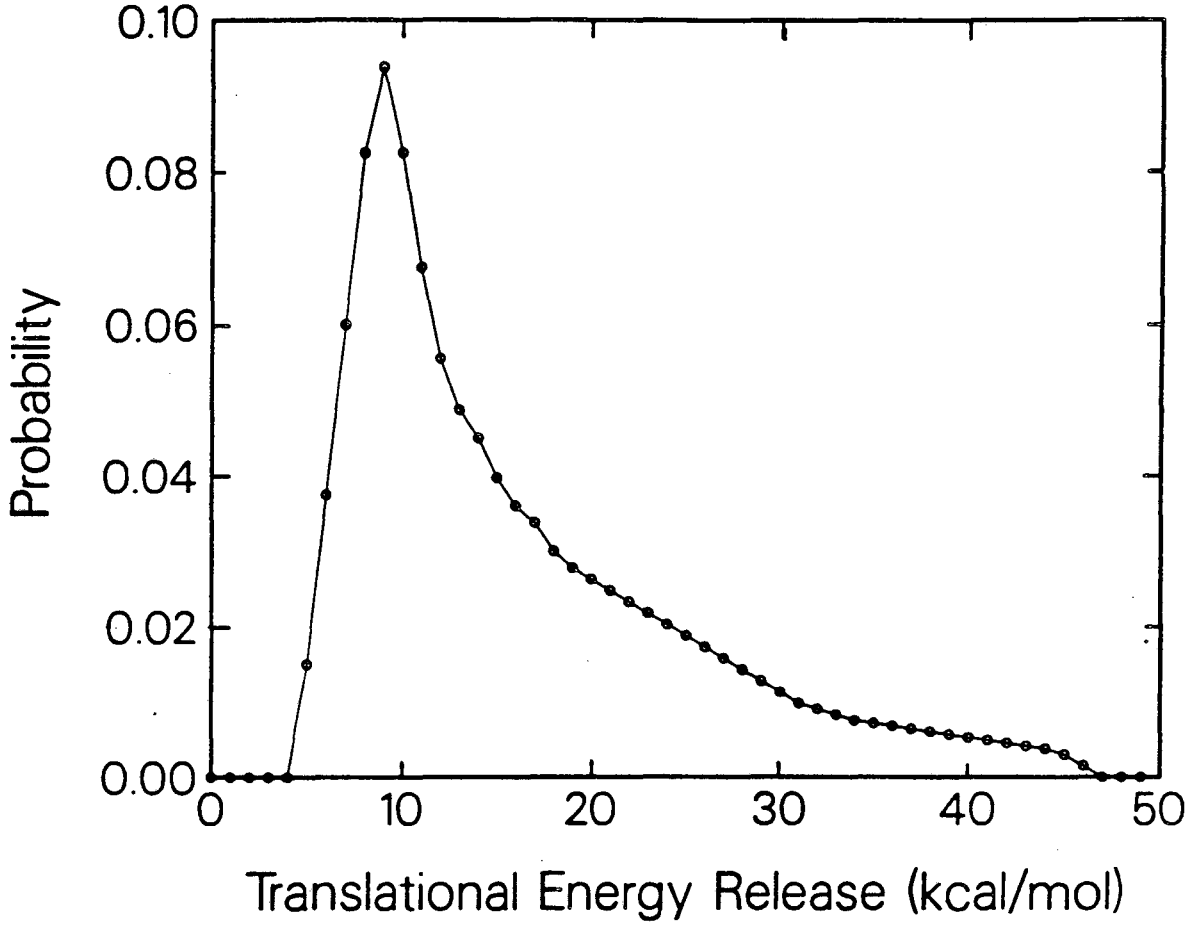

XBL 868-3132

Fig. 7. Translational Energy Distribution Used to fit C_2 Contribution to Fig. 6: Small open circles are separated by 1 kcal/mol.

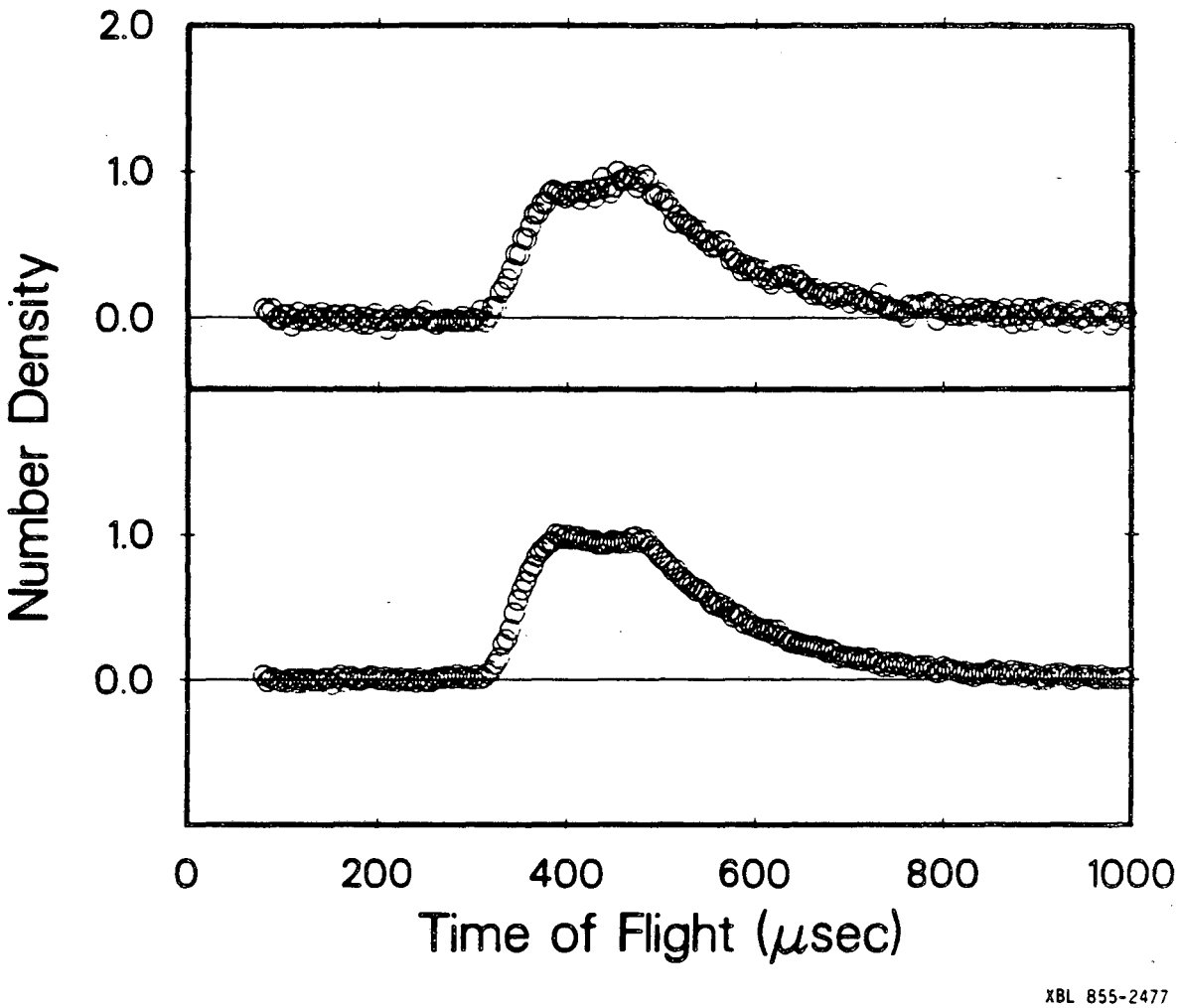

Fig. 8. Power Dependence of m/e=25 Time of Flight Spectrum: The lab angle is 20°. The upper trace is at 5 mJ/pulse and the lower trace is at 100 mJ/pulse.

acetylene at a laser power of 5 mJ/pulse, upper trace. This TOF spectrum is the result of primary process I only since at this power the m/e=25 and 24 TOF spectra are nearly identical. At 100 mJ/pulse, lower trace, substantial secondary photon absorption occurs. One can see that not only does the magnitude of the TOF spectrum increase, represented by the improved signal to noise, but the shape of the TOF spectrum changes as well. This is direct evidence for secondary photodissociation of the C_2H product. Moreover, it means that the absorption cross-section of the C_2H is strongly dependent on its internal energy. That is, C_2H formed with less translational energy and more internal energy, is depleted preferentially at the higher laser power.

C.4. Polarization Dependence of Process I.- By polarizing the laser light, it is possible to gain information on the lifetime of the excited state of acetylene. Because the transition dipole moment is anisotropic within the body fixed frame of the molecule, if the dissociation happens on a subpicosecond timescale, before the molecule has a chance to rotate, we would expect a strong polarization effect. The polarization effect should manifest itself as a substantial change in the shape of the m/e=25 TOF spectrum. This can be seen by consulting the newton diagram in fig. 2. At a fixed detector angle, say 20°, one can see that the center-of-mass recoil velocity vector of products appearing with small kinetic energy makes a much different angle with respect to the beam velocity vector than does the recoil

velocity vector of products appearing with a large amount of translational energy. Because in the case of prompt dissociation, the recoil direction is dependent upon the instantaneous orientation in space of the parent acetylene molecule, and because the orientation in space of the parent molecule has a substantial effect upon its probability to absorb a photon, if we were to polarize the laser light along the beam velocity direction, there would be a different absorption probability for the parent molecules that give rise to the low and high translational energy products.

On the other hand if the molecule rotates many times between excitation and dissociation, the recoil direction will have no relation to the initial orientation of the parent molecule in space. In this case no polarization effect will be observed in the experiment. β is the so-called anisotropy parameter which characterizes the center of mass frame angular distribution.[16] The limits of β, +2 and -1, describe $\cos^2$ and $\sin^2$ distributions around the polarization vector, respectively. β=0 indicates an isotropic angular distribution and a long excited state lifetime.

Experimentally, we can compare the shape of the TOF produced by light polarized along the recoil lab frame velocity vector with that produced by light polarized perpendicularly to this vector. Fig. 9a shows the fit to four TOF spectra using β=0 at two source-detector angles, 17° and 20°, and two polarization angles. The polarization angles are marked 'H' for along the lab recoil vector and 'V' for perpendicular to this vector. Fig.'s 9b and 9c show the resulting

Fig. 9a. Polarization Dependent Time of Flight Spectra: 'H' indicates polarization is along lab frame recoil vector and 'V' indicates that it is perpendicularly oriented. $\beta = 0.0$

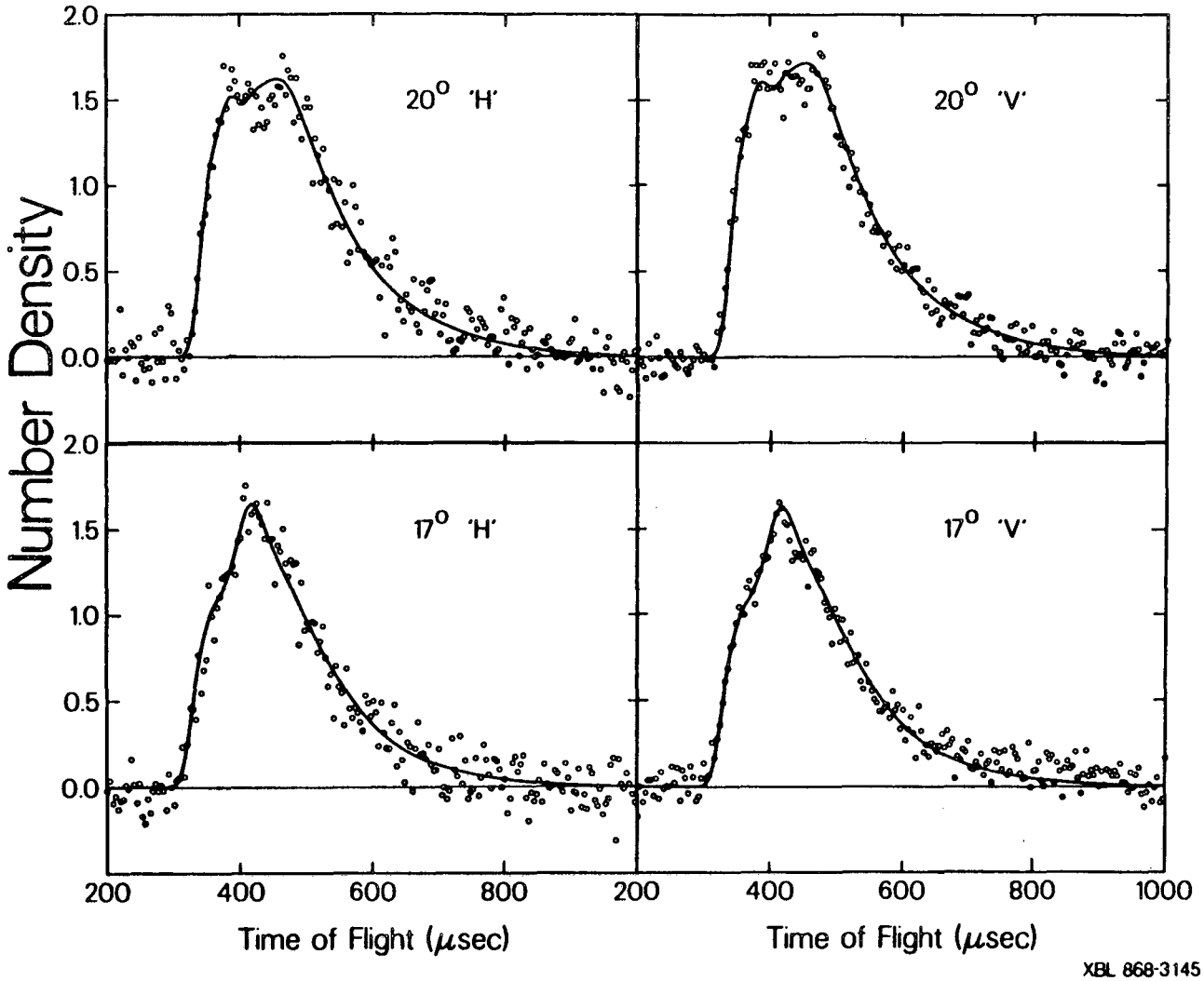
Number Density
2.0
1.5
1.0
0.5
0.0
20° 'H'
20° 'V'
17° 'H'
17° 'V'
200
400
600
800
1000
Time of Flight (μsec)
Time of Flight (μsec)

XBL 868-3145

Fig. 9b. Polarization Dependent Time of Flight Spectra: 'H' indicates polarization is along lab frame recoil vector and 'V' indicates that it is perpendicularly oriented. $\beta = 0.2$

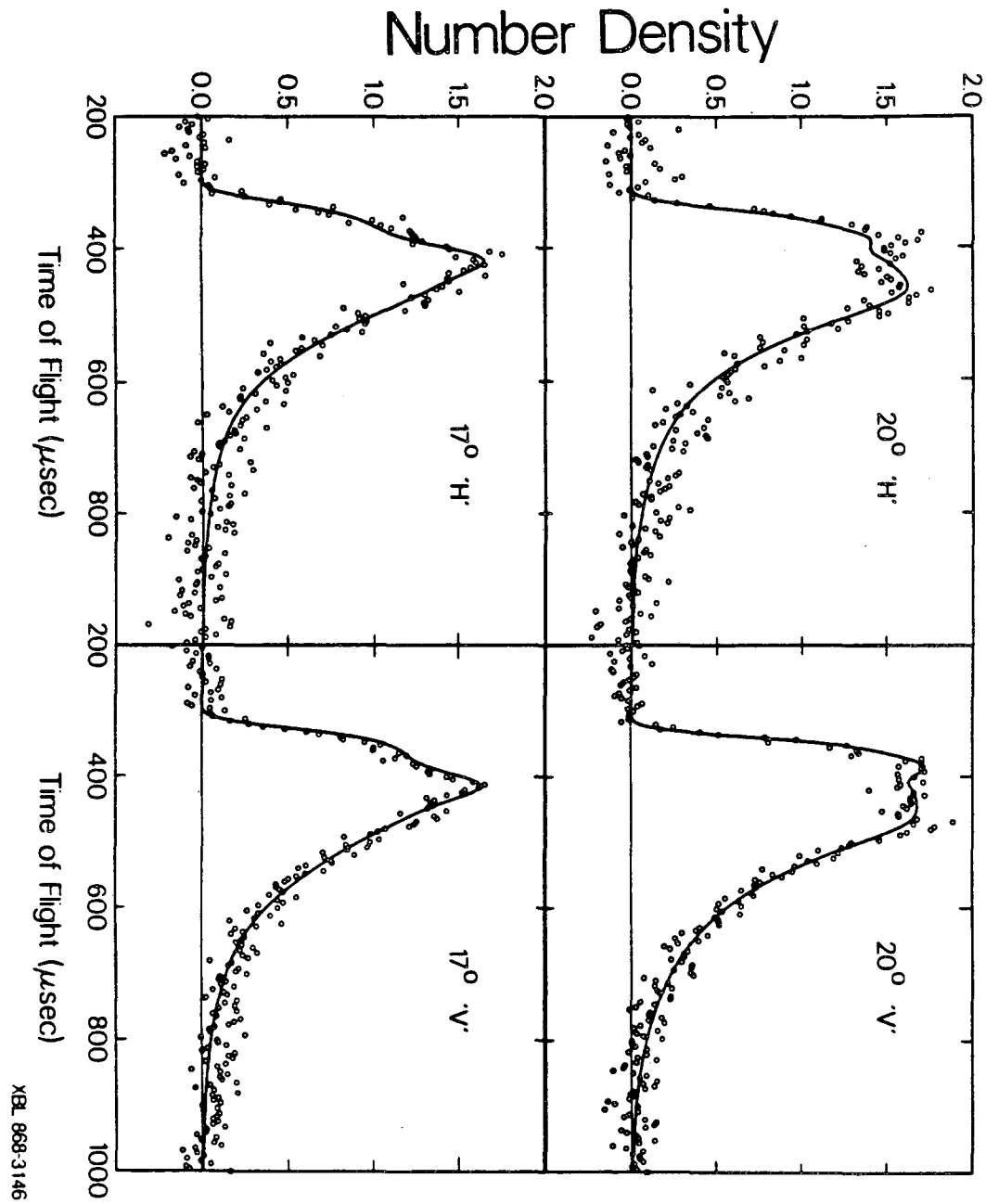
Number Density
0.0
0.5
1.0
1.5
2.0
200
400
600
800
1000
Time of Flight (μsec)
17° 'H'
20° 'H'
17° 'V'
20° 'V'

XBL 868-3146

Fig. 9c. Polarization Dependent Time of Flight Spectra: 'H' indicates polarization is along lab frame recoil vector and 'V' indicates that it is perpendicularly oriented. $\beta = -0.2$

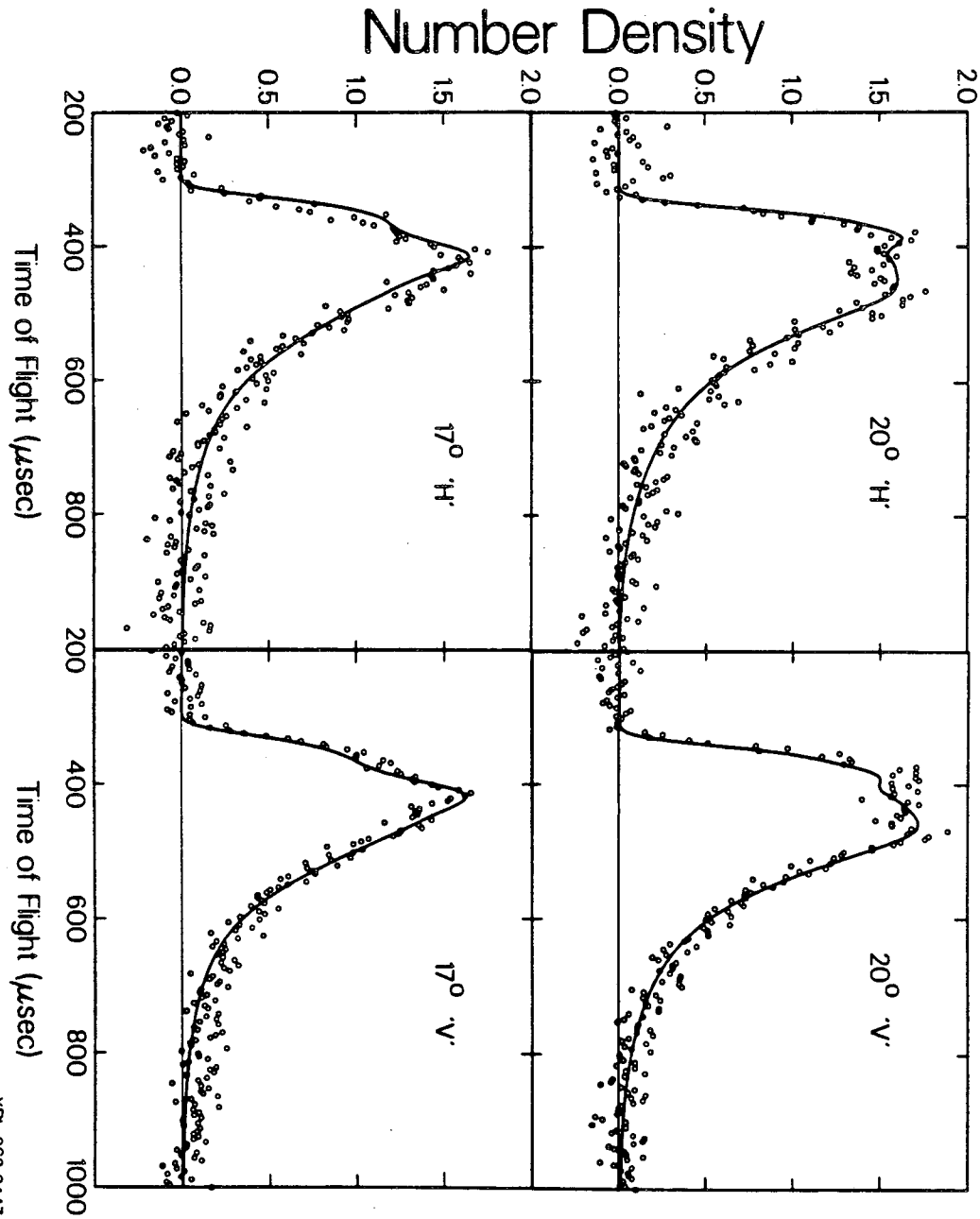
Number Density
0.0
0.5
1.0
1.5
2.0
200
400
600
800
1000
Time of Flight (μsec)
20° 'H'
17° 'H'
20° 'V'
17° 'V'

XBL 868-3147

fits for $\beta=\pm 0.2$. The experimental result with uncertainty is then $\beta = 0.0 \pm 0.1$.

D. Discussion.- D.1. Observed Collision Free Procceses.- The observation of laser induced m/e=25 signal at angles as large as 28°, and at lab velocities nearly twice that of the primary beam is conclusive evidence that C_2H radical is being photochemically produced in the collision free environment of a molecular beam. The amount of energy released as product translation is consistent with a single photon being absorbed. Although this is hardly a surprising finding, the presence of C_2H has always been inferred in past studies,[6,7,8] while this is the first direct observation of the nascent C_2H radical in the gas phase.

There are two conceivable explanations of our m/e=24 data. A sequential photodissociation described by processes I and II or a two photon absorption creating a very highly excited C_2H_2 and subsequent decay as shown in process III.

$$C_2H_2 \xrightarrow{2 \times 193 \text{ nm}} H + C_2 + H \qquad \text{(III)}$$

Consideration of the $P(E_T)$ for the two photon dissociation allows us to eliminate a simultaneous dissociation mechanism for process III. In a simultaneous three particle production process, conservation of linear momentum would require the two hydrogen atoms to be emitted in exactly the same direction in order to produce C_2 at as large a laboratory-frame velocity as we are observing. Even in a cis-bent

excited state it is difficult to imagine a concerted dissociation mechanism that would do this. If the two photon absorption of acetylene led to sequential loss of hydrogen atoms with time for the intermediate C_2H to rotate, it is possible that both hydrogen atoms could be emitted in the same direction. Similarly, the sequential mechanism involving proccesses I and II would have no problem conforming to this constraint.

While there is no way to prove that process III is unimportant, there is compelling evidence for the existence of process II in the power dependent TOF spectrum at m/e=25 shown in Fig. 8. If process III were dominant we would expect only the magnitude and not the shape of the TOF to change with power. If process II dominates it is not at all unlikely that certain internal states of the C_2H radical would have a higher absorption cross-section at 193.3 nm than others. This would give rise to a change in the shape of the m/e=25 TOF as a function of laser power, due to differential depletion of the C_2H radical, and that is exactly what has been observed in this experiment.

Further evidence in support of the importance of process II is the calculation of Shih et al..[17] The results of their ab-initio calculations on C_2H radical show that the two lowest doublet states above the $\tilde{A}^2\pi$ state are both in the vicinity of an ArF laser photon. Additionally, the calculations show that the only transitions with substantial oscillator strength are for $\tilde{A}^2\pi \rightarrow 3^2A'$ and distorted geometries of $\tilde{X}^2\Sigma \rightarrow 3^2A'$ and $2^2A''$. Any of these

transitions could account for the secondary absorption as will be seen below. This will be discussed further in section D.3..

We do not see any obvious evidence for the molecular elimination channel IV.

$$C_2H_2 \xrightarrow{193\ nm} C_2 + H_2 \qquad (IV)$$

The light H_2 products scatter in a much wider laboratory angular and velocity range than do the C_2 fragments. In addition, the smaller ionization cross section and shorter residence time in the ionizer for H_2 make it much harder to detect than heavier fragments such as C_2H and C_2. It is also very difficult to detect H_2 because of the very high m/e=2 background found in our mass spectrometer. We must, therefore, confine our search to C_2. Because of the small release of translational energy that is possible, 4 kcal/mol at most, we can look at m/e=24 at 20° and be assured that there is no contribution from process IV. If we then use the $P(E_T)$'s derived from the 20° data to fit the data at m/e=24 and 10°, where we would be able to see process IV if it were present, we can get an upper limit to the importance of this channel by adding in the contribution from process IV little by little until the data is no longer fit. Sensitivity to the observation of this channel depends upon the amount of translational energy released in process IV. If less translational energy is released, channel IV is easier to see. In estimating a conservative upper limit to the importance of this channel we have assumed the worst case, that all of the available 4 kcal/mole appears

as translation. This masks channel IV in the TOF spectrum so that it could appear very inconspicuously. Taking into consideration the relative ionization efficiences of C_2 and C_2H to give C_2^+, this leads to an upper limit for process IV of 15 percent of process I. This is a very conservative estimate, since if the translational energy release is less, say 2 kcal/mole, then the branching ratio would be less than 2 percent. It should be mentioned that if channel IV were to release less than 1 kcal/mol, we would not be able to detect the C_2 fragment, since there would not be enough kinetic energy for the fragment to get 10° away from the beam. Although this possibility seems highly unlikely, if it were true the importance of channel IV could be much greater.

The quantum yield for $C_2H_2 \rightarrow C_2 + H_2$ was estimated by Okabe[19] to be about 10 percent at 184.9 nm, however the quantum yield is expected to be much smaller at 193 nm, since the photon energy is much closer to ΔH of the reaction forming $C_2 + H_2$.

We also did not observe CH product which is presumably due to process V.

$$C_2H_2 \xrightarrow{2 \times 193 \text{ nm}} 2CH \qquad (V)$$

CH formation was a minor channel observed optically in ref. 7 and 8. McDonald et al. determined that V is less than 1 percent of the two-photon process that produces C_2. This would almost certainly be beyond our limit of detection. In summary, Table II lists the observed

Table II

Channel			Label	Observed
$C_2H_2(^1\Sigma_g^+)$	$\xrightarrow{193\ nm}$	$C_2H(^2\Sigma, ^2\pi) + H$	I	Yes
C_2H	$\xrightarrow{193\ nm}$	$C_2(^1\Sigma_g^+, ^3\pi_u) + H$	II	Yes
C_2H	$\xrightarrow{193\ nm}$	$C_2(^1\pi_u) + H$	II	Yes
$C_2H_2(^1\Sigma_g^+)$	$\xrightarrow{2 \times 193\ nm}$	$C_2 + H_2$		No
$C_2H_2(^1\Sigma_g^+)$	$\xrightarrow{193\ nm}$	$C_2 + H_2$	IV	< .15 of I

Table II: Possible Collision-free Dissociation Pathways in the Photolysis of Acetylene

channels in this work as well as some channels that have been postulated, but not observed in this experiment.

D.2. The Assignment of the $P(E_T)$ of Process I.- Because of the conservation of total energy, in an experiment with infinite resolving power the $P(E_T)$ would appear as a series of discrete peaks, one corresponding to each internal quantum state of the C_2H radical since only the $^2S_{1/2}$ state of H atom can be populated at these energies. Since acetylene is rotationally cold in the beam, the rotational excitation of C_2H comes only from the photon-induced repulsive bond rupture in which the orbital angular momentum of the departing fragments will be cancelled exactly by the rotational excitation of the triatom. The magnitude of this pair of antiparallel angular momenta is substantially limited by the small mass of the departing hydrogen atom, the small available energy and the impact parameter of the half-collision. Because of the resulting small rotational excitation, information on the vibrational and electronic structure of ethynyl is obtainable from the $P(E_T)$, although it is not practical to resolve rotational structure in velocity measurements. Moreover, because the experiment is performed under collision free conditions, the translational energy distribution is indicative of the nascent population distribution of C_2H and can lead to very detailed conclusions regarding the dynamics of the dissociation.

Ideally one would like to know all of the spectroscopic data on C_2H beforehand and attempt to derive this dynamical information from the $P(E_T)$. But despite its apparent simplicity, the determination of unambiguous spectroscopic information concerning the ethynyl radical has been very slow in coming. The ESR spectrum[20] yielded hyperfine splitting data which was used to assign the telescopically detected, interstellar emission at 87.3 GHz[21] to the N=1→0 transition. Since then, emission from other rotational states of interstellar ethynyl has been observed by a number of groups[22,23] and millimeter wave absorption spectra have been taken in the laboratory.[24-27] A very accurate rotational constant is now known for the dominant isotopic species.[28] It has only been in the last year that the millimeter wave spectrum for C_2D has been measured[29], allowing the derivation of the molecular geometry with high precision.[30]

Many infrared transitions have been measured by Jacox in rare gas matrices known to contain C_2H.[31] By very careful analysis of isotopic substitution data, the ν_1, C-H and ν_3, C-C harmonic stretching frequencies were surmised to be 3612 and 1848 cm^{-1}, respectively. A substantial effort was made to search for the ν_2 bend with no success. This lead to the supposition that ν_2 was below 400 cm^{-1}, the experimental limit of the infrared spectrometer. The ν_3 transition has very recently been confirmed by transient absorption diode laser spectroscopy.[32] In addition, the combination $\nu_2+\nu_3$ transition was observed in this work and has

shown indeed that the bend has a harmonic frequency very near to 250 cm^{-1}.[32]

Color center laser spectroscopy with magnetic rotation signal enhancement has been used to observe the 3612 cm^{-1} transition[33] as well as five others in this spectral region[34] in the gas phase with very high resolution. It is clear from this work that the observed $\sigma \rightarrow \pi$ transition at 3612 cm^{-1} is not the C-H stretch which would have a $\sigma \rightarrow \sigma$ symmetry.[33] All of the six transitions in the color center laser spectrum have been assigned as excitations of high vibrational levels of the ground electronic state whose transition moments are dramatically enhanced due to coupling with an excited electronic π state. Ab-initio calculations do confirm the presence of a very low lying excited electronic state anywhere from 2000[35] to 4000[17,18] cm^{-1} above the ground state. Unfortunately, due to the lack of knowledge concerning the precise value of the electronic origin, the fundamental vibrational frequencies in the ground and in the excited electronic states, and the effect of Renner-Teller coupling in the doubly degenerate excited electronic state, an unambigous assignment of these vibronic transitions is very difficult.

In addition, it was found that there is a strict curve crossing between the $^2\Sigma$ and $^2\pi$ states at extended C-C distances for exact linear geometries.[18] Any small deviation from linearity would induce a strong avoided crossing between the $1^2A'$ (formerly linear $^2\Sigma$) and the $2^2A'$ (formerly one of the doubly degenerate linear $^2\pi$ states). This would indeed imply that it is possible for high

vibrational states of the ground electronic state to be substantially mixed with the excited π state, especially for combination states involving C-C stretch and H-C-C bend since this motion will bring the system close to the avoided crossing.

The extremely low CCH bending force constant can be understood clearly from the ab-initio calculations of the bending potentials of the lowest three electronic states in ref. 17. If one constrains the nuclei to lie on a line, the lowest two states are $^2\Sigma$ and $^2\pi$ as has already been mentioned. Away from linearity the only symmetry operation is reflection across the molecular plane and when the molecule is allowed to bend, the ground state becomes $1^2A'$ while the doubly degenerate π state splits into the $2^2A'$ and $1^2A''$ states. The two A' states interact and repel one another. This pushes the $\tilde{X}$ state bending force constant down and one of the π state bending force constants up. In addition to producing a very low ground state bending force constant, this means that in the excited electronic state there is a larger restoring force when the H atom bends toward the half filled π orbital than when it bends perpendicularly to it. This will be discussed below in the context of the Renner-Teller effect.

Several critical structural quantities of C_2H are still open to question; for instance, the question of the C-H stretch in the $\tilde{X}$ state. Since the original assignment of 3612 cm^{-1} cannot be correct, it appears that there are no experimental observations of this state. Ab-initio calculations by Fogarasi et. al.[35] predict

ν_1=3350 cm^{-1}. However, despite the fact that this is a large basis set CI calculation, the use of only a single reference electronic configuration may be inauspicious when there is such a low-lying excited electronic state. Specifically, the calculated C-C bond length in ref. 35 is too short by .011 Å and the C-C stretching frequency is too high by 170 cm^{-1}. This is probably reflective of an under-representation of the low lying excited state in the basis set which has a bond order of 2.5 compared to the ground state bond order of 3. A longer C-C bond would also likely bring their ν_3 down, in line with ref.'s 31 and 32. Very recent multireference configuration CI calculations by Kraemer et. al. give a C-C bond length only 0.001 Å too short and a ν_3 frequency only 30 cm^{-1} to high.[36] The calculation of ν_1 by this method, which would appear more trustworthy, gives a value of 3497 cm^{-1}.

Another important open question is the value of the pure electronic excitation energy, T_{oo}. Because of the need to very accurately account for small correlation energy differences between the two states, this value is very difficult to obtain from ab-initio calculations. Curl et. al. observed a transition of $\pi \rightarrow \sigma$ symmetry which could clearly be assigned to an electronic excitation from ν_2=1, hence π symmetry for the lower state, to an odd quanta of ν_2 in the excited electronic state. Under the assumption that this was the (010)-→(010) transition, an estimation of T_{oo} was made.[34] Unfortunately, this assumption is impossible to verify. In fact, because of the probable large change in bending force constant upon

electronic excitaion, (010)-→(030) might be expected to possess a large transition moment.

Moreover, in order to obtain a quantitative value for T_{oo}, it is necessary to know the vibrational frequencies of the excited potential surface. These values have been calculated in ref. 36; however, the situation is further complicated by the presence of strong Renner-Teller mixing of the two bending potential surfaces which exist away from linearity. The Renner-Teller effect can shift the decoupled states by as much as 200 cm^{-1} or more.[37] Until this is sorted out, even an unambiguous assignment of the "pure electronic" transition observed in ref. 34 is quite difficult.

Because the $^2\pi$ state is so low in energy and clearly energetically accessible under our conditions where up to 5600 cm^{-1} of energy is available, in order to interpret the product translational energy distribution we must first decide which electronic states of C_2H are likely to be formed in the photolysis at 193.3 nm. To understand this, one would like to see the electronic state correlation diagram for process I. The calculation of the PES's that are involved in the dissociation has not, as yet, been done. However, Vazquez has calculated the eight lowest surfaces for bent geometries of HCN[38], which is isoelectronic with C_2H_2. Fig. 1 of their paper serves as a guide to what the surfaces for acetylene would look like. Our fig. 10 is a schematic representation of the corresponding curves for excited C_2H_2 based on the calculations of Vazquez.

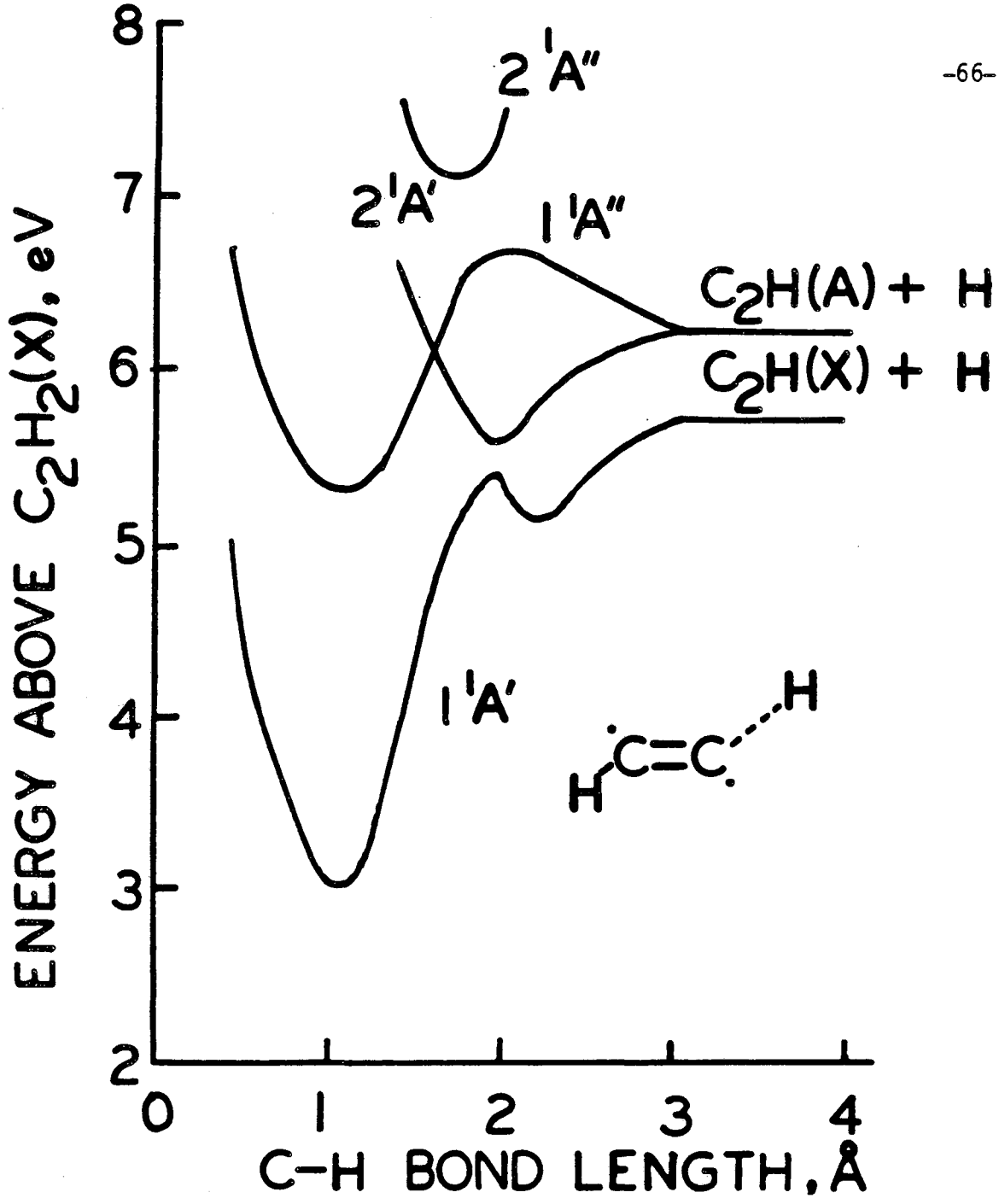

XBL 855-2478

Fig. 10. A Schematic Representation of the PES's for Acetylene Dissociation Based on the Calculations of Vasquez.

There are, undoubtedly, many differences between HCN and C_2H_2. For instance, the $1^1A"$ origin should be lower than the bond dissociation energy for acetylene. So, we expect that the avoided crossing between $1^1A"$ and $2^1A"$ will be lower in energy and occur at a longer C-H bond length than in HCN. Another difference occurs between CN and C_2H. In CN the $B^2\Sigma$ state is only 3.2 eV above the $X^2\Sigma$ state, while in C_2H the $B^2\Sigma$state is calculated to be 7.3 eV higher than $X^2\Sigma$.[17] For this reason, we don't expect that the surface that is analogous to the $3^1A'$ surface in fig. 1 of ref. 38 will influence the dynamics of acetylene at the energies found in our experiment.

Despite these differences, we do expect the qualitative features of Vazquez' fig. 1 to apply in the case of acetylene. In particular, the avoided crossing between the $1^1A"$ and the $2^1A"$ curves should be present. In our experiment we pump C_2H_2 to the $1^1A"$ curve of fig. 10. This state is di-radical like, with a C-C bond order of two and it is trans-bent.[3] It resembles ethylene with two diagonally opposed H's removed. The avoided crossing is the quantum mechanical representation of the rearrangement of the electronic configuration that is necessary in going from this di-radical structure with a C-C double bond to the electronic structure of C_2H ($\tilde{A}^2\pi$) where the bond order is 2.5 and there is only one free radical electron.

The avoided crossing between $\tilde{X}^1A'$ and $2^1A'$ shown in fig. 10 occurs only for significantly bent geometries. However, these are the molecular configurations that we are specifically interested in since

the initially pumped molecule has a trans-bent equilibrium structure. $X^2\Sigma$ C_2H has all π orbitals filled and a half filled σ_{pz} orbital. Thinking of the dissociation in reverse, for bent geometries the incoming H at first feels an attraction due to the σ_{pz} electron but upon deeper penetration is repelled due to its interaction with the closed π orbitals. In contrast, $^2\pi$ C_2H has a filled σ_{pz} orbital and a half filled π orbital (as well as a degenerate filled π orbital). For bent geometries the incoming H atom breaks the degeneracy of the π orbitals. There is a stong attraction to the half filled π orbital, A' symmetry, while there is a strong repulsion toward the filled π orbital, A" symmetry. It is likely that this avoided crossing occurs even more easily in C_2H since the separation of the $\tilde{X}$ and $\tilde{A}$ states is much smaller in C_2H than in CN.

Using fig. 10 as a guide we see that after acetylene is initially pumped to the $1^1A"$ it's total energy, which is 6.4 eV, will be close to and may well be less than the barrier height in the exit channel of this surface. Since the vibrational energy initially deposited in the molecule is mainly in the bending degree-of-freedom,[3] even if the photon energy is slightly above the barrier height, the barrier will act as a bottleneck to $C_2H(\tilde{A}^2\pi)$ formation. We expect that the barrier will at least slow down the production of C_2H $(\tilde{A}^2\pi)$ enough that vibronic coupling from $1^1A"$ to $2^1A'$ will become a competing dissociation pathway. This is consistent with the isotropic angular distribution observed with polarized light which implies that the lifetime of the excited molecule is at least 3 psec.[39] The fact

that the trajectory for dissociation would strongly sample the repulsive part of the $2^1A'$ surface, shown in fig. 10, and the consequent large departing H atom velocity could make the curve hopping to the $\tilde{X}^1A'$ surface very efficient. This argument is directly analogous to the explanation of ground state CN formation in the UV photodissociation of HCN.[38] In summary, on the basis of theoretical considerations alone, it is quite reasonable that both electronic states of the ethynyl radical should be formed. However, The possibility of forming π state C_2H depends critically upon the exact height of the barrier at ~6.4 eV.

We do not believe that vibronic coupling to the $\tilde{X}^1A'$ state is an important dissociation pathway. When formaldehyde was pumped 1 eV above its S_1 origin, it was found that vibronic coupling to S_o and subsequent C-H bond rupture was the dominant process[40]. However, because dissociation on the S_o PES involves a smooth and continuous rearrangement of the bonding electrons in formaldehyde to non-bonding, free-radical electrons in HCO and H, there is no barrier to dissociation. It is for this reason that simple bond rupture reactions that occur along the ground electronic surface so often lead to $P(E_T)$'s that peak near zero kinetic energy release as was indeed observed in the formaldehyde experiment. Since in sharp contrast to formaldehyde, acetylene photodissociation releases a large amount of translational energy and more importantly the $P(E_T)$ peaks substantially away from zero, implying a repulsive interaction between

the departing fragments, it is not likely that the ground electronic state plays a role in the photodissociation of acetylene.

It is important to note next the expected vibrational excitation in the photodissociation event. From the spectroscopic data we do have available to us, it is possible to trace the molecular geometry through the photodissociation. Before photon absorption the C-H bond length is that of ground state acetylene, 1.0585 Å.[41] From the UV absorption spectrum[3] we know that immediately after photon absorption, the C-H bond length is ~1.08 Å. Finally, from ref.'s 27-30, we know that the C-H bond length in C_2H is 1.0464 Å. From a typical C-H stretching force constant of 5.9 mdyne/Å, it can easily be calculated that zero point fluctuations are on the order of .07 Å. Therefore it is clear that the photodissociation represents a perturbation to the C-H stretch on the order of the zero point energy or smaller and we conclude that the C-H stretch will not be substantially excited. Actually, the energy required to displace H .02 Å from its equilibrium position is only about 50 cm^{-1}.

A similar view of the C-C bond can be explored. Here the ground state acetylene value of 1.2047 Å[41] becomes 1.383 Å[3] upon excitation. This must again relax to 1.2165 Å.[27-30] These motions which are on the order of tenth's of Å's as opposed to hundreth's of Å occur for a bond with approximately three times higher force constant than that of the C-H bond. For harmonic displacement of the C-C bond 0.2 Å from its equilibrium geometry, an energy on the order of 11,000 cm^{-1} is required. Although the actual potential

energy for this great a displacement must be smaller due to anharmonicity, it is easy to conclude that the C-C stretch should be a major player in the product energy distribution.

Similarly, The CCH bend should be very excited. Here the molecule goes from linear acetylene to the trans-bent excited state and back to the linear C_2H radical. The excited state acetylene has a bending angle of 120.2°[3] and considering the length of the C-H bond this is an overall motion of about one full Å. Of course the bending force constant in C_2H is quite small, nevertheless it requires about 2500 cm^{-1} to displace the $\tilde{X}$ state bend by one Å.

Since the bending force constant in the $\tilde{A}$ state is expected to be substantially stiffer than in the $\tilde{X}$ state, it is fair to say that the bend should be even more excited in the upper electronic state if it is formed.

With the following discussion in mind, the most reasonable assignment of the $P(E_T)$ in fig. 4 is as follows. Peak 1 is the vibrationless ground state of C_2H and peak 2 corresponds primarily to excitation of one quantum of C-C stretch. The energy separation from the rising edge of peak 1, 16.25 kcal/mol, to the rising edge of peak 2, 11 kcal/mol, is within 100 cm^{-1} of the known ν_3 energy. We then assign peak 3 to the onset of the excited electronic state and the peaks 3, 4 and 5 to v=0,1 and 2 of the π state bend. Because the $\tilde{X}$ state ν_2 is so low, 250 cm^{-1}, we would not expect to be able to resolve it though it may well be highly excited.

Since there should be no dynamical constraint, preventing C_2H from being formed in its vibrationless π state, if the assignment is correct, the implication is that the electronic excitation energy, T_{oo}, is 3000 ± 200 cm^{-1}. In fact, one of the transitions observed in Jacox's work reported at 2942 cm^{-1} may correspond to the pure 0←0 transition.[31] They were unable to assign this peak to a vibrational fundamental of C_2H but could determine that it was due to a reactive species.

It is not absolutely necessary to invoke formation of the excited electronic state in the photodissociation of acetylene in order to assign the $P(E_T)$, see below. Consequently, this last conclusion regarding T_{oo} should be taken with a full understanding of the assumption used to arrive at it.

The assignment of peaks 3, 4 and 5 as v = 0, 1 and 2 of $^2\pi$ C_2H must be appreciated within the context of the Renner-Teller effect.[42] As already mentioned, bending motion parallel and perpendicular to the free radical orbital is subject to two different Born-Oppenheimer surfaces. Because of the differing angular velocities about the C-C internuclear axis of the free electron and the H atom, at any instant the H atom may be moving parallel or perpendicular to the free-radical orbital or somewhere in between and to a first approximation the bending motion acts under the influence of an average potential energy surface. Renner-Teller spectra are reported as two numerical parameters, $\bar{\omega}$ and ϵ, neglecting spin-orbit interactions. $n\bar{\omega}$ is the harmonic energy progression of the average of

the two Born-Oppenheimer surfaces. The true vibronic states are clustered about each of these energy levels. ϵ can be used to calculate the precise energies for the actual vibronic states. Since it is unlikely that we would be able to resolve the splitting represented by the ϵ parameter, the observed 550 ± 100 cm^{-1} energy separation is best interpreted as the approximate value of $\bar{\omega}$.

It should be stated in no uncertain terms that this is not the only possible explanation of the observed translational energy distribution. A very interesting alternative supposes that the barrier to formation of $^2\pi$ C_2H in fig. 10 is high enough to essentially prevent formation of the excited state. Because it is expected that to a very good approximation, the fragmentation of excited state acetylene occurs in a plane, dynamically it is very improbable to produce C_2H with angular momentum about the C-C internuclear axis. This is especially true for the slower part of the translatioal energy distribution. Because of the cylindrical symmetry of the bending vibrational motion, only the even quanta of bending vibration can occur with vibrational angular momentum about the C-C axis equal to zero. Therefore, it is quite possible that only even quanta of ν_2 could be excited in the photodissociation process. Since the harmonic frequency has been found to be 250 cm^{-1} and a negative anharmonicity is expected,[36] an energy separation of 550 cm^{-1} is entirely consistent with this explanation. The disappearance of the progression at larger translational energy could be explained by the increase of product rotation at higher H atom

recoil velocities or by the inherently poorer experimental resolution at larger observed lab velocities.

Accurate ab-initio calculations of the barrier height to formation of $^2\pi$ C_2H would be very useful in resolving this interesting question. If it were to be found on the basis of theory that excited state C_2H could not be formed at photon energies of 6.4 eV, the dynamically preferential creation of even quanta of bending excitation would gain credibility.

D.3. The Translational Energy Distribution for Process II.- In order to understand the observation that internally excited C_2H absorbs a photon much more readily than does the ground state radical it is necessary to consult theory. According to ab initio calculations, there are two electronically excited states of C_2H in the energy range of a 6.4 eV photon that are of doublet spin multiplicity.[17] Their labels are $3^2A'$ and $2^2A''$ and are both considerably bent. These are the lowest two doublet states above $\tilde{A}^2\pi$. There is no optical absorption for C_2H at 193 nm in a rare gas matrix;[20] however, the calculations of ref.'s 17 and 18 show that there is strong oscillator strength between the $\tilde{A}^2\pi$ and the $3^2A'$ state. The vertical excitation energy that is calculated at the C-C bond length of the ground electronic state is 6.8 eV.[18] However, this result was shown to be very sensitive to the C-C bond length.[17] If the bond is stretched by 0.2 Å, the vertical excitation energy is lowered to 4.9 eV.[17] Since the $\tilde{A}^2\pi$ state is expected to have

about a 0.1 Å longer C-C bond than the $\tilde{X}$ state, it is clear that its vertical excitation energy to $3^2A'$ will be accessible with the 6.4 eV photon of the ArF laser.

Another possible explanation of the secondary absorption is that it is due to vibrationally excited ground state radical, since if $3600cm^{-1}$ of energy is put into the C-C stretch, displacements of 0.1 Å are also possible.

The $2^2A''$ may also play a role in the secondary absorption. While it is located even higher in energy than the $3^2A'$ at the equilibrium geometry of $\tilde{X}$ state C_2H, upon C-C stretching and bending it comes well down in energy and within reach of the ArF laser. Whatever the explanation, theory substantiates that at a photon energy of 6.4 eV, ground state C_2H will not absorb while internally excited C_2H can have a substantial absorption probability. This is precisely what we have observed in the power dependence experiment. See section C.3. and D.1..

In the $P(E_T)$ shown in Fig. 7, it is easy to see a sharp peak at around 10 kcal/mole which we attribute to $^1\pi_u$ of C_2. This sharp peak has underlying it a broad feature originating from one or both of two low lying electronic states of C_2 ($^1\Sigma_g$ or $^3\pi_u$ or both). This is consistent with fluorescence emission work,[7,8] where the C_2 $^1\pi_u$ state has been observed.

It is a tantalizing feature of this experiment that the dynamics of dissociation appear to channel so much of the available energy into translation for formation of electronically excited C_2 whereas the

ground electronic state appears to be very vibrationally hot. The emmision studies agree that the vibrational population distibution in the $^1\pi_u$ state is peaking at or near v=0. Unfortunately, no information on the ground state population distribution is possible by this method. Under high resolution conditions using a well prepared beam of C_2H radicals, very interesting information might be obtained using the photofragmentation translation method. It would almost certainly be possible to resolve each vibrational state of the C_2 product. Unfortunately under the present conditions, i.e. peering through a very dirty window at something quite interesting, little can be learned. One might postulate however that the ground state C_2 is formed only after internal conversion of C_2H to the ground state, while the $^1\pi_u$ state is predissociated by a directly repulsive state.

D.4. The C-H Bond Energy in Acetylene.- In previous experiments, the C-H bond energy was determined indirectly by measuring the dissociative ionization threshold for acetylene and the IP for the C_2H radical, processes VI and VII respectively.

$$C_2H_2 \longrightarrow C_2H^+ + H + e^- \qquad E_{VI} \qquad \text{(VI)}$$

$$C_2H \longrightarrow C_2H^+ + e^- \qquad E_{VII} \qquad \text{(VII)}$$

DWM measured E_{VI} very carefully, looking at the temperature dependence of hotbands near threshold to get a value of 17.37 ± 0.01 eV.[10] Recently, ON have disputed this value on the basis of a

very sensitive molecular beam photoionization threshold measurement. ON claim the threshold to be 16.79 ± 0.03 eV.[11]

The IP of C_2H was measured directly by Wyatt and Stafford[43] (WS) using electron impact threshold ionization and they obtain a value of 11.6 ± 0.5 eV. In two much more precise experiments, Okabe and Dibeler[12] (OD) and Miller and Berkowitz[13] (MB) have obtained 11.96 ± 0.05 eV and 11.51 ± 0.05 eV respectively. Their experiments are conceptually shown in Fig. 11 and 12 where the numbers with asterisks are the measured values and the underlined values are well known. Table III shows all possible values of the C-H bond energy obtained by combining in all possible ways the various experiments.

In addition to these determinations, Janousek et. al.[14] have come up with a value for $D_0(C_2H\text{-}H)$ of 132±5 kcal/mol by combining processes VIII, IX and X in a thermochemical cycle.

$$C_2H^- \longrightarrow C_2H + e^- \qquad \text{(VIII)}$$

$$C_2H_2 \longrightarrow C_2H^- + H^+ \qquad \text{(IX)}$$

$$H^+ + e^- \longrightarrow H \qquad \text{(X)}$$

This result is in good agreement with the present work although the uncertainty is still fairly large.

Very recently, the photoionization threshold for proton formation from acetylene was measured using synchrotron radiation. Because of the well known IP for H, the bond energy was obtained in a very direct manner. This approach is qualitatively simpler than the other

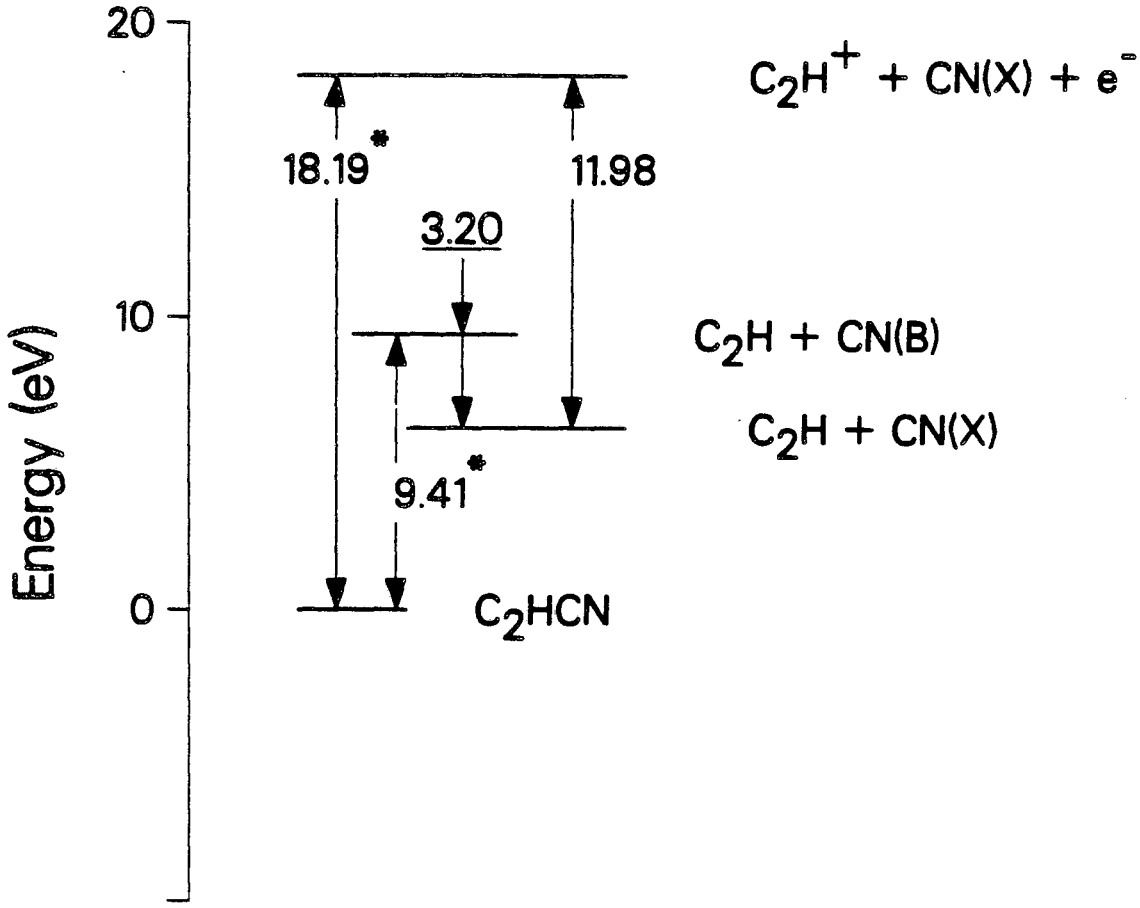

XBL 855-2479

Fig. 11. Energy Diagram for C_2H Ionization Potential Determination of Okabe and Dibeler (Ref. 12): The numbers with asterisks are the measured thresholds and the underlined numbers are well known. The numbers with no symbols is the derived IP.

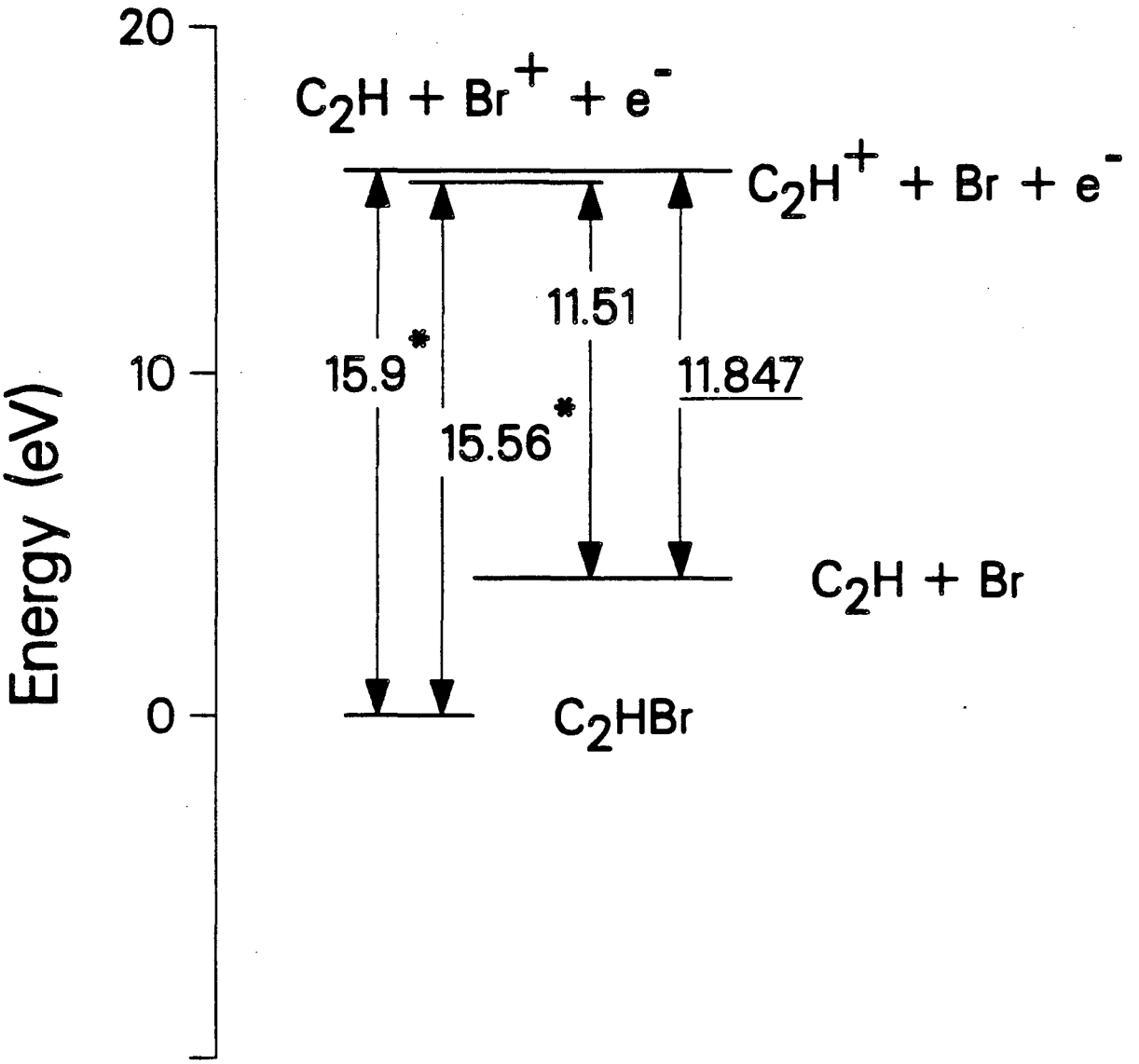

Fig. 12. C_2H Ionization Potential Determination of Miller and Berkowitz (Ref. 13): See fig. 11 for explanation.

XBL 855-2480

Table III

Combination	C-H Bond Energy
DWM a WS	133 kcal/mole ± 12 kcal/mole
DWM a MB	135 kcal/mole ± 1.4 kcal/mole
DWM a OD	125 kcal/mole ± 1.4 kcal/mole
ON a WS	116 kcal/mole ± 1.2 kcal/mole
ON a MB	118 kcal/mole ± 1.8 kcal/mole
ON a OD	107 kcal/mole ± 1.8 kcal/mole
This work	132 kcal/mole ± 2 kcal/mole

Table III: Combinatorial Possibilities of Acetylene's C-H Bond Energy.

photoionization experiments described above and gave 132.6 ± 1 kcal/mol in very good agreement with this work.[44]

Very accurate calculations have also been performed by Melius et al..[45] These have given a value of 127 kcal/mole for the bond energy. Single reference configuration calculations of this type suffer from spin contamination due to the many low lying quartet states in C_2H. Therefore, the error in this calculation is higher than in other molecules. In the isoelectronic case of HCN, which also has the spin contamination problem, the calculated value was slightly lower than the experimental value. This leads us to believe that 127 kcal/mol is a lower limit to $D_0(C_2H-H)$.

The experiment of Abramson et. al. should also be mentioned. They performed laser induced fluoresence experiments on the excited A state of acetylene in the 220 nm region, very close to the bond dissociation energy.[46] It was observed that the fluoresence quantum yield was still about 1 even at a total excitation energy of 129.5 kcal/mol. They also observed quantum-beat oscillations in the time resolved fluoresence. The frequency of the quantum beats implied a density of states so high that it could only be reconciled by postulating that S_0 is coupled to S_1, through a trans-bent triplet state. Stimulated emmision pumping on acetylene has shown that even at much lower total energies the motion is essentially completely ergodic.[47] Therefore if it were really true that the bond energy was lower than the excitation energy in the quantum beat experiment, one would expect that when the molecules reached the S_0 surface,

dissociation would occur on a time scale much faster than the recurrence time of the observed oscillations. However, if the dissociation energy were really to be as high as 132 kcal/mol, the presence of discrete energy levels in S_0 would not be at all surprising. The implication is that the energy at which quantum beats are observed is a lower limit to the dissociation energy. The disappearance of these quantum beats at higher excitation energies may in time provide the most precise experimental method for the determination of the C-H bond energy in acetylene.

Considering again table III, our work substantiates the values reported by DWM and MB. All the values calculated using the results of ON are far too low by about the electron affinity of H, 0.75 eV. This suggests that ON may be looking at the threshold for the ion pair production channel. We could understand OD's value for the IP of C_2H being too high if there were to be a barrier to the dissociative ionization of C_2HCN. This, in fact is not at all unreasonable. If one ionizes C_2HCN, one of the π electrons from the C-C bond will be ejected. If this ion were to homolytically cleave the C-N bond an electronically excited state of C_2H^+ would be formed where there are two free radical electrons, one π and one σ. The ground state of C_2H^+ has a closed shell electronic configuration. Even if it were possible to form the ground electronic state of the ion near threshold, it would be necessary to cross to another electronic PES. This could very easily give rise to a dissociation barrier. A barrier

would give OD a value for the IP of C_2H which is somewhat too high and consequently a $D_o(C_2H-H)$ which is too low.

As mentioned previously, our $D_o(C_2H-H)$ determination rests upon the assumption that it is possible for all available energy to appear as translation in some of the products, in other words, some of the products should be in the ground state. Even though we have surmised that the bending vibration is highly excited, it is not likely that it would be so highly inverted that no ground state is formed. This is due to the high amplitude motion possible in a CCH bend. For instance, in the C_2H even the energy present as total molecular zero point energy is sufficient to allow bending excursions as large as 60°.

It is possible, although unlikely, that peak 2 of fig. 8 is misassigned as v=1 of the C-C stretch and should be assigned to v=2. However, this assignment would pedict a very odd product vibrational distribution indeed. From fig. 4, one can see that the trend going from high CC stretching excitation to low excitation is going down rather gradually, and a sudden drop-off at low vibrational states would seem highly unreasonable.

Another reason that favors the possibility of ground state product formation is the light mass of the H atom. The H atom cannot impart a large impulse to the partner C_2H fragment and hence, it cannot act to excite it vibrationally with any degree of efficiency. Additionally, the large release of translational energy peaking well away from zero is indicative of a repulsive fragment interaction as

discussed in sec. D.2.. This type of interaction is particularly efficient at channeling available energy into translation.

Putting aside assumptions of any kind, our result of 132 ± 2 kcal/mol for the bond energy in acetylene is a rigorous upper limit. Because the result of ref. 45, 129.5 kcal/mol, is a lower limit, the ground state fragment assumption is justified empirically.

Because of all of the following arguments and the excellent signal/noise of our data, we conclude that 16.25 ± 2 kcal/mole is an accurate determination of the maximum release in translational energy and hence, the bond energy in acetylene is 132 ± 2 kcal/mole. For a more general disscusion of the validity of the ground state fragment assumption, see chapter IV.

E. Conclusions.- We have measured the translational energy distribution for acetylene photodissociation at 193.3 nm. The collision free processes are indicated by equations I and II.

$$C_2H_2 \xrightarrow{193\ nm} C_2H + H \qquad (I)$$

$$C_2H \xrightarrow{193\ nm} C_2 + H \qquad (II)$$

Process II is important even at fluences as low as 10^{26} photons/cm^2 s. The translational energy distribution for I shows up to 16.25 kcal/mole energy release implying a $D_o(C_2H\text{-}H)$ of 132 ± 2 kcal/mole. This is the most direct measurement of this quantity to date and there is a growing quantity of data to support this value.

The internal structure of C_2H is partially resolved in the translational energy distribution. It is clear that the C-C stretch and the CCH bend are highly excited in the photolysis; however, an unambiguous interpretation of the observed features will require further theoretical and experimental effort. There appear to be two quite reasonable possibilities. One proposes that both electronic states of C_2H can be formed in roughly equal amounts by the photolysis. Peaks 3, 4, and 5 of fig. 4 are then assigned to v=0, 1 and 2 of the excited π state bending vibration. This assignment implies that the adiabatic excitation energy is ~3000 ± 200 cm^{-1} while the π electronic state bending fundamental, $\bar{\omega}$, is in the neighborhood of 550 cm^{-1}. Dynamically preferential population of even bending quanta of the ground electronic state of C_2H due to conservation of angular momentum about the C-C internuclear axis during the photodissociation could also explain the observed data. If this explantion were to be true, it is unlikely that $^2\pi$ C_2H would be formed in the photolysis of acetylene. Accurate theoretical calculations of the barrier to excited state C_2H formation would be very useful in resolving this question.

The translational energy distribution for II is consistent with fluorescence work showing population of $C_2(^1\pi_u, {}^1\Sigma_g, {}^3\pi_u)$. The first information on the product internal energy distribution for the lowest two electronic states of C_2 shows that these states are much more vibrationally excited than is C_2 $^1\pi_u$, observed in dispersed fluoresence.

REFERENCES

1. J.G. Calvert, J.N. Pitts, Photochemistry, John Wiley and Sons, 1966, pp 493-497

2. R. Brurnham, N. Djeu, Appl. Phys. Lett., 29, 707 (1976)

3. C. K. Ingold, G. W. King, J. Chem. Soc. 2702 (1953).

4. K. Keith Innes, J. Chem. Phys. 22, 863 (1954).

5. S. Trajmar, J. K. Rice, P. S. P. Wei, A. Kuppermann, Chem. Phys. Lett. 1, 703 (1968).

6. M. P. Irion, K. L. Kompa, Appl. Phys. B27, 183 (1982).

7. J. R. McDonald, A. P. Baranovski, V. M. Donnelly, Chem. Phys. 33, 161 (1978).

8. H. Okabe, R. J. Cody, J. E. Allen Jr., Chem. Phys. 93, 67 (1985).

9. Miziolek, private communication.

10. Vernon H. Dibeler, James A. Walker, K. E. McCulloh, J. Chem. Phys. 59, 2264 (1973).

11. Y. Ono, C. Y. Ng, J. Chem. Phys. 74,. 6985 (1981).

12. H. Okabe, V. H. Dibeler, J. Chem. Phys. 59, 2430 (1973).

13. J. Berkowitz, Photoabsorption, Photoionization, and Photoelectron Spectroscopy, Academic Press, New York, 1979, pp. 285-290.

14. B.K. Janousek, J.I. Brauman, J. Simons, J.Chem. Phys., 71, 2057 (1979)

15. G.I. Mackay, D.K. Bohme, Int. J. Mass Spectrom. Ion Phys., 26, 327 (1978)

16. R.N. Zare, Mol. Photochem., 4, 1 (1972)

17. S.K. Shih, S.D. Peyerimhoff, R.J. Buenker, J. Molec. Spectr., 74, 124, (1979)

18. S.K. Shih, S.D. Peyerimhoff, R.J. Buenker, J. Mol. Spectr., 64, 167 (1977)

19. H. Okabe, J. Chem. Phys. 78, 1312 (1983).

20. W.R.M. Graham, K.I. Dismuke, W.Weltner Jr., J. Chem. Phys., 60, 3817 (1974)

21. K.D. Tucker, M.L.Kutner, P.Thaddeus, Ap. J., 193, L115 (1974)

22. A. Wootten, E.P. Bozyan, D.B. Garrett, R.B. Loren, R.L. Snell, Ap. J., 239, 844 (1980)

23. L.M.Ziurys, R.J.Saykally, R.L.Plambeck, N.R. Erickson, Ap. J., 254, 94 (1982)

24. L.Å. Nyman, Astron. Astrophys., 141, 323 (1984)

25. K.V.L.N. Sastry, P. Helminger, A. Charo, E. Herbst, F.C. De Lucia, Ap. J., 251, L119 (1981)

26. C.A. Gottlieb, E.W. Gottlieb, P.Thaddeus, Ap. J., 264, 740 (1983)

27. R.J. Saykally, L. Veseth, K.M. Evenson, J. Chem. Phys., 80, 2247 (1984)

28. For $^{12}C^{12}CH$, B_o=43674.3607(37)MHz from ref. 27.

29. M. Bogey, C. Demuynck, J.L. Destombes, Astron. Astrophys., 144, L15 (1985)

30. R_{C-H}= 1.0464 Å and R_{C-C}=1.2165 Å.

31. Marylin E. Jacox, Chem. Phys. 7, 424 (1975).

32. Hideto Kanamori, private communication.

33. R.F. Curl, private communication.

34. (a) P. G. Carrick, A. J. Merer, R. F. Curl Jr., J. Chem. Phys. 78, 3652 (1983). (b) R.F. Curl, P.G. Carrick, A.J. Merer, J. Chem. Phys., 82, 3479 (1985)

35. G. Fogarasi, J.E. Boggs, P. Pulay, Mol. Phys., 50, 139 (1983)

36. W.P. Kraemer, B.O. Roos, P.R Bunker, P. Jensen, to be published.

37. For example see: R.N. Dixon, Phil. Trans. A, 252, 165 (1960)

38. G.J. Vazquez, Il Nuovo Cimento, 63, 446 (1981)

39. Based on a beam temperature of 50°K the average rotational period is 3 psec for C_2H_2.

40. Pauline Ho, Douglas J. Bamford, Richard J. Buss, Yuan T. Lee, C. Bradley Moore, J. Chem. Phys. 76, 3630 (1982).

41. Vibrational Spectra of Polyatomic Molecules, L.M. Sverdlov, M.A. Kovner, E.P. Krainov, p. 314, John Wiley and Sons, New York 1974, Library of Congress cat. no. QC454.S9413

42. (a) J.M. Brown, F. Jorgenson, Adv. Chem. Phys., 52, 117 (1983), (b) Ch. Jungen, A.J. Merer, Mol. Spectrosc, Modern Research, Ed. K.N. Rao, Academic Press, New York, 2, p. 127, (1976)

43. J.R. Wyatt, F.E. Stafford, J. Phys. Chem., 76, 1913 (1972)

44. H. Shiromaru, Y. Achiba, K Kimura, Y.T. Lee, J. Chem. Phys., (to be published)

45. Carl Melius, D.O.E. Proceedings of the Combustion Research Contractor's Meeting, Sponsored by the Office of Basic Energy Sciences, U.S. Department of Energy, p. 39, 1984..

46. (a) E.H. Abramson, "Molecular Acetylene in States of Extreme Vibrational Excitation", Ph.D. Thesis, Massachusetts Institute of Technology, (1985); (b) E. Abramson, C. Kittrell, J.L. Kinsey, R.W. Field, J. Chem. Phys., 76, 2293 (1982)

47. (a) E.H. Abramson, R.W. Field, D. Imre, K.K. Innes, J.L. Kinsey, J. Chem. Phys., 83, 453 (1985); (b) R.L. Sundberg, E.H. Abramson, J.L. Kinsey, R.W. Field, J. Chem. Phys., 83, 466 (1985)

CHAPTER IV: The Photodissociation of Vinyl Bromide at 193 nm
-The Heat of Formation of the Vinyl Radical and an Investigation of the Validity of the "Ground State Fragment" Assumption

A. Background Information.- Because of their role as highly reactive, chemical intermediates, molecular free-radicals are certainly one of the most intriguing subjects of chemical research. The presence of unpaired electrons gives them very interesting behavior that, due to their very high reactivity and concommitant elusiveness, is very difficult to study.

The determination of reliable, thermochemical data for molecular radicals is one area that promises to shed a great deal of light on their chemistry[1] as is graphically illustrated by the reaction of vinyl radical with molecular oxygen.

$$C_2H_3 + O_2 \longrightarrow C_2H_2 + HO_2$$

Erroneous values of the heats of formation of the radicals in this reaction led chemists to believe that the reaction was endothermic by 10 kcal/mol and it was assumed that there was a substantial activation barrier, limiting its rate and therefore its importance.[2] More recent values of the heat of formation of C_2H_3 and HO_2 [3] imply that the reaction is exothermic. While it is true that dynamical features of the potential energy surface (PES) play a role in the rate of a reaction, a quantitative misunderstanding of thermochemistry can lead to incorrect conclusions concerning the rate of a reaction, especially for near thermoneutral ones.

Traditionally, thermochemical data has been obtained from activation energy measurements of reactions which involve the radical of interest, for example, bond fission reactions. However, the ambiguities of bulk experiments and the blossoming of mass spectrometric technology have triggered the advent of more direct, "microscopic" experiments. A good example is the determination of the heat of formation of the C_2H radical by the photoionization method.[4] This has already been mentioned and is illustrated in fig. 12 of chapter III. Here the photoionization threshold difference between reactions I and II

$$C_2HBr \xrightarrow{h\nu} C_2H^+ + Br + e^- \qquad (I)$$

$$C_2HBr \xrightarrow{h\nu} C_2H + Br^+ + e^- \qquad (II)$$

is measured to get the ionization potential of C_2H, by knowing the ionization potential of Br. By combining this result with the

dissociative photoionization threshold of acetylene,[5] reaction III,

$$C_2H_2 \xrightarrow{h\nu} C_2H^+ + H + e^- \qquad \text{(III)}$$

the C-H bond energy in acetylene and hence the heat of formation of C_2H is obtained.

While the precision of these experiments is typically very high, ~1 kcal/mol, there are a number of possible systematic difficulties associated with threshold measurements that give rise to large deviations between experiments, far outside this uncertainty. First of all, by definition the photoionization cross-section near threshold is very small and it can be quite difficult experimentally to identify the true threshold. Secondly, since it is difficult to anticipate the nature of electronically excited molecules at energies as high as 15 eV, it is often an implicit assumption that ion formation is possible at the thermodynamic threshold. Problems may result from wave function symmetry restrictions which prevent the formation of ground state ionic products or for dissociative ionization, barriers to dissociation on the excited PES's may impede the determination of the true threshold.[6]

Thirdly, ordinarily only positive ions are detected. Since almost all atoms and molecules have non-negative electron affinities, there will be the possibility of an ion pair production channel that may form the positive ion of interest at or slightly below the true threshold for dissociative photoionization.[7]

Fourthly as with any thermodynamic determination, in photoionization threshold measurements it is often necessary to rely on other thermodynamic determinations in order to build a thermochemical cycle, the missing leg of which is the process of interest. These cycles can be very complex; see fig. 12 of chapter III. For example in the above photoionization experiment, the cycle begins at $C_2HBr + H$. The energy required to go to $C_2H^+ + H + Br + e^-$ is measured, process I, and the energy released in going to $C_2H_2 + Br$ is obtained from another experiment, process III. The well known IP of Br informs how much energy is required to make $C_2H_2 + Br^+ + e^-$ and the missing leg of the cycle takes us to $C_2H + H + Br^+ + e^-$. Finally the second measured step, process II ends up at the beginning. Since the energy change around the cycle is zero the energy of the missing leg can be gotten. While this strategy provides the experimentalist with an endless number of possible approaches to the heat of formation of a given molecule, each additional leg of a thermochemical cycle is an opportunity for the accumulation of error in the data and the refinement or redetermination of a previously well accepted thermochemical quantity can have a ripple effect on many different experiments.[8]

Another common feature of free-radicals is the existence of low-lying excited electronic states, since free-radical electrons are often less tightly bound than bonding electrons in similar closed-shell molecules and the presence of a low-lying half-filled molecular orbital lowers the possible excitation energies of the

bonding electrons. The understanding of excited state free-radical chemistry is quite important because radicals are typically found in high temperature environments where these states can be populated and they may behave very differently than the ground state as in the case of CH_2.[9] Unfortunately, photoionization threshold measurements yield little information on the electronically excited states of radicals, so other methods must be employed to obtain thermochemical data of this sort.

The method of photofragmentation translational spectroscopy has been shown to yield very accurate thermochemical results since by photodissociating at wavelengths substantially above the dissociation threshold where the absorption cross-section is large and measuring the maximum release of translational energy, E_T^{MAX}, the bond energy can be determined in a very direct manner, avoiding many of the problems already alluded to.[10] Reaction IV illustrates the determination of the heat of formation of C_2H by this method which is, by comparison to the photoionization experiment just described, simple indeed. See chapter III of this thesis.

$$C_2H_2 \xrightarrow{193.3\ nm} C_2H + H + E_T \qquad D_o(C_2H\text{-}H) = E_{photon} - E_T^{MAX} \qquad (IV)$$

In addition to obtaining heats of formation for ground state radicals, the possibility of forming electronically excited radicals is a general feature of UV photodissociation and by doing high resolution translational energy measurements, these states can be resolved and studied.

In a similar way, one can perform crossed-molecular beam experiments to obtain thermochemical information for ground state radicals by measuring the maximum release of translational energy of the products of reactive scattering. For quite some time it has been realized that the crossed beam experiment on the reaction $F + C_2D_4 \longrightarrow C_2D_3 + DF(v'=4)$ of Parson and Lee[11] could be used to determine the heat of formation of C_2H_3 within ±0.5 kcal/mol. However, it has not been clear until recently[12] that the highest vibrational state of the DF product observed in the reactive scattering experiment might not be v'=3. A misassignment would have caused the determination to underestimate the heat of formation of C_2H_3 by 7.5 kcal/mol.

The heat of formation of the vinyl radical is important not only because it yields the C-H bond energy of ethylene and therfore has a tremendous influence on the initiation steps of ethylene chemistry, but also because the exact energy required to eliminate a highly reactive H atom from vinyl will have a major impact on the complex reaction mechanisms used to simulate combustion and pyrolysis of small hydrocarbons. The suggested values for vinyl's heat of formation range over ~13 kcal/mol and there is no clear reason to accept one value as the correct one, reflecting many of the problems already mentioned.[13]

Ab-initio calculations have predicted the presence of a low-lying electronically excited state, created by moving one of the π bonding electrons into the sp^2 non-bonding free radical orbital and the

visible absorption spectrum involving this state has been observed.[14] However, an unambiguous assignment was impossible, since the origin band could not be clearly identified, due to the large geometry change upon excitation.

The purpose of this chapter is to present the analysis of the crossed beam reactive scattering experiment mentioned above, which gives the most accurate and precise value for the heat of formation of the vinyl radical to date, and to descibe and compare results on the UV photodissociation of C_2H_3Br. The C_2H_3 heats of formation derived from these two very different experiments are in good agreement despite the many possible factors that could make the UV photodissociation experiment inaccurate. This good agreement is indicative of the general usefulness of the method. In addition, a very interesting feature of the photodissociation experiment was the observation of a metastable state of C_2H_3, containing enough energy to dissociate to C_2H_2 + H but with a ~100 μs lifetime. The possible identity of this metastable state and the resulting implications will also be discussed.

B. Experimental Supplement.- The experimental apparatus has been described in detail in chapter II so only those experimental features peculiar to this study will be presented here. A continuous molecular beam was formed by expanding 150 torr of vinyl bromide out of a 125 μm diameter orifice which was heated to 280°C to prevent cluster formation. The vinyl bromide beam had a peak velocity of 6.9×10^4

cm/s and a full width at half maximum 2.7 x 10^4 cm/s. Due to the large release of translational energy in the photodissociation of C_2H_3Br, this relatively large spread in beam velocities is essentially negligible. Most of the experiments were performed using the light from an unpolarized ArF laser, emmiting at 193.3 nm; however, in order to obtain information on the vinylbromide excited state lifetime, the laser was polarized with a MgF_2 prism as has already been described in chapter III.B..

C. Results.- C.1. Photodissociation Using an Unpolarized Laser.- TOF spectra were obtained for mass to charge ratio's (m/e's) of 82, 81, 80, 79, 27, and 26. The two important dissociation channels are reactions V and VI.

$$C_2H_3{}^{81,79}Br \xrightarrow{193\ nm} C_2H_3 + {}^{81,79}Br(^2P_{3/2,1/2}) \quad (V)$$

$$C_2H_3{}^{81,79}Br \xrightarrow{193\ nm} C_2H_2 + H{}^{81,79}Br \quad (VI)$$

The m/e=27 TOF spectrum, measured at an angle 90° from the molecular beam, is shown in fig. 1 and is due solely to vinyl radicals produced in reaction V. Fig. 2 is an energy level diagram for reaction V, from which it is clear that unless at least 25 kcal/mol of energy goes into translation there will be sufficient energy for C_2H_3 to decompose into C_2H_2 + H even in the event of spin orbit excited $Br(^2P_{1/2})$ formation.

$$C_2H_3Br \longrightarrow C_2H_2 + H + Br(^2P_{1/2}) \quad \Delta H = 123 \text{ kcal/mol} \quad (VII)$$

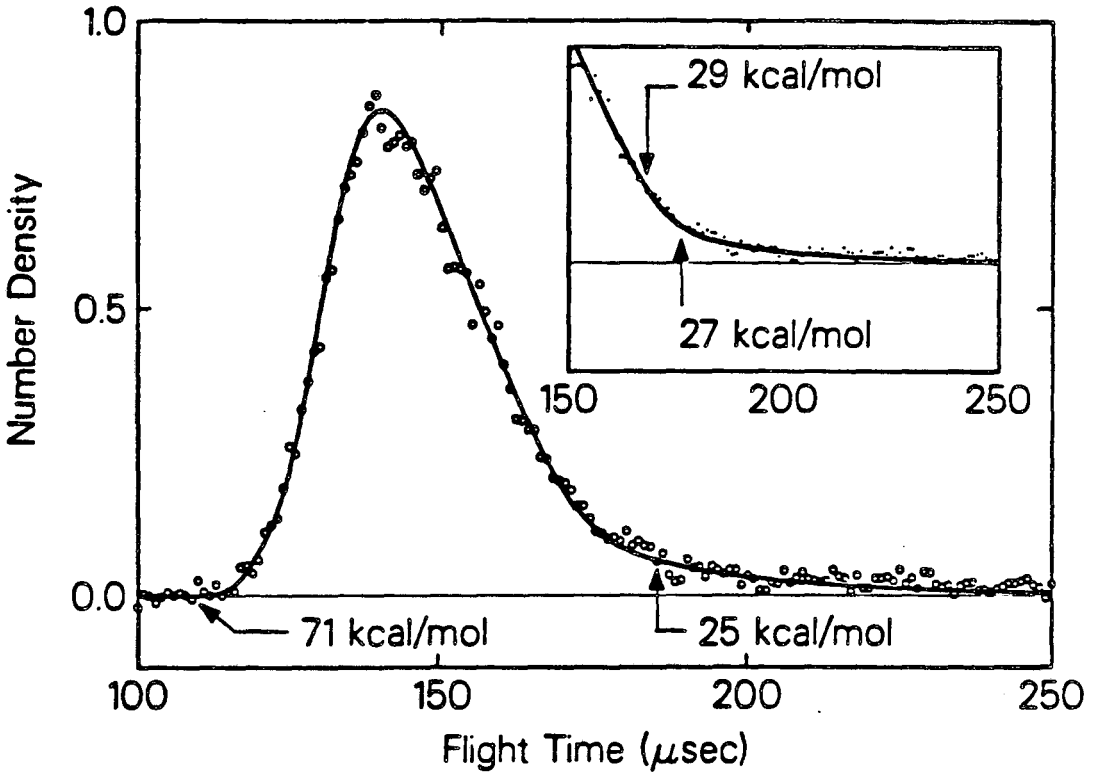

Fig. 1 TOF Spectrum at m/e=27, 90 deg. from beam. Open circles are data and the solid line is the fit to the data based on the translational energy distribution shown as the solid curve in fig. 4.

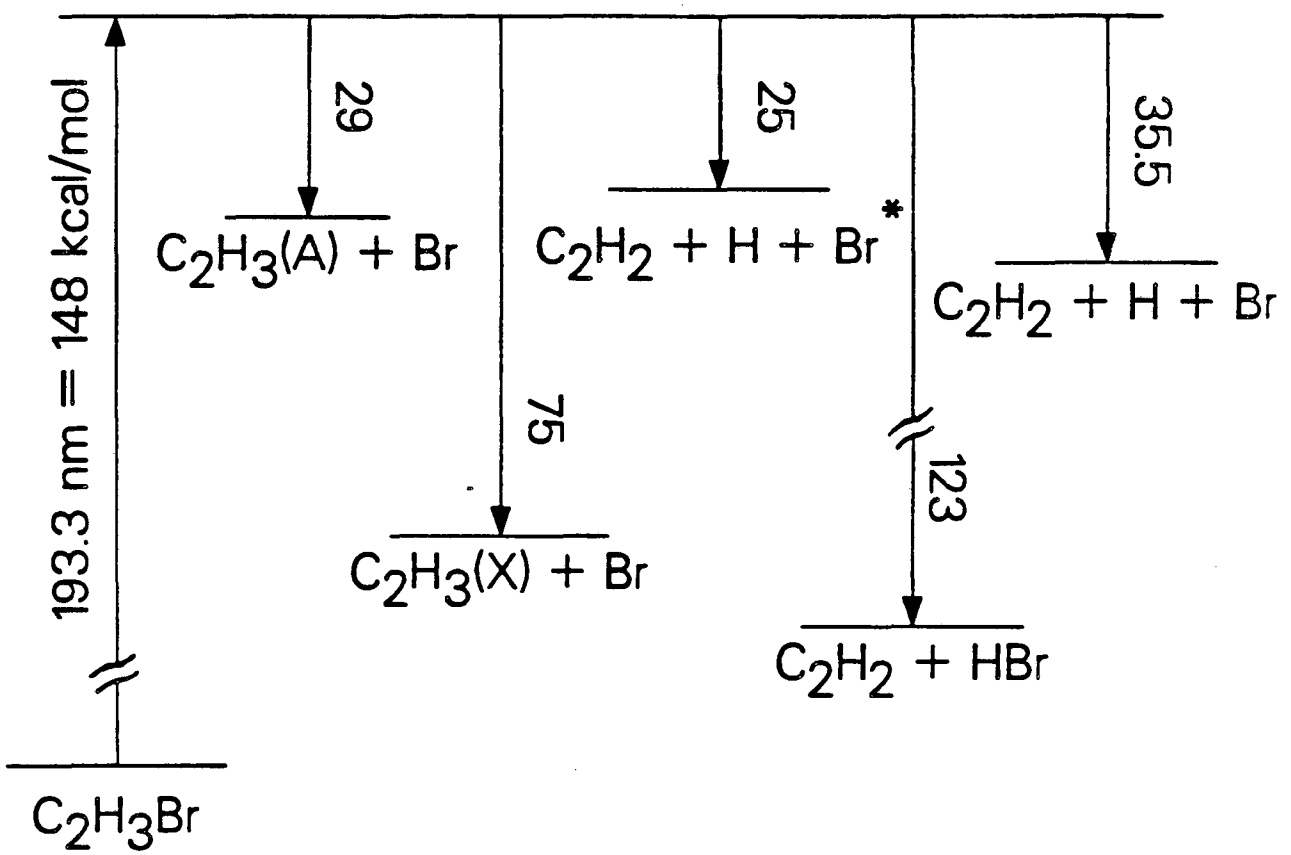

Fig. 2 Energy level diagram for the photodissociation of vinylbromide. Energies are in kcal/mol.

This is predicted simply on the basis of the heats of formation of molecules which are well known.[15] An inspection of the inset in fig. 1 reveals a pronounced change in the slope of the data between 29 and 27 kcal/mol translational energy release. In addition, the existence of substantial signal below 25 kcal/mol implies the existence of some metastable state of C_2H_3.

If secondary decomposition were unimportant, detection of either C_2H_3 or Br would by itself be enough to give the $P(E_T)$ for reaction V, since linear momentum must be conserved. In reality because C_2H_3 can decompose we must make an effort to observe the Br atom in order to get this information.

In order to observe Br atoms produced in reaction V which appear at m/e=81, we must first determine the contribution of $H^{81}Br$ from reaction VI that can appear at this mass due to fragmentation in the electron impact ionizer. By measuring and analyzing the m/e=82 TOF spectrum, due to $H^{81}Br^+$ and shown in fig. 3a, where only products from reaction VI can appear, we can account for the long slow tail in the m/e=81 TOF spectrum, shown as the dot-dashed curve in fig. 4b. The portion of the m/e=81 TOF spectrum that remains unfit by the dashed curve is due solely to reaction V.

The $P(E_T)$ for production of Br atoms in reaction V (dashed curve) along with the $P(E_T)$ for production of vinyl radicals (solid curve) is shown in fig. 4 . The $P(E_T)$'s are identical on the fast side of the distribution where products appear with low internal energy, but below a translational energy of about 40 kcal/mol the

Fig. 3 TOF spectra of the Br containing products: (a) m/e=82 at 30° from the molecular beam. (b) m/e=81 at 30° from the molecular beam. Open circles are the data points. The solid lines are the fit to the data. In (b) the dot dashed curve is due to HBr coming from reaction VI and the dashed curve is due to Br atoms coming from reaction V.

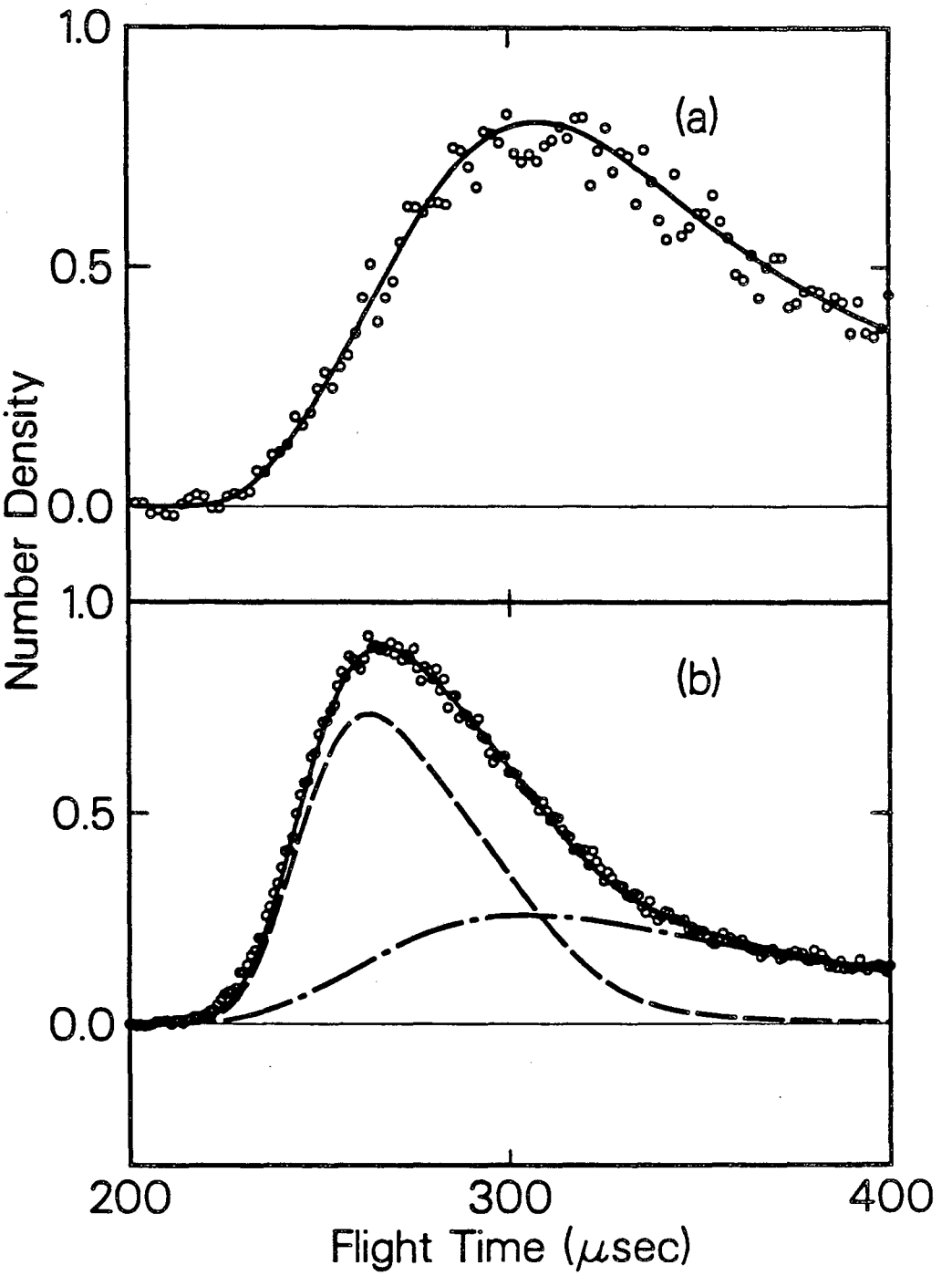
1.0
0.5
0.0
(a)
1.0
0.5
0.0
(b)
Number Density
200
300
400
Flight Time (μsec)

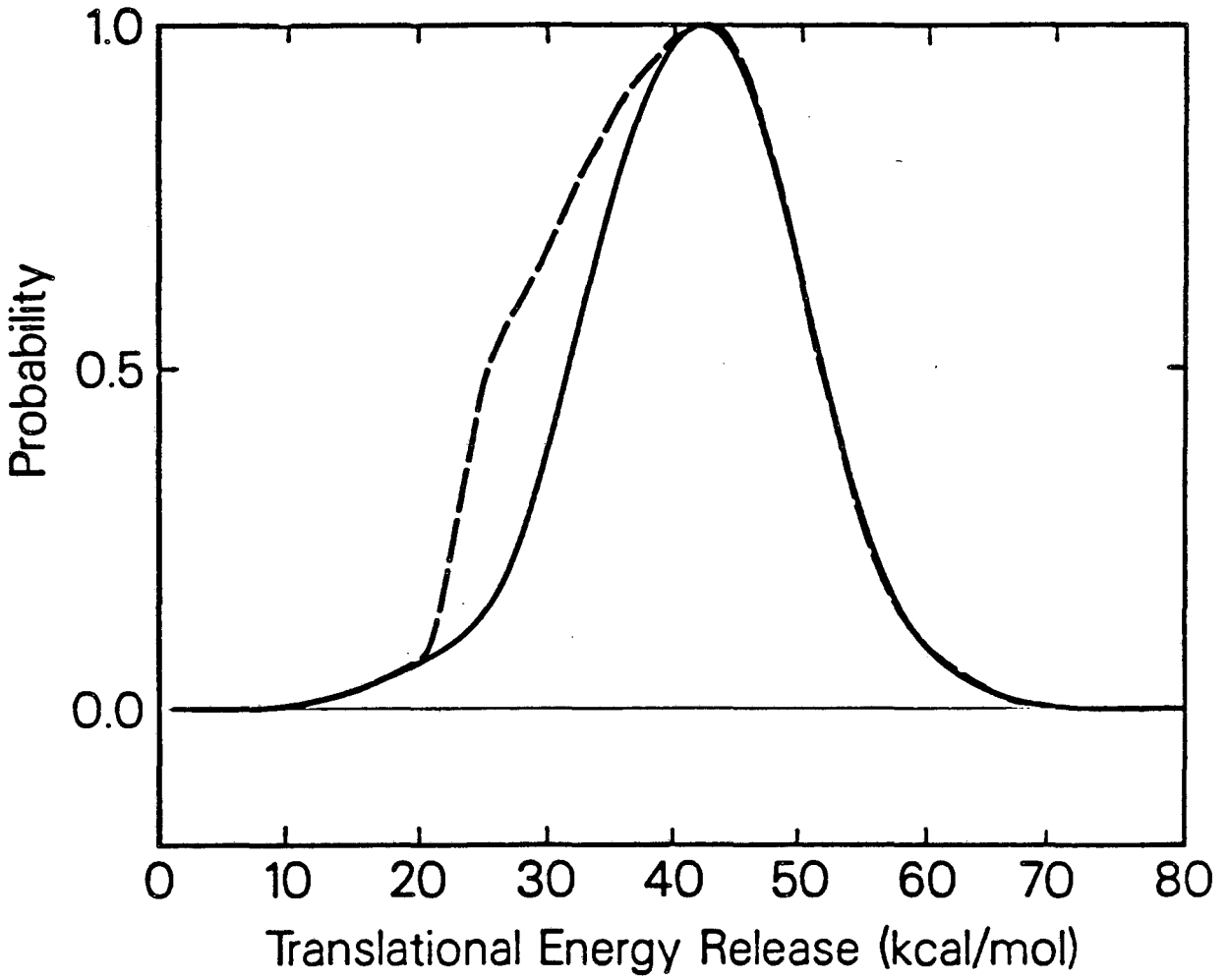

Fig. 4 Translational energy distributions for: production of vinyl radical (solid curve) and production of Br atoms (dashed curve).

$P(E_T)$ derived from the m/e=27 TOF spectrum drops below the one derived from the m/e=81 spectrum due to the secondary decomposition of C_2H_3. At translational energies below about 20 kcal/mol the $P(E_T)$'s converge again, indicating the presence of the metastable component in the data. By subtracting the solid curve from the dashed curve in fig. 4, the translational energy distribution of radicals that decompose is obtained. See fig. 5.

As mentioned previously if only $Br(^2P_{1/2})$ were formed, we would expect C_2H_3 molecules to survive down to kinetic energies as low as 25 kcal/mol. Because the molecular beam is heated, there may be some unrelaxed vibrational energy in the parent C_2H_3Br that could end up in the vinyl radical after C_2H_3Br dissociation and cause it to decompose even if more than 25 kcal/mol appeared as translation. However taking this effect into consideration only shifts the translational energy required for radical survival to 30 kcal/mol. The secondary loss of molecules produced with even as much as 40 kcal/mol of translational energy is unambiguous evidence that $Br(^2P_{3/2})$ is produced in the photodissociation of vinylbromide, where the 10.5 kcal/mol of spin-orbit excitation energy is available for vinyl radical vibration.

The most direct observation of secondary decomposition is the m/e=26 TOF spectrum taken at 90° from the molecular beam, shown in fig. 6. There are three components to this TOF spectrum, two of which are determined from other data. These are: (1) vinyl radical, shown as the dashed curve, (2) acetylene from reaction VI, shown as the

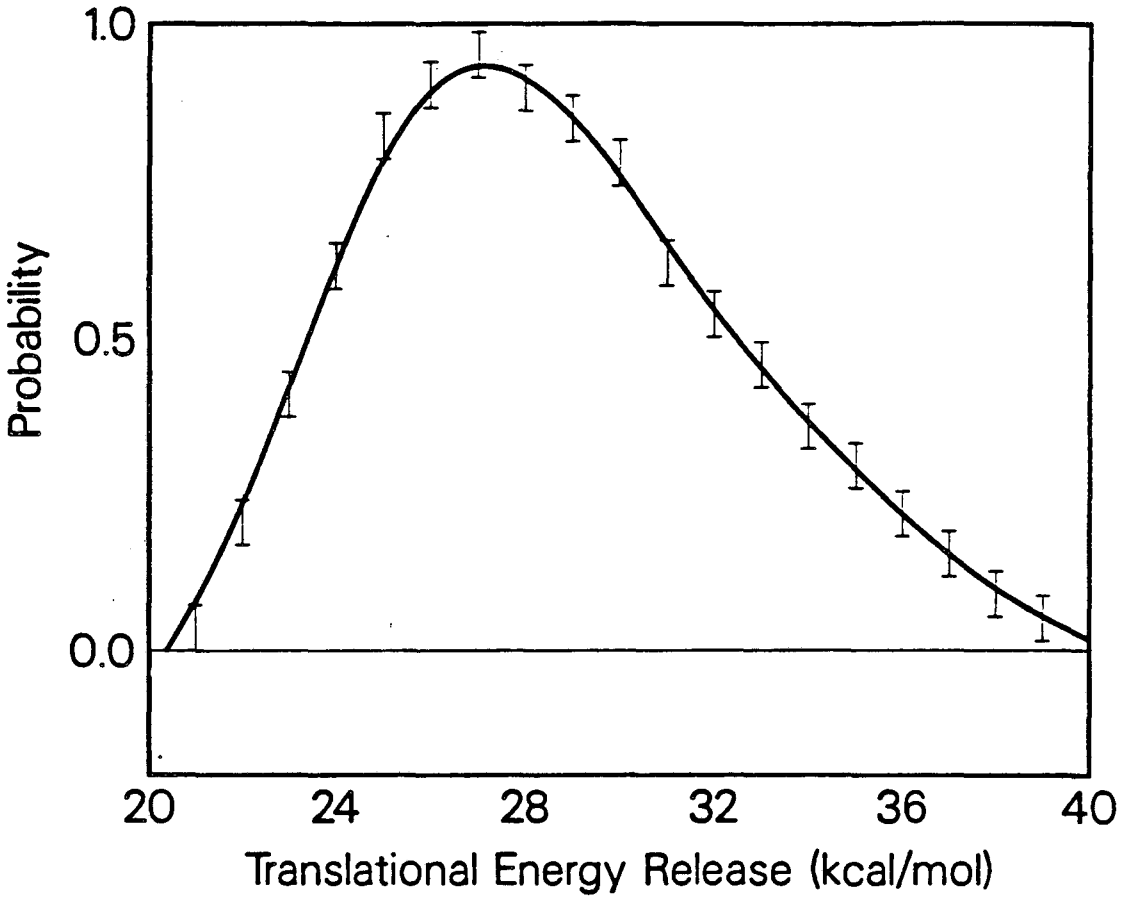

Fig. 5 Translational energy distribution for those vinyl radicals that undergo secondary decomposition.

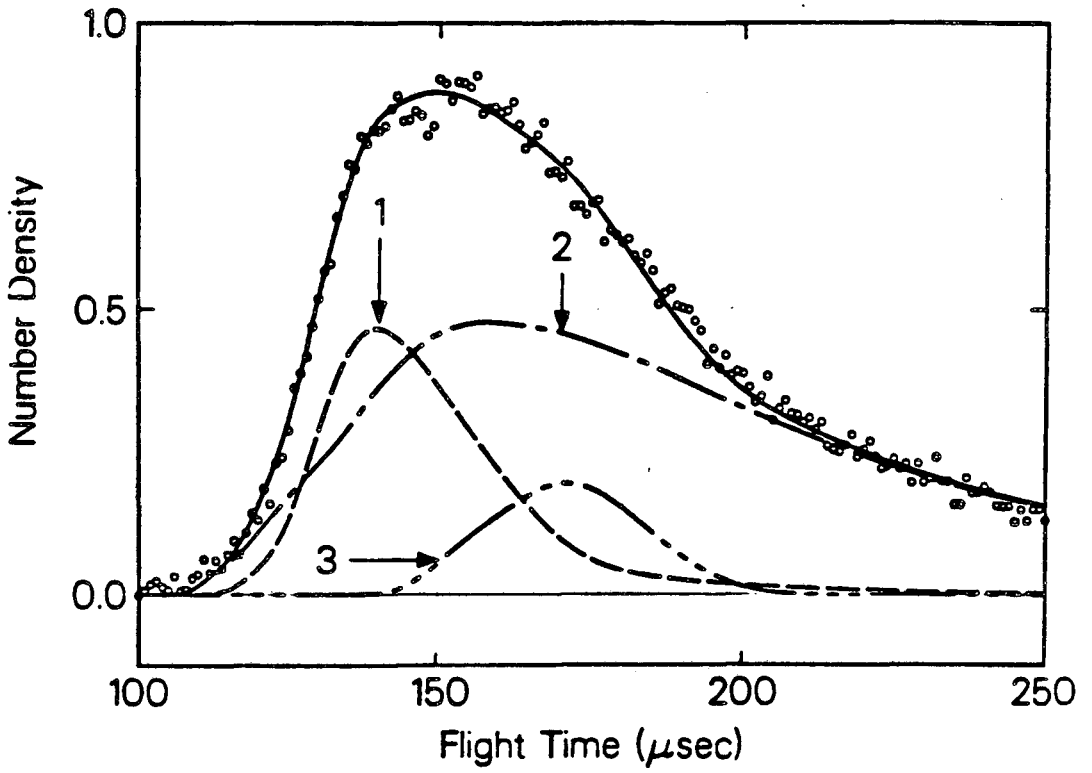

Fig. 6 TOF spectrum for m/e=26 at 90 deg. from the beam. Open circles are data. Solid line is the fit to the data based on three components. The three components are (1) vinyl radicals, dashed curve, (2) acetylene from reaction VI, dot-dashed curve, and (3) acetylene from the secondary decomposition of vibrationally hot vinyl radicals, triple dot dashed curve.

dashed-dot curve and (3) acetylene from spontaneous secondary decomposition of vibrationally hot vinyl radical, shown as the dashed-triple dot curve. Curve (1) is due to fragmentation of $C_2H_3^+$ to $C_2H_2^+ + H$ in the ionizer and is therefore determined by the m/e=27 data. Curve (3) is from reaction VI and is derived from the m/e=82 data.

The analysis of secondary decomposition in molecular beam experiments is descibed in the appendix. In short, there are two $P(E_T)$'s used to generate curve (3). The first is shown in fig. 5 and is used to calculate the lab frame velocity vector distribution of the primary vinyl radicals which undergo secondary decomposition. The second $P(E_T)$ is the translational energy release of the secondary process, reaction VIII.

$$C_2H_3 \longrightarrow C_2H_2 + H \qquad \text{(VIII)}$$

Because Br is three times heavier than C_2H_3 and there is a large translational energy release for reaction V, the recoil velocity of the vinyl radical is very large. In contrast, reaction VIII releases very little energy and the loss of a light H atom in reaction VIII changes the original large velocity of the vinyl radicals by so little that curve (3) in fig. 6 is only dependent on the $P(E_T)$ shown in fig 5. The fit to the m/e=26 data, curve (3) of fig. 6, was generated without modification of this $P(E_T)$ and as such is a good second check of the two $P(E_T)$'s shown in fig. 4.

C.2. Photodissociation Using Polarized Light.- The general form of the product angular distribution in the center of mass frame was derived by Zare[16] and is given in equation 1.

$$P(\theta) \sim 1 + \beta P_2(\cos\theta) \qquad (1)$$

where:

$P(\theta)$: Probability density for products to recoil with a velocity vector θ° from the polarization vector, $\underline{\varepsilon}$

β: Experimentally determined anisotropy parameter

$P_2(\cos\theta)$: Second Legendre polynomial of $\cos\theta$

β is limited between +2 and -1, the former value corresponding to a $\cos^2\theta$ and the latter to a $\sin^2\theta$ distribution about $\underline{\varepsilon}$.

It is possible to observe the manifestation of a polarized angular distribution in several ways. In the acetylene experiment, (see chapter III, sec. C.4.) the signal at different points in the C_2H TOF spectrum came from products with recoil vectors making substantially different angles with respect to $\underline{\varepsilon}$. In that case it was found that the shape of the TOF spectrum was independent of the polarization of the laser, indicating that after excitation C_2H_2 can rotate many times before dissociating, loosing all memory of its spatial orientation at the moment of excitation. If, however, the molecule were to dissociate promptly before rotation had a chance to

occur, the shape of the TOF spectrum would have been strongly dependent on the polarization of the laser.

In contrast to acetylene, the vinyl radical detected at 90° from the beam comes within a very small range of recoil vector-polarization vector angles at all points along the TOF spectrum. This can be seen by inspection of fig. 7, which shows the newton diagram for this experiment. Consequently, no change in the shape of the TOF spectrum can be observed with changing polarization angle. However, it is possible to see a marked change in the magnitude of the signal, depending on the polarization of the laser, from which we can derive β with high precision.

Because of the very large absorption cross-section of vinylbromide at 193 nm, 10^{-17} cm^2, one must be aware of possible saturation effects. Even though the laser pulse is very long compared to the rotational period of the molecule and one might think that every molecule would have an equal probability to rotate into a favourable alignment before dissociation, this is not really true. The case of a perpendicular transition in a diatomic molecule is most easily understood, since the transition dipole moment, $\underline{\mu}$, is parallel to the angular momentum vector, $\underline{J}$. Imagine that at very low laser powers, the angular distribution is a perfect $\sin^2\theta$ function about $\underline{\varepsilon}$. Since $\underline{J}$ must be conserved and $\underline{\mu}$ is parallel to $\underline{J}$, we can divide the ensemble of isotropically rotating molecules into subsets defined by the angle that $\underline{J}$ and $\underline{\mu}$ make with $\underline{\varepsilon}$. This angle is a constant of the rotational motion within each subset. Now it is clear that if we

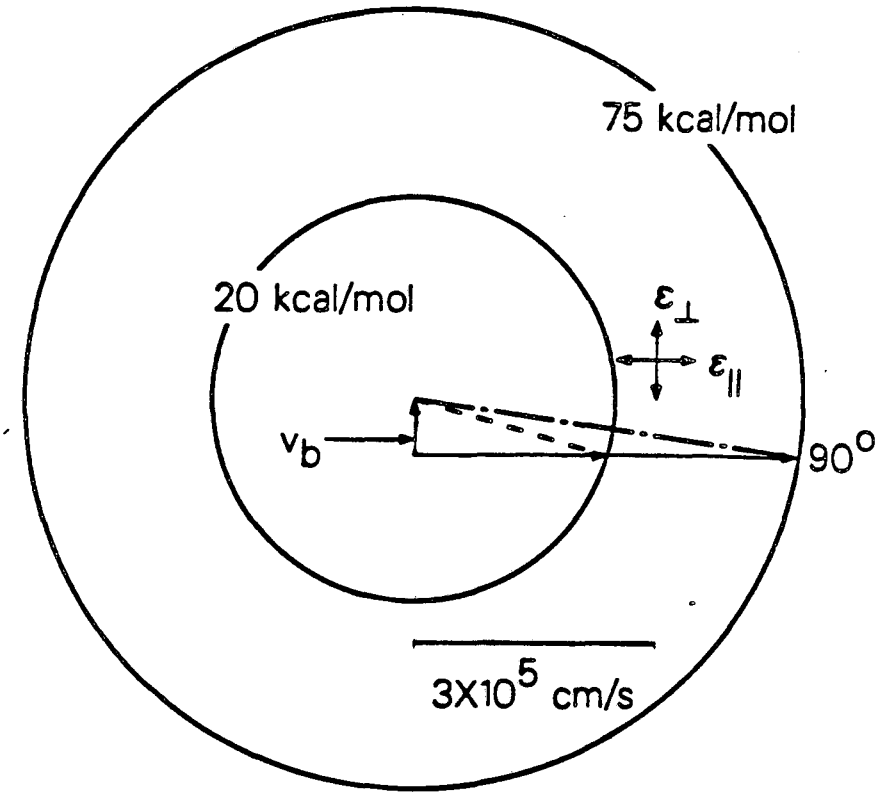

Fig. 7 Newton diagram for the photodissociation of vinylbromide to form vinyl radical and Br atom. v_b shows the beam velocity vector. The dashed curve shows the c.m. recoil vector of vinyl radicals produced with 20 kcal/mol of translational energy. The dot dashed curve shows the c.m. recoil vector for those formed with 75 kcal/mol. Note that the range of angles between the recoil vectors and either of the polarization vectors is very limited for different releases of translational energy.

turn up the laser power, the subsets whose $\underline{\mu}$'s are nearly aligned with $\underline{\varepsilon}$ will saturate before those whose $\underline{\mu}$'s are not so well aligned. This means that the product angular distribution will be dependent upon the laser power.[17]

Fig. 8 shows the magnitude of the m/e=27 signal for $\underline{\varepsilon}$ parallel and perpendicular to the detector direction as a function of laser power. The ratio of the two is directly related to β. While the parallel signal is always larger than the perpendicular signal, the ratio is not constant above a laser power of ~3 mJ/pulse, indicating orientation dependent saturation. In the linear regime, however, the ratio is constant and a value for β of 0.45 ± 0.02 is derived for process V.

By analyzing the m/e=82 TOF spectrum, β for process VI can be derived. Although there is a substantial change in the shape of the TOF spectrum as a function of polarization angle, simultaneously fitting both the shape and the relative magnitudes of the two TOF spectra, for either $\underline{\varepsilon}$ parallel or perpendicular to the detector direction, provides the most precise result. Fig. 9 shows the two TOF spectra as the open circles and the fit to the data as the solid line. This analysis leads to β = 0.70 ± 0.02 for process VI.

D. Discussion.- D.1.The Heat of Fromation of $C_2H_3(\tilde{X}^2A')$ by the Photodissociation Method.- Fig. 2 shows clearly that the difference between the energy of the photon, E_{photon} and the maximum release of translational energy, E_T^{MAX} is the C-Br bond energy in

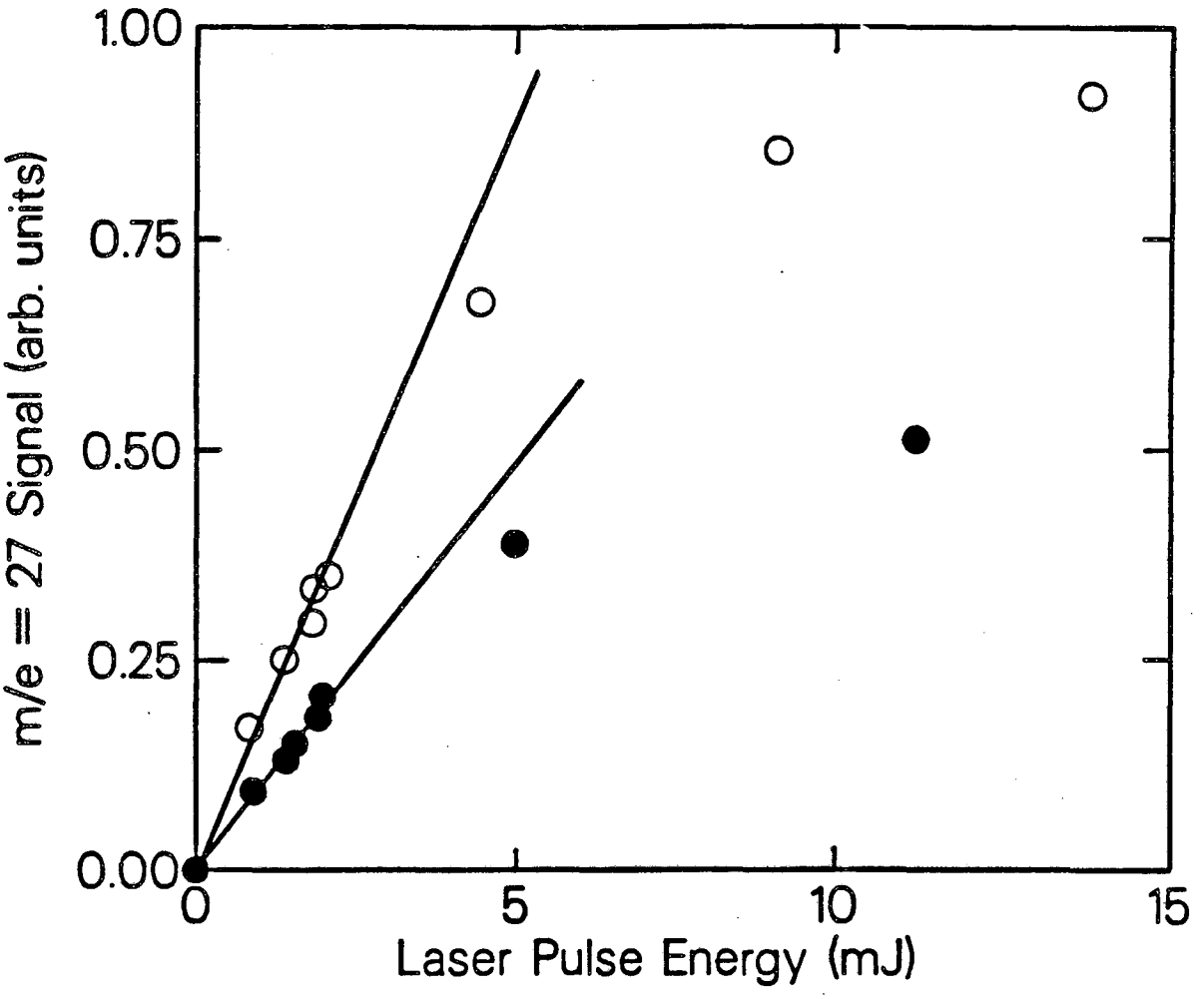

Fig. 8 m/e=27 signal intensity as a function of laser power for two laser polarization angles. The open circles correspond to the parallel polarization of fig. 7 while the closed circles correspond to the perpendicular polarization angle of the same fig..

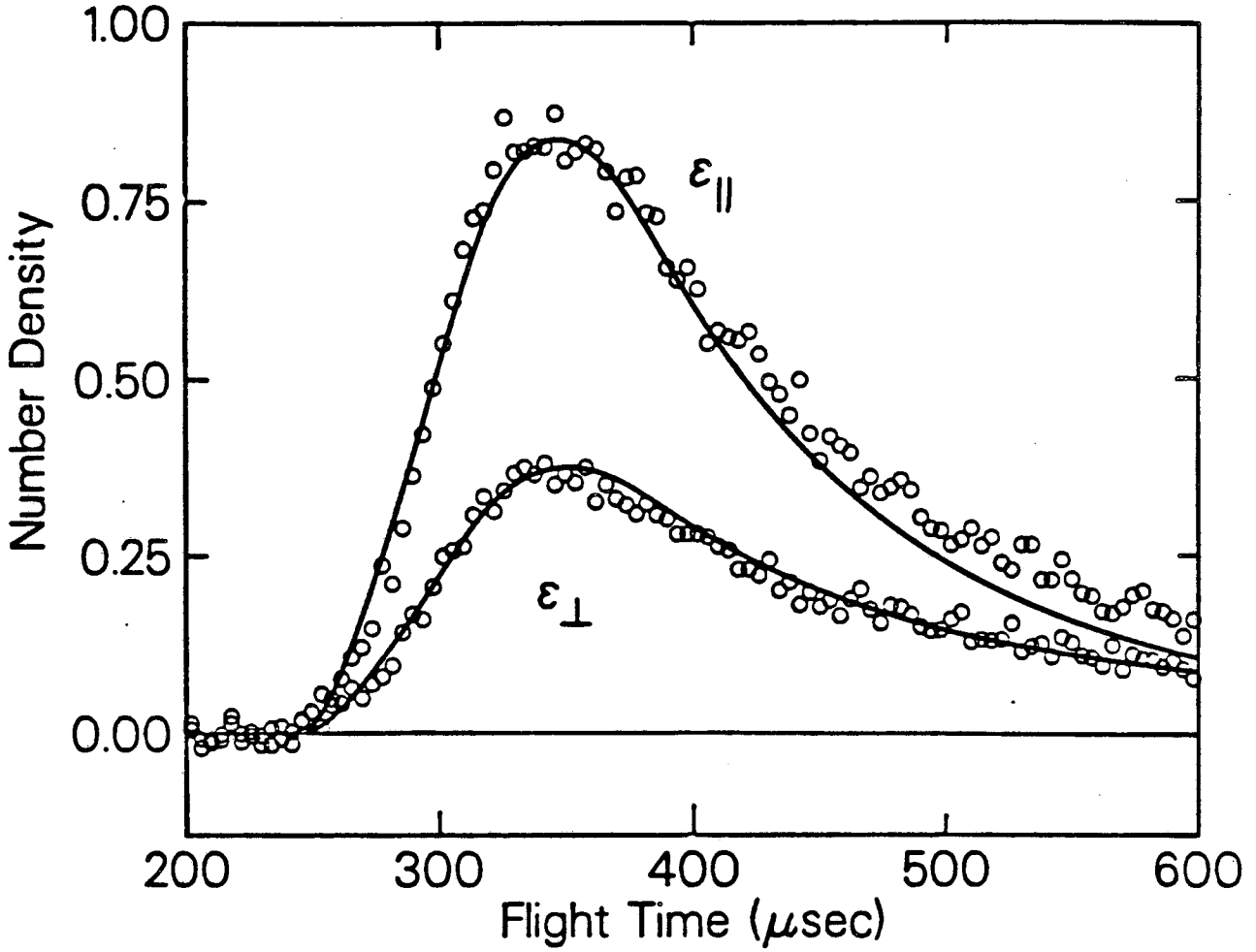

Fig. 9 m/e=82 TOF spectra as a function of laser polarization. Symbols refer to fig. 7. Open circles are data and solid line is fit to the data based on an anisotropy parameter of 0.70.

vinylbromide assuming that it is possible to form the products in their lowest quantum states. Fig. 1 shows that E_T^{MAX} is 71 ± 3 kcal/mol and since the photon energy is 148 kcal/mol, an upper limit to the C-Br bond energy in vinylbromide is 77 ± 3 kcal/mol.

By knowing the heats of formation of C_2H_3Br and $Br(^2P_{3/2})$, one can derive an upper limit to the heat of formation of vinyl radical of 71 ± 3 kcal/mol, corresponding to a C-H bond energy in ethylene of 108.1 ± 3 kcal/mol. Since the thermochemical data upon which this experiment is based is quite well established, the only sources of error are the experimental measurement of E_T^{MAX} and the validity of the assumption that products can be formed in their lowest quantum states.

There are a number of ways that this assumption could be wrong. For example, if it were impossible to form Br in anything but the spin orbit excited $^2P_{1/2}$ state, our determination of E_T^{MAX} would be off by 10.5 kcal/mol, the spin-orbit splitting in Br. As shown in section C.1. however, we know that both states of Br are formed.

Another way the assumption of lowest quantum state products could be wrong is due to the conservation of angular momentum. When the C-Br bond breaks in reaction V, it is quite unlikely that the Br atom departs along a trajectory with zero impact parameter. Consequently, there will be a substantial amount of orbital angular momentum generated between the C_2H_3,Br pair. The classical expression for this angular momentum is given by equation 2.

$$\vec{L} = \mu^* v b \qquad (2)$$

where: μ^* = reduced mass between C_2H_3 and Br

v = relative recoil velocity

b = deparing impact parameter

Because of the large mass of Br and the relative stiffness of C_2H_3 radical, we constructed a pseudotriatomic model that partitions energy only between rotation of the C-C framework in the radical and translation, based on the conservation of angular momentum. One can easily derive equation 3.

$$\frac{E_T}{E_{TOT}} = \left(1 + 0.25 \frac{\mu^*}{\mu_e} \sin^2(\pi-\theta)\right)^{-1} \qquad (3)$$

where: E_T = kinetic energy release

E_{TOT} = total available energy

θ = C-C-Br bond angle

μ^* = reduced mass between C_2H_3 and Br

μ_e = reduced mass of the C_2 rotor

To the extent that this model is correct, there is a one-to-one correspondence between the kinetic energy release and the departing impact parameter of the half collision. The opacity function derived by this analysis from the experimental $P(E_T)$ is shown in fig. 10. This model works best for large translational energy release, where vibrational excitation is small and it becomes increasingly inaccurate

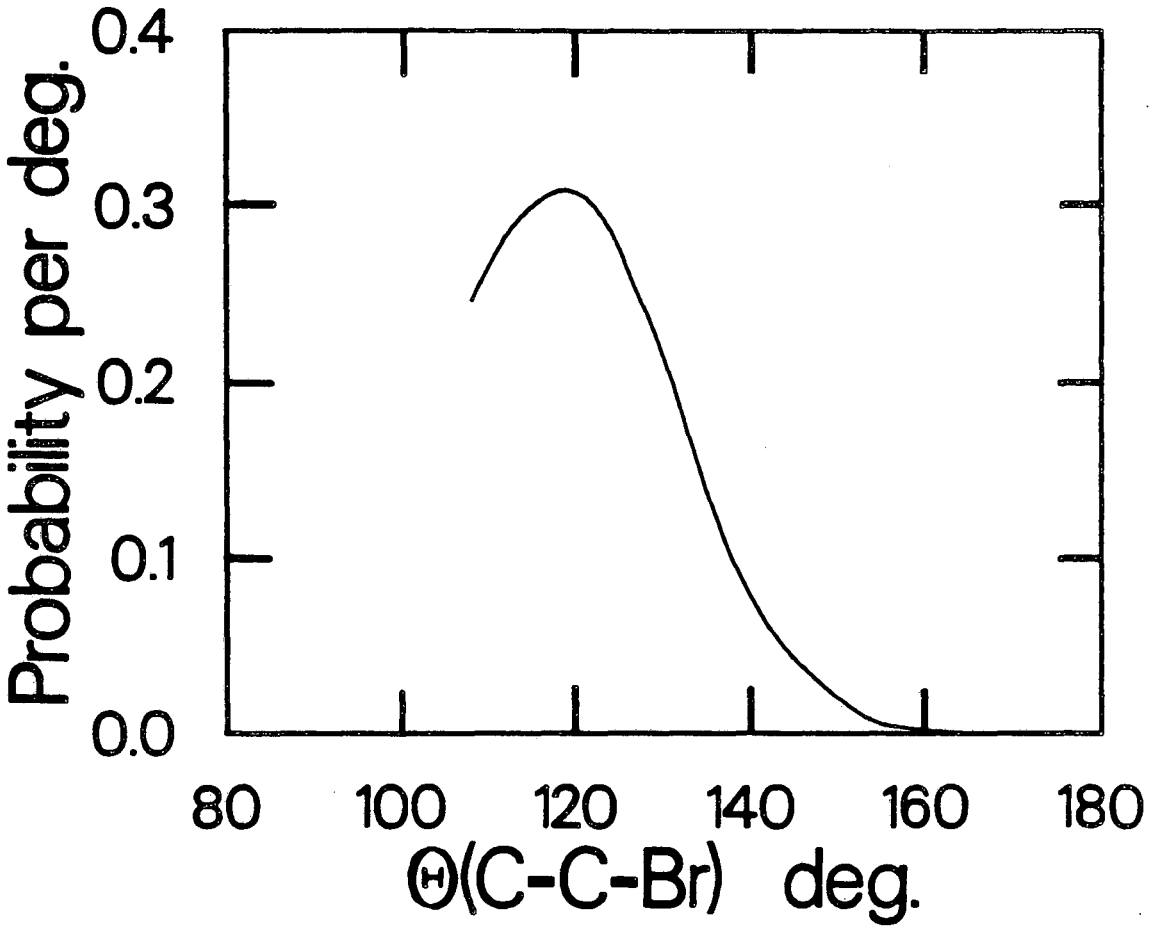

XBL 869-3252

Fig. 10. The Opacity Function for C-Br Bond Rupture in the Photodissociation of Vinylbromide at 193 nm. θ is the C-C-Br bond angle.

at smaller translational energies where vibrational excitation becomes more important. Consequently we have truncated the distribution somewhat arbitrarily at a C-C-Br bond angle of 105°. It is worth noting that at least the qualitative features of this model are correct. The most probable impact parameter for the half-collision is very close to the equilibrium bond angle of the ground state and there is a diminishingly small probability for dissociation near linearity, where all of the available energy can go into translation. Because of this, it might be expected that the determination of accurate thermochemical data in this experiment is impossible and we must evaluate more thoroughly this possible source of error. Of course, the best way to do this is to perform an experiment that gives a very accurate value for the heat of formation of C_2H_3. This is the subject of the next subsection.

D.2. The Heat of Formation of $C_2H_3(\tilde{X}^2A')$ by the Reactive Scattering Method.- In a like manner to photodissociation, we can measure the E_T^{MAX} with which the products of reactive scattering are formed. Reaction IX

$$F + C_2D_4 \longrightarrow C_2D_3 + DF(v'=4) + E_T \qquad (IX)$$

is almost thermoneutral so the exact value of the heat of formation of C_2D_3 will cause a large fractional change in the product's E_T^{MAX}. Practically speaking, because of the conservation of product flux in the transformation between the lab frame and the c.m.

frame in reactive scattering experiments, the amount of energy released as product translation has a dramatic effect on the intensity of the signal observed in the lab frame. The experiment is much more sensitive to processes that release a small amount of translational energy, since the products will be scattered in a very small laboratory angular range. Even for products with DF in the next lowest vibrational state, there is about 7X more translational energy released and this causes the the observed lab-frame signal from such scattering events to be very small. Consequently, the angular distribution of DF products measured in ref. 11 is almost entirely due to formation of DF in its highest energetically allowed vibrational level, almost regardless of the DF vibrational population distribution. This was assumed to be v'=4 in ref. 11. Measuring E_T^{MAX} for reaction IX gives a very accurate determination of its endothermicity and because the internal energies of the rovibrational states of DF[18] and the heats of formation of F[15(a)] and C_2D_4[19] are very well known, this is equivalent to deriving the heat of formation of the C_2D_3 radical. The angular distribution measured by Parson and Lee is shown in fig. 11 along with three calulated fits to the data. The solid curve is the best fit to the data using the $P(E_T)$ shown in fig. 12 and assuming a c.m. product angular distribution that is forward-backward symmetric. The dashed line and the dotted line in fig. 11 show the resulting fit to the data if the $P(E_T)$ is offset by + or - 0.5 kcal/mol respectively. This

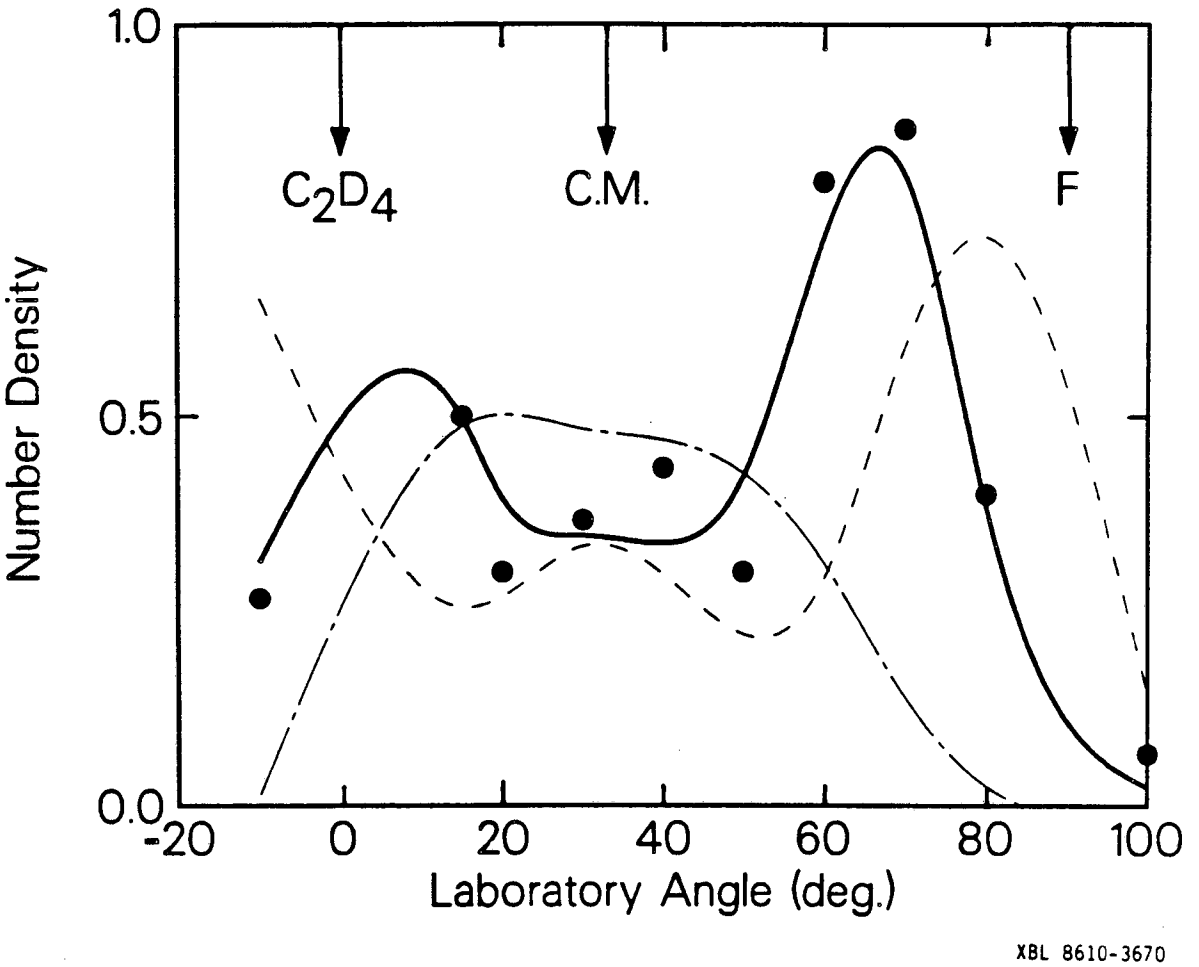

XBL 8610-3670

Fig. 11 Angular Distribution of the DF Product from the Reaction of $F + C_2D_4 \rightarrow C_2D_3 + DF(v'=4)$: The circle are the data points. The solid line shows the best fit to the data based on the $P(E_T)$ in fig. 12. Offsetting the $P(E_T)$ by ± 0.5 kcal gives the other two fits.

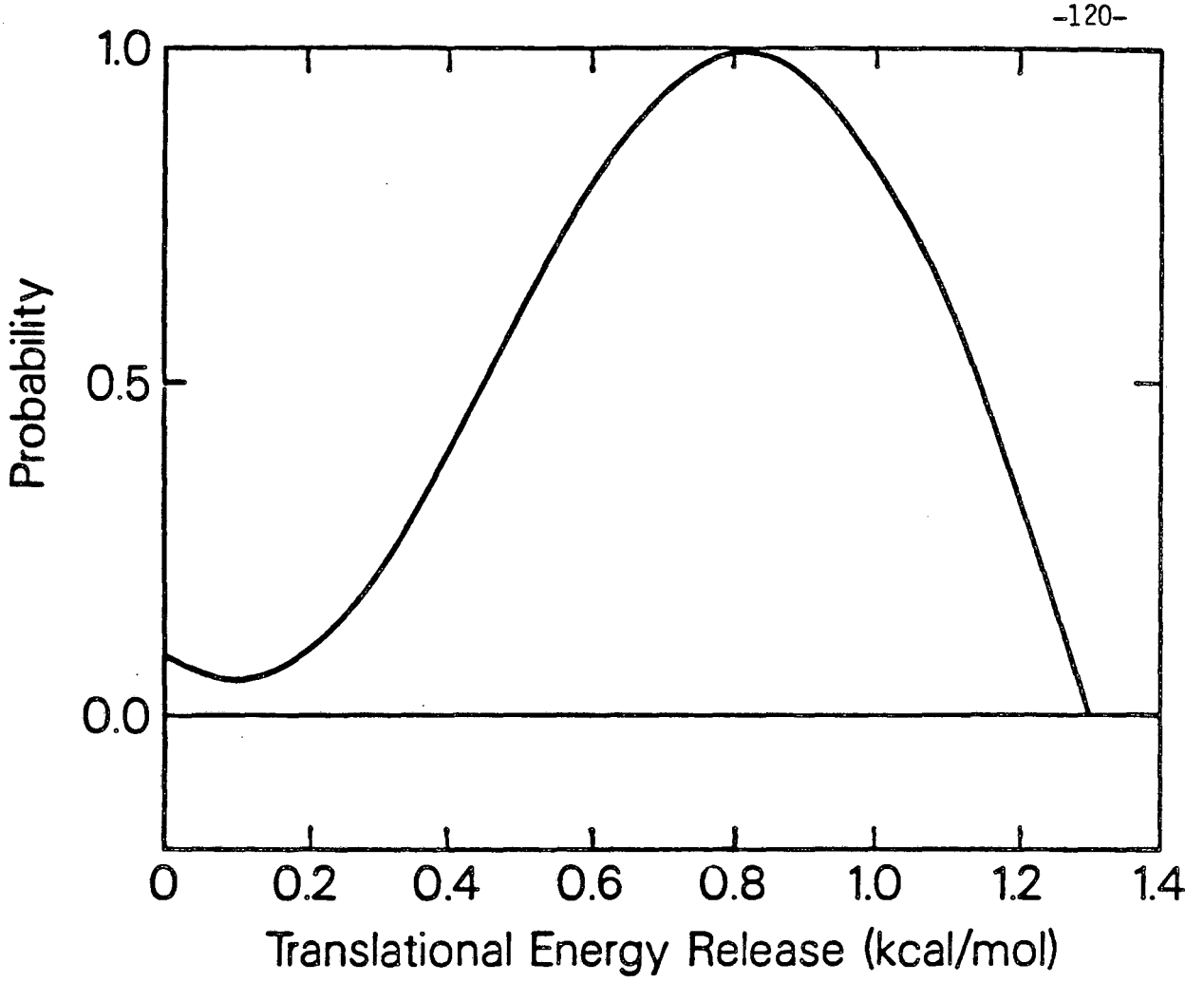

Fig. 12 Translational energy distribution for the products of reaction IX.

high sensitivity to the maximum release of translational energy accounts for the very high precision of the determination.

By working through a very similar analysis to that of the photodissociation experiment, one finds the heat of formation of C_2D_3 at 0°K to be 64.1 kcal/mol based on an experimental collision energy of 2.1 kcal/mol. By correcting for zero point energies, the heat of formation for C_2H_3 radical at 0°K is found to be 66.7 kcal/mol.[20] The precision of this result, ±0.5 kcal/mol, is not limited by our ability to determine E_T^{MAX} as much as it is by the spread of collision energies which arises from the velocity spreads of the molecular beams. Table I shows our result expressed in several different forms for the convenience of the reader.

Of course, we have no way to know from the crossed-beam experiment alone, that the assignment of the highest available vibrational state to DF(v'=4) is correct. If it is correct, we would predict that in the infrared chemiluminesence experiment of Sloan et. al[12] the highest rovibrational level observable from the reaction $F + C_2H_4 \longrightarrow HF + C_2H_3$ should be HF(v'=3,J'=3). This assumes 1.5RT of possible collision energy that may contribute to population of states of the product. This prediction is in excellent agreement with the observed experimental result.[12] In conclusion, we believe this determination of the heat of formation of the vinyl radical is the most accurate and precise value obtained to date.

Table I

Thermochemical Quantity[a]	C_2H_3	C_2D_3
$\Delta H^o_{f,0°K}$	66.7	64.1
$\Delta H^o_{f,298°K}$	65.7	63.1
$D_o^{0°K}(C_2X_3\text{-}X)$[b]	103.8	105.9
$D_o^{298°K}(C_2X_3\text{-}X)$[c]	105.3	107.4

a. Units are kcal/mol

b. This is C-H bond energy in C_2H_4 or C-D bond energy in C_2D_4

c. This is the enthalpy of the bond cleavage reaction at 298°K

Table I: Various Representations of the Heat of Formation of the Vinyl and the Perdeuterated Vinyl Radical.

D.3. The Identity of the Metastable State of C_2H_3.- As mentioned before, the slow tail on the m/e=27 TOF spectrum, fig. 1, is due to metastable C_2H_3. It is clear that if the internal energy of the photochemically produced vinyl radicals is in the form of molecular vibration, there will be nothing to keep it from decomposing at energies where signal directly attributable to vinyl radical at m/e=27 is still observed. However, since the $\tilde{A}^2A''$ state does not correllate adiabatically with ground electronic states of C_2H_2 + H, if the molecule were to be electronically excited, the decomposition rate could be very slow. Then the molecule might be able to survive long enough either to reach the detector or to fluoresce. If fluoresence is the deactivation mechanism, internal conversion to the $\tilde{X}^2A'$ state must occur on a time scale slower than about 50 μs based on the magnitude of the absorption cross-section.[14]

If this assignment is correct, the maximum release of translational energy for the formation of excited state vinyl radical is assigned to the point where the slope of the data begins to change, 29 ± 2 kcal/mol. Combining this with the reactive scattering result for the heat of formation of ground state C_2H_3 gives a $T_{oo}(\tilde{A}\leftarrow\tilde{X})$ of 46.4 ± 2.5 kcal/mol. We saw that even for the ground state where there was 75 kcal/mol available energy, the photodissociation method overestimated the bond dissociation energy by only ~4 kcal/mol. Since for the excited state there is less than half the available energy, we would expect the error to be proportionatly smaller. Also it is much

easier experimentally to distinguish a small difference in the translational energy release when the overall release is small.

As mentioned earlier, The absorption spectrum of the C_2H_3 radical in the 500 nm range has been observed and ab-initio calculations have verified the presence of an excited electronic state in the region of 2 eV.[14] The considerable change in geometry upon electronic excitation make it difficult to observe the (0→0) transition in absorption, however a 1205 cm^{-1} progression was observed and attributed to the C-C stretch in the A state. By extrapolating this progression, one obtains a predicted T_{oo} of 46.9 kcal/mol in excellent agreement with this work, assuming that the lowest observed transition is from v=0→v=3.

We have already seen that it is very reasonable to expect that the internal energy in C_2H_3 may be largely rotational. It is very interesting to ask what would be the expected lifetime of a molecule with enough rotational energy to dissociate but only a small amount of molecular vibration. One can imagine that as the C-H bond stretches, the centrifugal energy gets channeled into potential energy of the breaking bond, in the same way as a skater channels rotational energy into potential by extending his arms. At some point the bond will break and the C_2H_2 will rotate freely as the H atom departs. The point at which the two fragments decouple determines how much rotational energy will be left in the rotation. Ab-intio calculations place the saddle point in the PES at a C-H bond length of about 2Å. If this is really the point where the two fragments decouple, it will

be impossible to form the C_2H_2 product without substantial rotational energy. This would make the effective bond dissociation energy of the molecule substantially higher than the thermodynamic value and could give rise to a very long lifetime. This experiment points out the very interesting possibility that the unimolecular decomposition of highly rotationally excited molecules may have little to do with statistical theories of dissociation.

E. Conclusions.- In the photodissociaition of C_2H_3Br, the important collision-free dissociation processes were found to be the following.

$$C_2H_3{}^{81,79}Br \xrightarrow{193\ nm} C_2H_3 + {}^{81,79}Br(^2P_{3/2,1/2})$$

$$C_2H_3{}^{81,79}Br \xrightarrow{193\ nm} C_2H_2 + H^{81,79}Br$$

By finding the E_T^{MAX} for process V, an upper limit to the heat of formation of C_2H_3 was found. The results were compared to a very accurate determination based on measuring the E_T^{MAX} for the products of the reaction $F + C_2D_4 \rightarrow DF(v'=4) + C_2D_3$. The good agreement between the methods, despite the presence of many factors that could lead to difficulties with the photodissociation experiment is a good indication of the general usefulness of the method of photofragmentation translational spectroscopy in detemining thermodynamic quantities.

A metastable state of C_2H_3 was found to be formed in the photodissociation of C_2H_3Br. This is due either to electronically

or highly rotationally excited vinyl radical neither of which can decompose to ground state C_2H_2 + H within less than ~100 μs. If the interpretation of the metastable signal as observation of $C_2H_3(\tilde{A}^2A")$ is correct, we would derive an adiabatic electronic excitation energy, $T_{oo}(\tilde{A}\leftarrow\tilde{X})$, of 46.4 ± 2.5 kcal/mol.

REFERENCES

1. S. W. Benson, "Thermochemical Kinetics"; John Wiley and Sons: New York, 1976

2. D. F. Cooke, A. Williams, Symp. (Int.) Combust. [Proc.], 1971, 13, 757

3. C. J. Howard, J. Am. Chem. Soc., 1980, 102, 6937

4. J. Berkowitz, "Photoabsorption, Photoionization, and Photoelectron Spectroscopy"; Academic Press: New York, 1979, PP. 285-290

5. V. H. Dibeler, J. A. Walker, K. E. McCulloh, J. Chem. Phys., 1973, 59, 2264

6. One of these last two phenomena may explain why the I.P.(C_2H), derived from photoionization of C_2HCN, is substantially higher than that derived in ref. 5. See H. Okabe, V. H. Dibeler, J. Chem. Phys., 1973, 59, 2430

7. This is probably the cause of the discrepancy in the ionization potentials of ref. 6 and Y. Ono, C. Y. Ng, J. Chem. Phys., 1981, 74, 6985

8. A good example of this is the disagreement over the absolute proton affinity of NH_3 upon which a huge amount of proton affinity depends. See (a) S. T. Ceyer, P. W. Tiedemann, B. H. Mahan, Y. T. Lee, J. Chem. Phys., 1979, 70, 14 and (b) F. A. Houle, J. L. Beauchamp, J. Am. Chem. Soc., 1979, 101, 4067

9. A. H. Laufer, Rev. Chem. Int., 1981, 4, 225

10. A. M. Wodtke, Y. T. Lee, J. Phys. Chem., 1985, 89, 4744

11. J. M. Parson, Y. T. Lee, J. Chem. Phys., 1972, 56, 4658

12. (a) D. J. Donaldson, D. G. Watson, J. J. Sloan, Chem. Phys., 1982, 68, 95

13. (a) F. P. Lossing, Can. J. Chem., 1979, 49, 357; (b) D. J. DeFrees, R. T. McIver, W. J. Hehre, J. Am. Chem. Soc., 1980, 102, 3334; (c) J.H. Holmes, F. P. Lossing, Int. J. Mass Spectr. Ion Process, (1984) 58, 113; (d) A. F. Trottman-Dickenson, G. J. O. Verbeke, J. Chem. Soc., 1961, 2590; (e) G. A. Chappell, H. Shaw, J. Phys. Chem., 1968, 72, 4672; (f) D. M. Golden, S. W. Benson, Chem. Rev., 1969, 69, 125; (g) G. Ayranci, M. H. Back, Int. J. Chem. Kinet., 1983, 15, 83; (h) R. B Sharma, N. M. Semo, W. S. Koski, Int. J. Chem. Kinet., 1985, 17, 831

14. H. E. Hunzicker, H. Kneppe, A. D. McLean, P. Siegbahn, H. R. Wendt, Can. J. Chem., 1983, 61, 993

15. The heats of formation of C_2H_2, H, and Br can be found in (a) "Janaf Thermochemical Tables"; 2nd ed., D. R. Stull, H. Prophet eds., Nat. Stand. Ref. Data Ser., Nat. Bur. Stand., (1971), 37,: Obtainable from U.S. Govt. Printing Office, Wash., D.C. 20402. (order by cat. no. C 13.48:37). The heat of formation of C_2H_3Br is 22.26 kcal/mol and can be found in (b) J. Phys. Chem. Ref. Data (1982), 11, suppl. 2, p. 2-101

16. R.N. Zare, Mol. Photochem., 4, 1 (1972)

17. The theory of this phenomenon has been worked out by J.H. Ling, K.R. Wilson, J. Chem. Phys., 65, 881 (1976)

18. K.P. Huber, G. Herzberg, "Molecular Spectra and Molecular Structure IV. Constants of Diatomic Molecules"; Van Nostrand and Reinhold Co.: New York, 1979

19. The heat of formation of C_2D_4 was obtained by correcting the difference in zero point energies between C_2H_4 and C_2D_4. The heat of formation for C_2H_4, can be found in ref. 15 (a) and the vibrational frequencies of C_2H_4 and C_2D_4 can be found in: L. M. Sverdlov, M. A. Kovner, E. P. Krainov, "Vibrational Spectra of Polyatomic Molecules"; John Wiley and Sons: New York, 1945, pp. 414-426

20. The zero point energies of C_2H_3 and C_2D_3 were estimated by using the vibrational frequencies of C_2H_4 and C_2D_4, see ref. 19, ommiting one C-H or C-D stretch and two C-C-H or C-C-D bends.

CHAPTER V: The Infrared Multiphoton Dissociation of Three Nitroalkanes

A. Background Information.- The discovery of infra-red, multiple-photon absorption (IRMPA) and dissociation (IRMPD) in isolated polyatomic molecules raised great hopes that one could direct chemical reactions, since IRMPA allows one to put a great deal of energy directly into the nuclear motion of a polyatomic molecule through a specific vibrational degree of freedom.[1-5] The subsequent discovery that IRMPD could be isotopically selective,[6-8] aroused continued enthusiasm among some scientists about the possibilities of bond selective chemistry. A plethora of review articles has appeared on these and related topics.[9] It is now generally realized that the quest for mode specific chemistry by

IRMPD is not technologically possible because of very fast intramolecular vibrational redistribution (IVR) in highly vibrationally excited polyatomic molecules. Several experiments have shown that this typically occurs on a picosecond time scale or faster.[10,11] The profound implications of this can be appreciated if one realizes that even for strong IR absorbers ($\sigma = 10^{-17}$ cm^2) and intense IR sources (I = 10^{26} photons cm^{-2} sec^{-1}), the average time it takes to absorb a single photon is 10^{-9} sec.

In spite of the "problem" of picosecond IVR, in fact because of it, there are certain advantages to studying the dissociation of polyatomic molecules by IRMPD. The first of these is that statistical theories of unimolecular decomposition[12] which assume the free flow of vibrational energy in the dissociating molecule can be used to describe the dissociation process and thus interpret experimental results. The validity and usefulness of various statistical theories, especially the most commonly used RRKM theory, have been widely documented in the literature.[13-18]

The second advantage to studying IRMPD stems from the ability to "thermally heat" isolated molecules by IRMPA. This can be done either at low pressure in a gas cell or in the collision free environment of a molecular beam. While it is true, as has been pointed out, that IRMPA does not give rise to a vibrational population distribution that can be characterized by a temperature,[19] the difference between the population distribution created by IRMPA and that created by true thermal heating is not substantial. A coupled set of differential

rate equations can be solved to quantitatively determine these IRMPA induced "thermal" distributions of total vibrational energy based on IR absorption cross sections as a function of vibrational energy.[19] This offers the very intriguing possibility of quantitatively accounting for the differences between thermal, collisional experiments which measure phenomenological quantities such as activation energies and IRMPD, molecular beam experiments which measure microscopic quantities such as potential energy barriers and do not use the concept of temperature.

One important class of reactions where RRKM theory cannot be used to predict product energy distributions is that of concerted molecular elimination reactions.[20] In this case the transition state is generally at the top of a substantial, mechanical barrier in the potential energy surface (PES). The detailed dynamics which occur as the reaction proceeds down the exit barrier must be taken into consideration if one wishes to understand the product energy distribution. In general, a large fraction of the exit barrier is converted into product kinetic energy and the translational energy distribution peaks well away from zero, in contrast to simple bond rupture reactions with no exit barrier, whose translational energy distributions typically peak at zero. Consequently, the presence of an exit barrier in the PES can be easily determined by a direct measurement of the product translational energy distribution.

In this chapter we will present an application of some of these ideas to the understanding of the energetics and dynamics of the

competition between two decay channels in three prototypical nitro-compounds. In these molecules simple bond rupture competes with isomerization or concerted dissociation. Because RRKM theory can predict the translational energy distribution for simple bond rupture reactions based on the internal energy of the dissociating molecules, we can use the measured translational energy distributions for simple bond rupture reactions as a "thermometer" to derive information on the average level of internal excitation in the dissociating molecules. With this information the potential energy barrier for isomerization or concerted dissociation can be obtained based on the measured branching ratio of the two dissociation channels.

Three nitroalkanes: nitromethane (CH_3NO_2), nitroethane ($C_2H_5NO_2$) and 2-nitropropane ($CH_3CHNO_2CH_3$) have been investigated in the collision free environment of a molecular beam. The work on nitromethane has been reported cursorily before.[21] We were interested to see if there was any validity to the suggestion of an exit barrier for simple C-N bond rupture.[22] In addition, we wanted to look for the isomerization channel to methylnitrite, CH_3ONO, and subsequent dissociation to CH_3O and NO that had been predicted theoretically.[23,24] With the application of RRKM theory, a branching ratio measurement between simple bond rupture and isomerization would then provide information upon which a good estimation of the barrier height to isomerization could be made.

Our interest in nitroethane and 2-nitropropane was due to the fact that in these two systems simple bond rupture and concerted

molecular elimination occur competitively. This allows us to study the translational energy release for concerted molecular elimination reactions through a five membered ring transition state. The nitroethane experiment also provided us with a way to test the reliability of our branching ratio matching approach to the determination of the barrier height to isomerization in nitromethane, since the method can easily be applied to the determination of the barrier height to concerted molecular elimination in nitroethane, a quantity that is quite well known from activation energy measurements.

B. Experimental Supplement.- The experimental apparatus is identical to that described in chapter II. The laser used in these experiment was a GENTEC, TEA, pulsed CO_2 laser operating on the R(20) line of the 9.6 μm branch. Typically, the laser emmited 200 mJ/pulse of unpolarized light at 35 Hz and the output was focussed down to a 0.06 cm diameter circular spot to give a laser fluence of ~75 J/cm^2. The laser pulse had the characteristic 200 nsec "spike" of IR emmission followed by a 600 nsec tail.

Due to the low translational energy release in many of the reactions studied in these experiments it was neccesary to obtain data close to the molecular beam. Therefore all of the data were taken at 10° from the molecular beam. In order to lower the background which at this angle mainly originates from effusion at the second skimmer of the molecular beam source, an extra defining slit (circular, 0.4 cm dia.) was placed 3.81 cm from the interaction region, between the

interaction region and the detector. This had the effect of cutting out 80 percent of the background without losing any signal by limiting the viewing window of the detector to the minimum necessary to "see" the entire interaction region.

The chemicals used in these experiments were commercially obtained and used without purification. The characteristics of the molecular beams used are shown in table I.

C. Results and Data Analysis.- The data in this experiment appear in three forms. First, the mass spectra of the laser induced dissociation products contain information on the identity of the collision free dissociation pathways. Second, the intensities of the signal at each mass (actually m/e) yield information on the branching ratios of competing dissociation channels. Third, the TOF spectrum for each mass is reflective of the translational energy distribution of the products of each channel. Although we normally measure the TOF spectra of both recoiling fragments of a given dissociation channel, in principle this is not necessary since in the center-of-mass (c.m.) frame, the velocity of the second fragment can be obtained from the first by conservation of linear momentum. In practice, because we do measure the TOF spectra of each fragment we can use the conservation of linear momentum to unambiguously determine which products belong to the same dissociation channel in complex reaction systems with more than one important decomposition pathway. This is extremely important

Table I

Parent Molecule	Stagnation[a] Temperature	Stagnation[b] Pressure	Percent Parent[c] in Beam	Nominal[d] Velocity	$\frac{\Delta V}{V}$[e]
CH_3NO_2	308°C	140 torr	17	1.3×10^5	.22
$C_2H_5NO_2$	345°C	170 torr	13	1.4×10^5	.18
$2\text{-}C_3H_7NO_2$	358°C	200 torr	12	1.4×10^5	.17

a. Same as nozzle temperature.

b. Pressure immediately behind nozzle.

c. All molecules were seeded in Helium.

d. Units are cm/sec.

e. (full width at half maximum) ÷ (Nominal beam velocity).

Table I: Experimental Conditions of Parent Molecular Beams.

when dissocation products do not yield parent ions due to fragmentation in the ionizer.

C.1. IRMPD of CH_3NO_2.- Table II lists the IRMPD mass spectrum of nitromethane. Signal was observed at m/e = 46, 30, 29, 15. The TOF spectrum of m/e=46 (NO_2^+), shown in fig. 1a, is from NO_2 produced in reaction I.

$$CH_3NO_2 \xrightarrow{nh\nu} CH_3NO_2^{\ddagger} \longrightarrow CH_3 + NO_2 \qquad (I)$$

The TOF spectrum for m/e=15 (CH_3^+) which is from CH_3 radical product in reaction I is shown in fig. 1b.

The solid lines drawn through the m/e=46 and 15 TOF spectra are both calculated from the $P(E_T)$ for reaction I shown in fig. 2 which is characteristic of the translational energy distribution of a simple bond rupture reaction with no exit barrier, that is, it peaks at zero and releases on the average only a small amount of translational energy. The arrows in the TOF spectra mark the expected arrival time of the parent molecules if they were to travel in the same direction as the products. The small release of translational energy is indicated by the closeness of the observed TOF signal to the arrow. Because of the nature of electron-impact ionization, there will be substantial fragmentation of the NO_2 to NO^+ which should be detectable at m/e=30. The m/e=30 TOF spectrum is shown in fig. 1c. The dashed curve shows the contribution to this TOF spectrum from NO_2 which fragments to NO^+ in the ionizer, calculated from the

Table II

m/e	Identity of Ion	Product Detected	Signal(a) Intensity
46	NO_2^+	NO_2	0.05
15	CH_3^+	CH_3	0.14
30	NO^+	NO_2	0.11
30	NO^+	NO	0.06
30	CH_2O^+	CH_3O	0.08
29	HCO^+	CH_3O	0.02

a. units are (ion counts/laser shot)

Table II: IRMPD Mass Spectrum of Nitromethane.

Fig. 1 TOF Spectra from the IRMPD of Nitromethane: The circles are the data and the solid lines are the fit to the data using the forward convolution method. Data was taken at 10° from the molecular beam. (a) NO_2 product from reaction I. (b) CH_3 product from reaction I. (c) NO_2 product from reaction I (---), NO as well as CH_3O product from reaction II (-·-·-). (d) CH_3O product from reaction II observed as HCO^+ (see ref. 25).

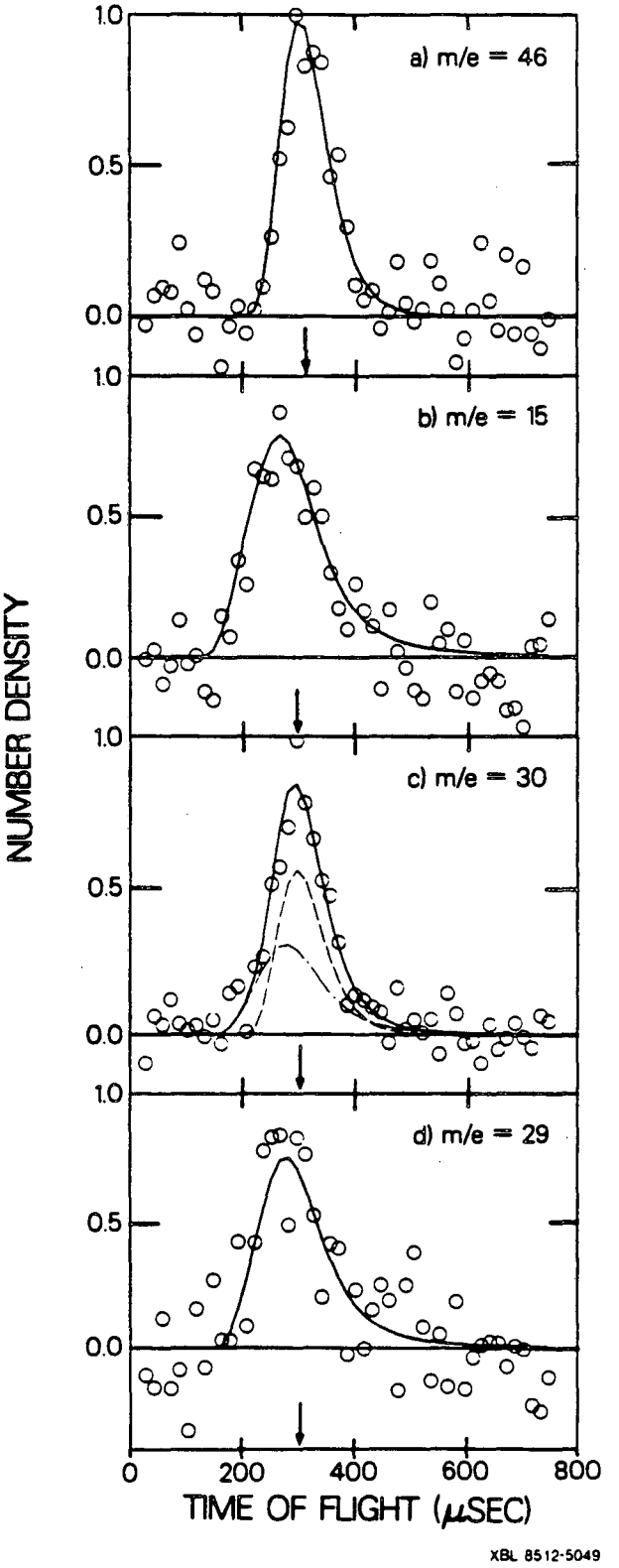
a) m/e = 46
b) m/e = 15
c) m/e = 30
d) m/e = 29
1.0
0.5
0.0
NUMBER DENSITY
0
200
400
600
800
TIME OF FLIGHT (μSEC)
XBL 8512-5049

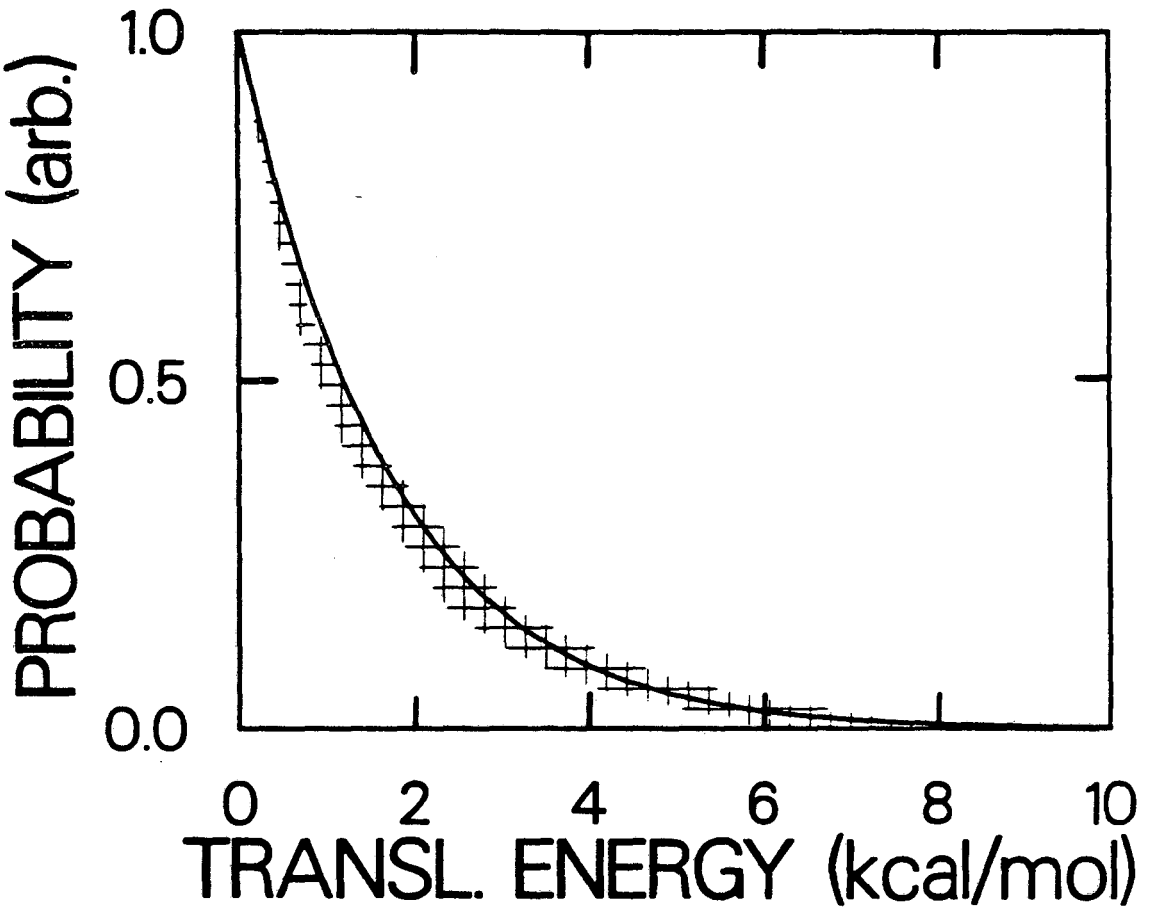

XBL 8512-5042

Fig. 2 Translational Energy Distribution of the Products of Reaction I: The cross-hatched area represents the uncertainty associated with the measurement and the solid line is the result of the model calculation described in section D.1..

$P(E_T)$ in fig. 2. Careful inspection of the experimental data reveals that while the falling edge of the TOF spectrum is accurately simulated by the dashed curve in fig. 1c, there is an indication of substantial signal coming faster than the dashed curve which cannot be explained by reaction I alone. This is not at all surprising because the observation of a second reaction channel yielding m/e=29 (HCO^+), shown in fig. 1d, which cannot be formed by any of the products of reaction I, implies that there is a second source of NO^+. Recently it has been suggested that the barrier to isomerization of nitromethane to methylnitrite (CH_3ONO) may be low enough to compete with reaction I.[23,24] Due to the fact that the endoergicity of CH_3O + NO formation is lower than the barrier height to isomerization (see section IV. A.), isomerized CH_3ONO should contain enough internal energy to dissociate and manifest itself in the production of NO (which would appear at m/e=30) and CH_3O (which would appear at m/e=30 and 29), which is exactly what has been observed.

$$CH_3NO_2^{\ddagger} \longrightarrow CH_3ONO^{\ddagger} \longrightarrow CH_3O + NO \qquad (II)$$

If we are observing CH_3O product one might expect signal at m/e=31 (CH_3O^+). However, because electron impact ionization produces ions that are, at least initially, in the same geometrical configuration as the neutrals, i.e. a vertical transition, CH_3O^+ (methoxy cation) produced by electron impact ionization is not stable and will spontaneously decompose to form HCO^+ and H_2. The most

stable form of the ion with the chemical formula CH_3O^+ is protonated formaldehyde (H_2COH^+) and not methoxy cation.[25] If reaction II is occurring, the fast part of the m/e=30 TOF spectrum that cannot be fit with reaction I alone must be momentum-matched in the c.m. coordinate system to the m/e=29 TOF spectrum through the mass ratio of the products of reaction II. By using the $P(E_T)$ shown in fig. 3 which releases somewhat more translational energy than the one for reaction I, it is possible to calculate the dashed-dot curve in the m/e=30 TOF spectrum and the solid line in the m/e=29 TOF spectrum. The $P(E_T)$ for formation of CH_3O and NO should peak at zero for the same reason that the $P(E_T)$ for the IRMPD of CH_3ONO would. This and the resulting good fit to the data confirm the existence of reaction II. Previously the formation of CH_3O has been assumed to proceed through secondary reaction of CH_3O with NO_2.[26] This is the first experimental evidence for the primary production of CH_3O in the unimolecular decomposition of CH_3NO_2.

We obtain the branching ratio of reaction II to reaction I by comparing the amount of NO_2 to NO formed, measured at m/e=30. The expression for the branching ratio is shown by equation (1) which contains the proper transformation Jacobian between the lab frame and the c.m. frame for isotropic product angular distributions. Such distributions would be expected for IRMPD in which an unpolarized laser is used.

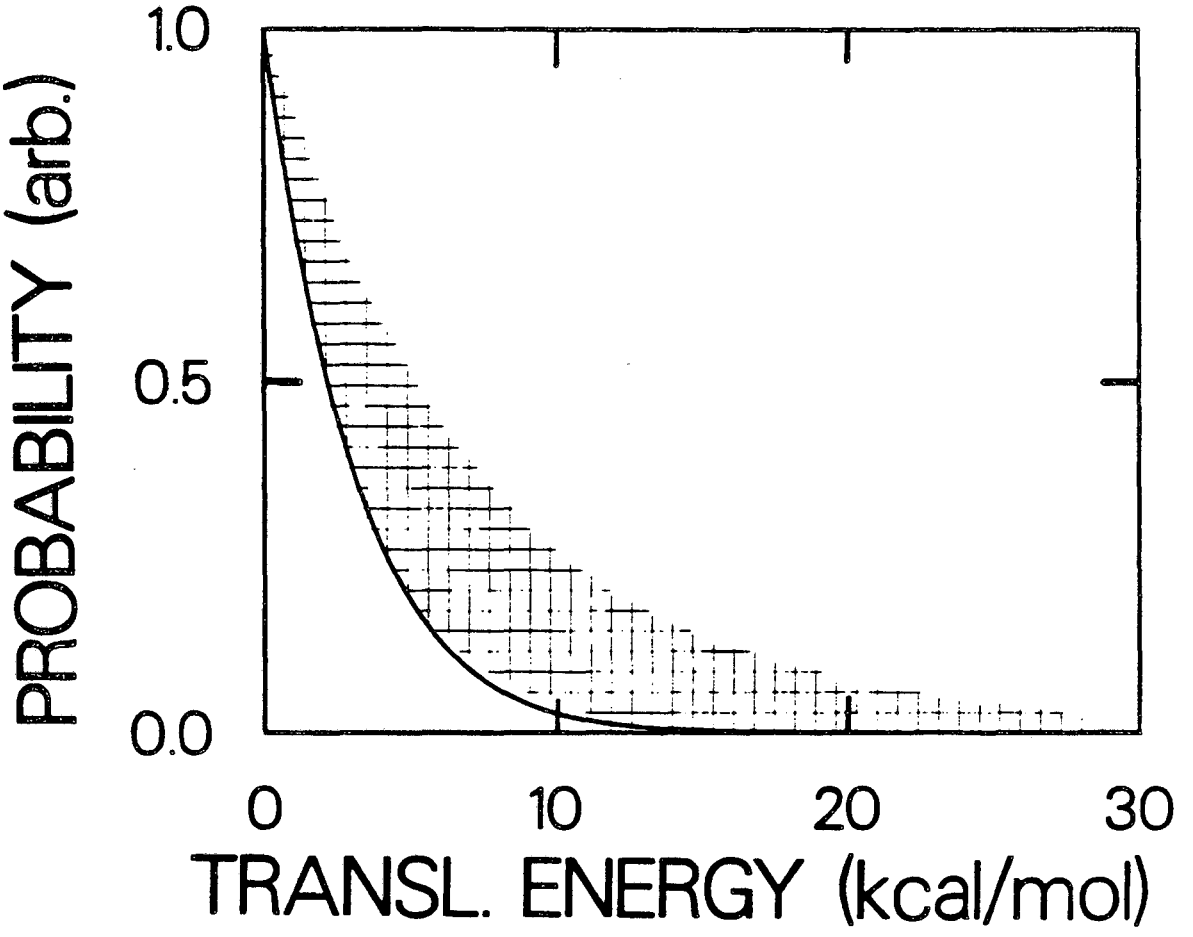

Fig. 3 Translational Energy Distribution of the Products of Reaction II: See caption of fig. 2.

$$R = \frac{N_{NO^+/NO}(10^\circ)\ \sigma_{ion}(NO_2)\ F(NO^+/NO_2)\ (31)(46)}{N_{NO^+/NO_2}(10^\circ)\ \sigma_{ion}(NO)\ F(NO^+/NO)\ \ (15)(30)} \frac{\int P_I(E_T)\ \frac{v_{NO_2}}{u_{NO_2}}\ dv_{NO_2}}{\int P_{II}(E_T)\ \frac{v_{NO}}{u_{NO}}\ dv_{NO}} \qquad (1)$$

where:

R = Branching ratio (Reaction II/Reaction I)

$N_{NO^+/NO_X}(\theta)$ = Time integrated TOF signal (number density of NO_X) appearing as NO^+ at a detector angle measured from the direction of the beam.

$\sigma_{ion}(NO_X)$ = electron impact ionization cross section for NO_X.

$F(NO^+/NO_X)$ = fraction of NO_X that fragments to NO^+ in the ionizer.

v_{NO_X} = lab frame velocity of NO_X.

u_{NO_X} = c.m. frame velocity of NO_X.

The ionization cross sections used in this calculation are derived from the empirical formula of Center and Mandl.[27]

$$\sigma_{ion} = [36(\alpha)^{0.5} - 18]\ \text{Å}^2 \qquad (2)$$

where α is the molecular polarizability in Å^3

By plugging in the measured values and performing the indicated integrals, a branching ratio of 0.6 in favor of reaction I is obtained. In this calculation, the fraction of the fast component of mass 30 that is NO^+, as opposed to CH_2O^+ is calculated to be

0.41 by requiring that in the c.m. frame, the sum of the mass 29 signal and the part of the fast contribution to mass 30 that is CH_2O^+ must equal the amount of the fast contribution to mass 30 that is NO^+ when corrected for ionization cross sections. In other words, it is required that for each NO molecule that is formed there must be one CH_3O molecule and it is assumed that ions from CH_3O only appear at masses 29 and 30.

C.2. IRMPD of $C_2H_5NO_2$.- Table III shows the IRMPD mass spectrum of nitroethane. Signal was observed at m/e=46, 30, 29, 28, 27, and 26. The TOF spectra for these masses are shown in fig. 4a-e. The m/e=28 spectrum is not shown since, due to the large background in the detector at this mass it is impossible to obtain any useful information from this TOF spectrum. Fig. 4a shows the m/e=46 (NO_2^+) TOF spectrum and, analagously to the nitromethane case, is unambiguous evidence for the C-N bond rupture channel in the collision free unimolecular decomposition of nitroethane.

$$C_2H_5NO_2 \xrightarrow{nh\nu} C_2H_5NO_2^{\ddagger} \longrightarrow C_2H_5 + NO_2 \qquad \text{(III)}$$

The $P(E_T)$ for reaction III, shown in fig. 5, generates the solid lines shown in the m/e=46 (NO_2^+) and m/e=29 ($C_2H_5^+$) TOF spectra. Further verification of this assignment is given by the fact that the slow part of the m/e=30 TOF spectrum (shown as the dashed curve) is fit simply assuming fragmentation in the ionizer of NO_2 to NO^+. Similarly, the slow parts of the m/e=27 and 26 TOF spectra (shown as

Table III

m/e	Identity of Ion	Product Detected	Signal(a) Intensity
46	NO_2^+	NO_2	0.03
30	NO^+	NO_2	0.14
30	NO^+	HONO	0.02
29	$C_2H_5^+$	C_2H_5	0.09
27	$C_2H_3^+$	C_2H_5	0.07
27	$C_2H_3^+$	C_2H_4	.002
26	$C_2H_2^+$	C_2H_5	0.07
26	$C_2H_2^+$	C_2H_4	0.01

a. Units are (ion counts/laser shot)

Table III: IRMPD Mass Spectrum of Nitroethane.

Fig. 4 TOF Spectra from the IRMPD of Nitroethane: See caption of fig. 1. (a) NO_2 product of reaction III. (b) C_2H_5 product of reaction III. (c) NO_2 product of reaction III (---), HONO product of reaction IV (-·-·-). (d-e) C_2H_5 product of reaction III (---), C_2H_4 product of reaction IV (-·-·-)

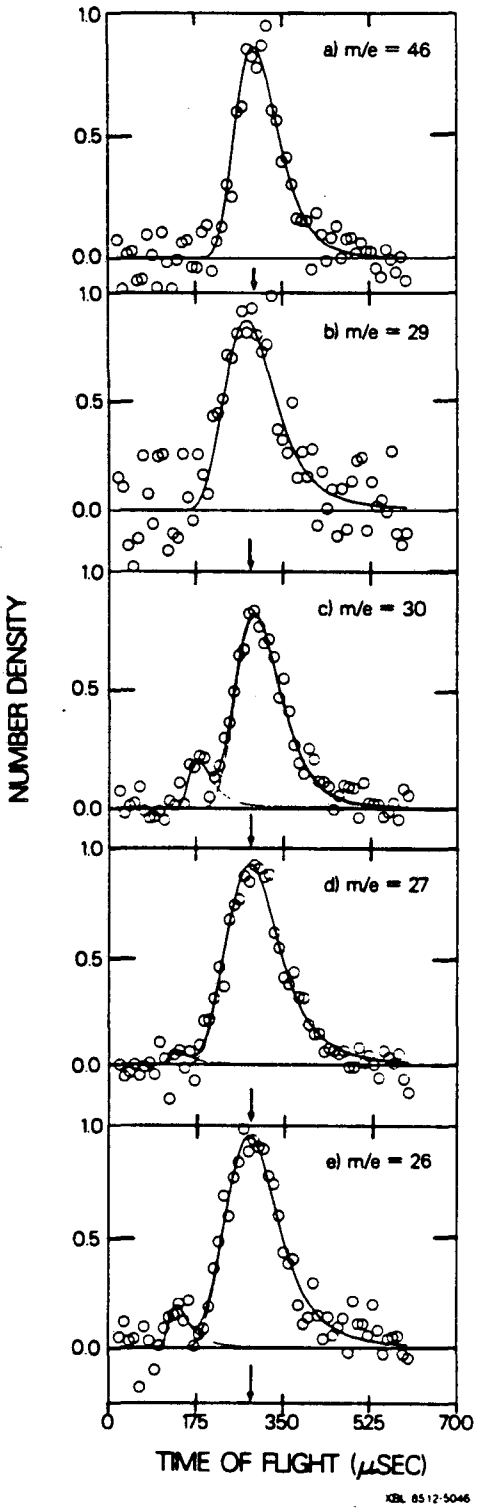
a) m/e = 46
b) m/e = 29
c) m/e = 30
d) m/e = 27
e) m/e = 26
1.0
0.5
0.0
NUMBER DENSITY
0
175
350
525
700
TIME OF FLIGHT (μSEC)
XBL 8512-5046

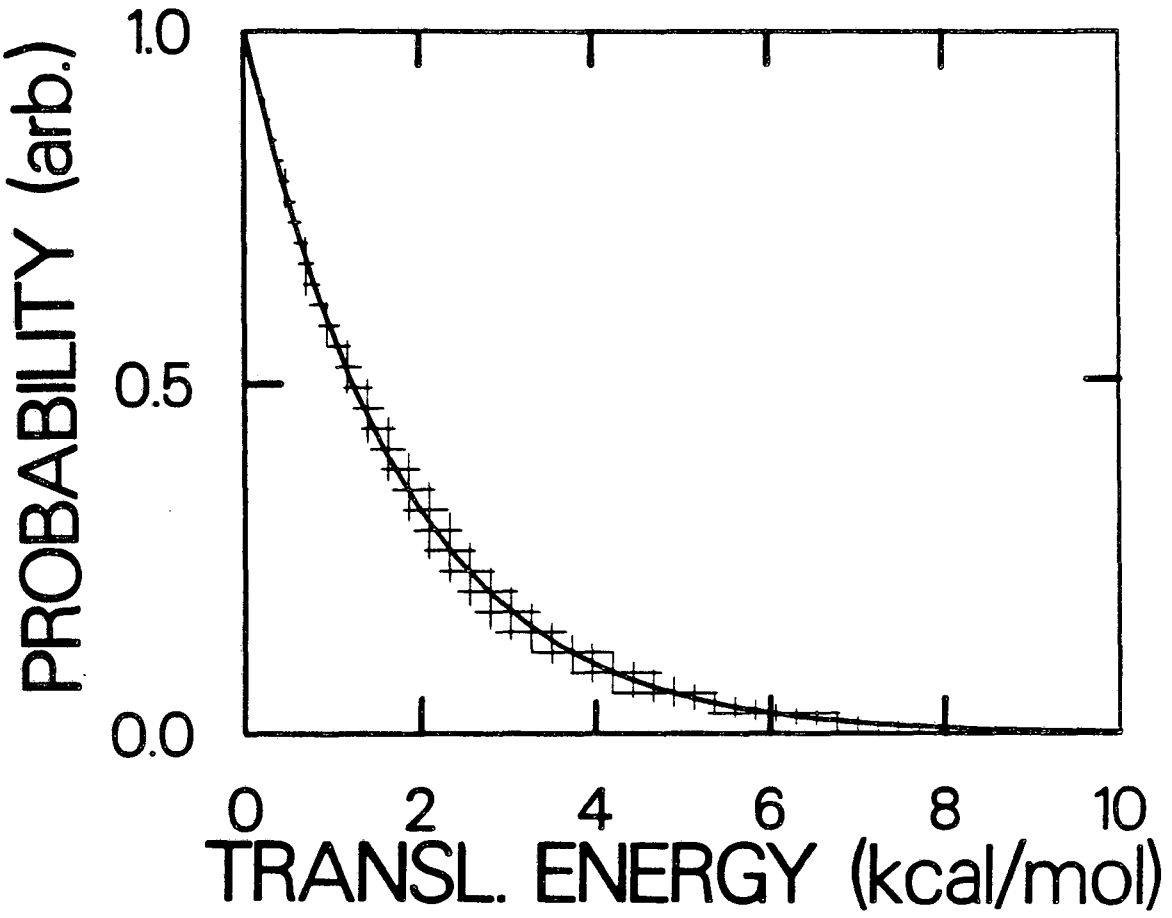

XBL 8512-5045

Fig. 5 Translational Energy Distribution of the Products of Reaction III: See caption of fig. 2. Solid line is the result of the model calculation described in section D.2..

dashed curves) are based on the fragmentation in the ionizer of ethyl radical to these masses.

One can see from the m/e=30, 27 and 26 TOF spectra that there is also a second reaction channel appearing which is releasing a much larger amount of translational energy than reaction III. It is known from thermal decomposition studies that reaction IV is a low energy decomposition pathway.[28]

$$C_2H_5NO_2 \longrightarrow C_2H_4 + HONO \qquad (IV)$$

This reaction occurs through a five-membered cyclic transition state and forms products which are substantially more stable than the radical products of reaction III. The activation energy is 45 kcal/mol.[28] Comparing this to an endothermicity of 18 kcal/mol, it is clear that the PES must have a substantial exit barrier. Therefore, it is not surprising that the products of reaction IV should be formed with qualitatively more translational energy than the products of reaction III. The TOF spectra of the fast products can be fit by a single $P(E_T)$ shown in fig. 6, assuming reaction IV to be their source. This argument is based on the assumption that ethyl radical appears at m/e = 29, 28, 27, 26; that ethylene appears at 28, 27, 26 and that HONO is observed only at 30. While it is clear that the observed mass spectra of ethyl radical and ethylene are reasonable, as far as we can tell, the mass spectrum of HONO has never been measured. By comparison with the mass spectrum of methylnitrite

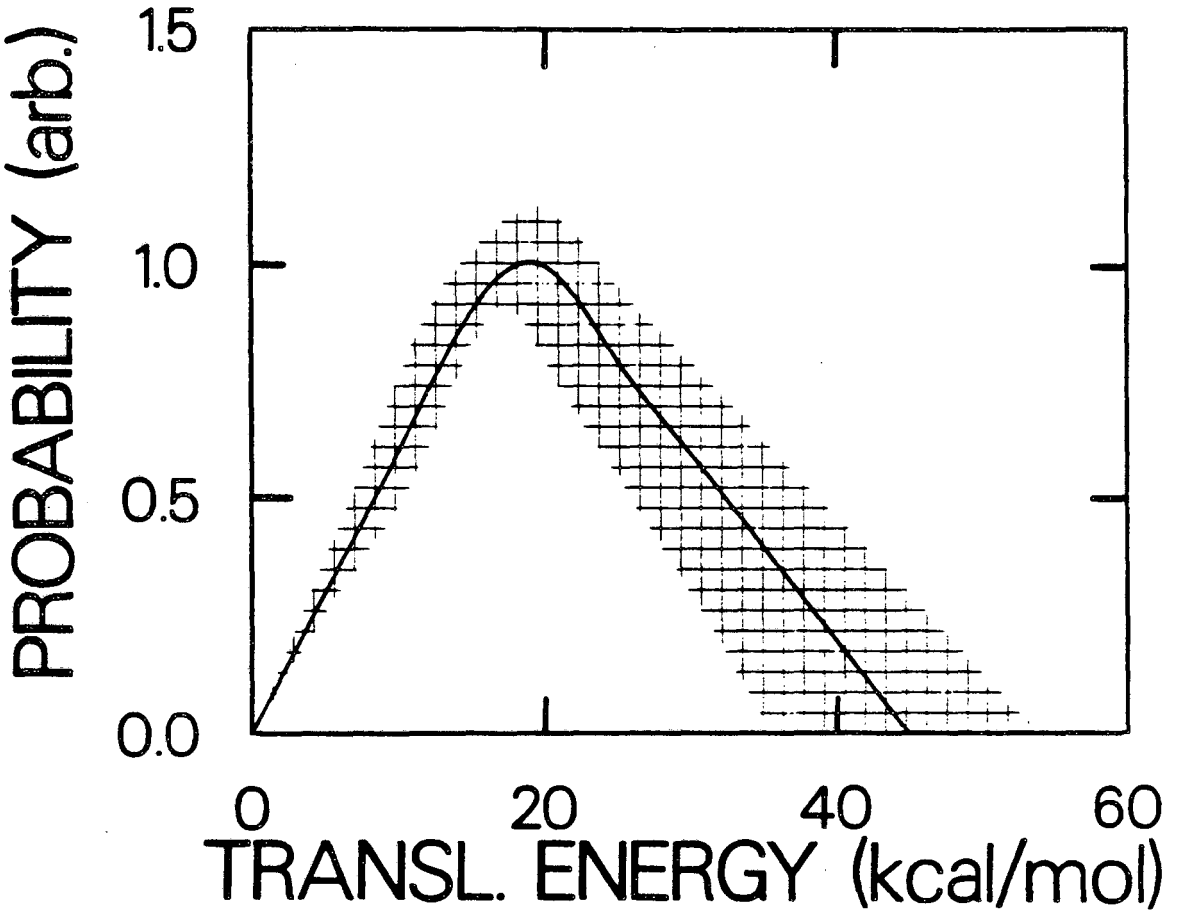

XBL 8512-5041

Fig. 6 Translational Energy Distribution of the Products of Reaction IV: The cross hatching represents the uncertainty associated with the measurement and the solid line is the $P(E_T)$ which gives the best fit to the data.

(the methyl ester of HONO), which gives no parent or mass 46,[29] it seems reasonable that HONO also should appear mainly at m/e=30.

The branching ratio between reactions III and IV can be calculated in the same way as was done above for nitromethane based on analysis of the m/e=30 TOF spectrum. The derived branching ratio of reaction IV to reaction III is 0.5 in favor of C-N bond rupture.

C.3. IRMPD of $2\text{-}C_3H_7NO_2$.- The IRMPD mass spectrum of 2-nitropropane is shown in table IV. The data is completely analagous to the nitroethane system. There is clear evidence for the simple bond rupture reaction V

$$CH_3\underset{\displaystyle NO_2}{\underset{|}{C}}HCH_3 \xrightarrow{nh\nu} CH_3\overset{\ddagger}{\underset{\displaystyle NO_2}{\underset{|}{C}}}HCH_3 \longrightarrow CH_3CHCH_3 + NO_2 \qquad (V)$$

in the m/e=46 (NO_2) TOF spectrum shown in fig. 7a which is momentum matched in the c.m. frame to the m/e=43 (2-propyl radical) TOF spectrum shown in fig. 7b. Both of these TOF spectra are fit by the $P(E_T)$ shown in fig. 8. The m/e=41 TOF spectrum shown in fig 7c, and the m/e=30 TOF spectrum shown in fig. 7d both show products which are appearing with a great deal of translational energy release, and it is clear that this is evidence for HONO elimination in 2-nitropropane, exactly as in nitroethane.

$$CH_3\underset{\displaystyle NO_2}{\underset{|}{C}}H\,CH_3 \xrightarrow{nh\nu} CH_3\overset{\ddagger}{\underset{\displaystyle NO_2}{\underset{|}{C}}}H\,CH_3 \longrightarrow CH_2{=}CH{-}CH_3 + HONO \qquad (VI)$$

Table IV

m/e	Identity of Ion	Product Detected	Signal(a) Intensity
46	NO_2^+	NO_2	0.04
43	$C_3H_7^+$	C_3H_7	0.10
41	$C_3H_5^+$	C_3H_7	0.11
41	$C_3H_5^+$	C_3H_6	0.01
30	NO^+	NO_2	0.25
30	NO^+	HONO	0.06

a. Units are (ion counts/laser shot)

Table IV: IRMPD Mass Spectrum of 2-Nitropropane.

Fig. 7 TOF Spectra from the IRMPD of 2-Nitropropane: See caption of fig. 1. (a) NO_2 product of reaction V. (b) C_3H_7 product of reaction V. (c) C_3H_7 product of reaction V (---), C_3H_6 product of reaction VI (-·-·-). (d) NO_2 product of reaction V (---), HONO product of reaction VI (-·-·-).

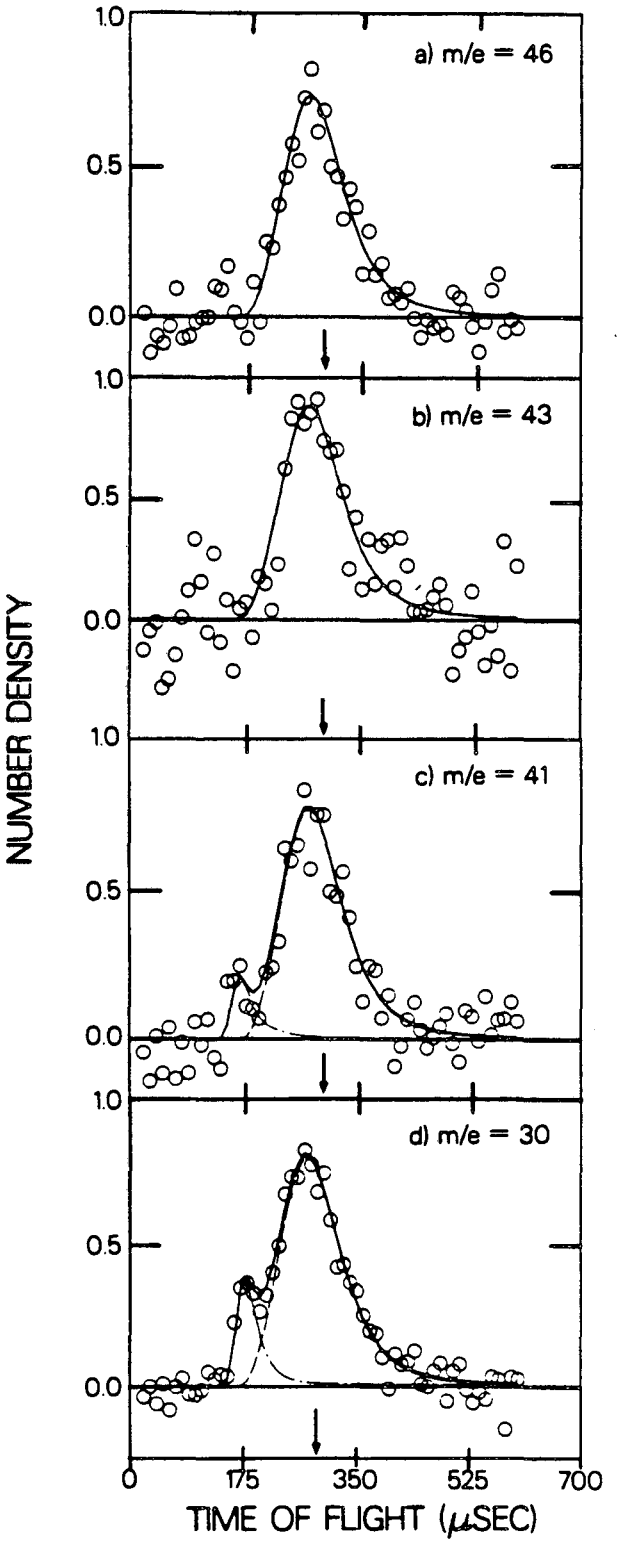
a) m/e = 46
b) m/e = 43
c) m/e = 41
d) m/e = 30
1.0
0.5
0.0
NUMBER DENSITY
0
175
350
525
700
TIME OF FLIGHT (μSEC)
XBL 8512-5048

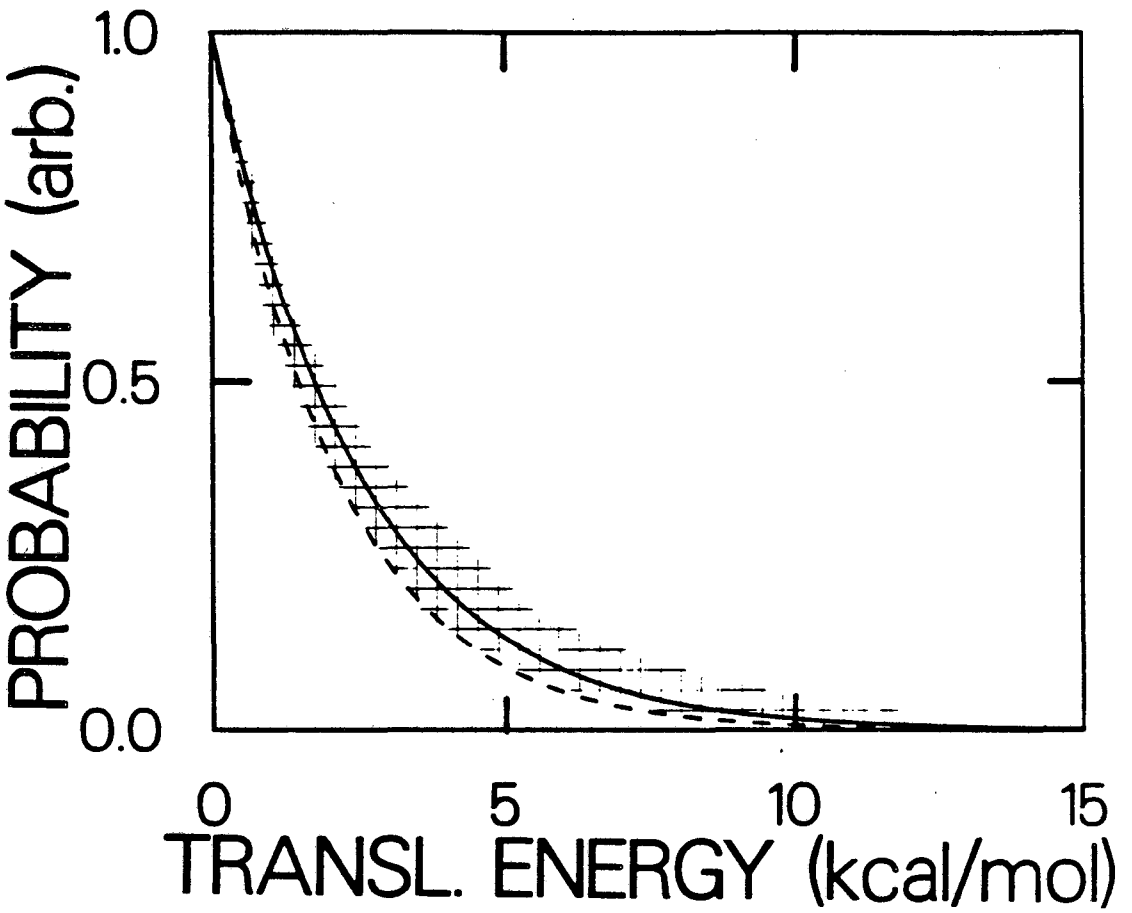

Fig. 8 Translational Energy Distribution of the Products of Reaction V: See caption of fig. 2. The dashed line is the result of the model calculation using absorption cross-sections in the OC of 0.25 x 10^{-19} cm^2 as described in section D.2..

The $P(E_T)$ for reaction VI is shown in fig. 9.

The branching ratio between reaction V and reaction VI can be found by comparing the amount of NO_2 formed to the amount of HONO that is formed just as in the case of nitroethane. This can be done by analysis of the mass 30 TOF spectrum, the fast component of which is due to HONO and the slow component of which is due to NO_2. By knowing the fragmentation pattern of NO_2, which we measured, and by using equations 1 and 2 (see above) we arrive at a branching ratio of 0.5 in favor of simple C-N bond rupture.

D. Discussion.- Because of the ability of RRKM theory to calculate both internal and translational energy distributions of products from simple bond rupture reactions without exit channel potential energy barriers,[30] given the total internal energy of the dissociating parent, we can use measured translational energy release distributions of simple bond rupture reactions to work backward and obtain information on the level of internal excitation in the dissociating parent molecule. Of course, in an IRMPD experiment the measured translational energy release distribution is the result of parent molecules dissociating with a range of internal energies, determined by the competition between photon absorption, stimulated emission and dissociation of excited molecules. In order to treat this problem in an adequate way, it is necessary to model the competing rate processes in detail. We first calculate the simple bond rupture product yield probability distribution as a function of

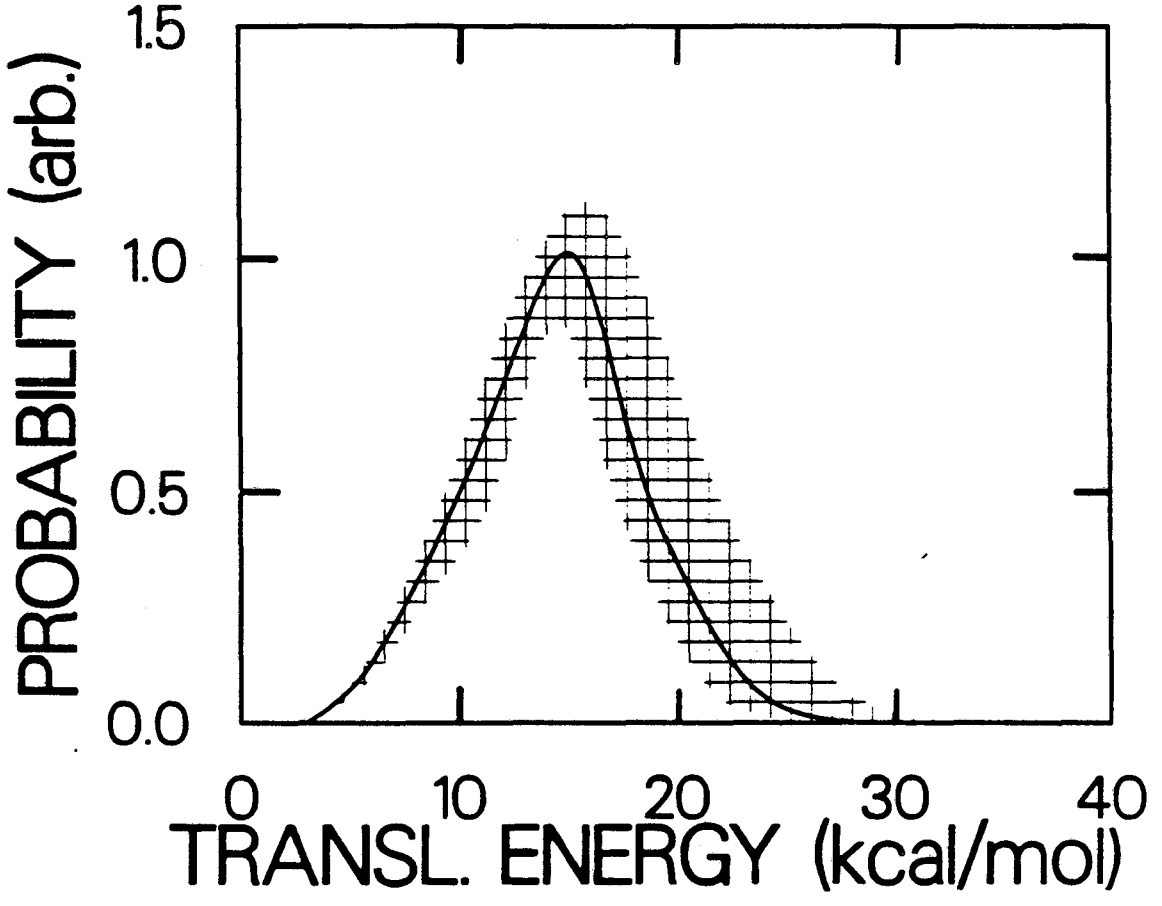

XBL 8512-5039

Fig. 9 Translational Energy Distribution of the Products of Reaction VI: See caption of fig 6.

the level of excitation of the dissociating molecules by using a computer program which solves the system of coupled differential rate equations which governs the IRMPD process. We then combine these results with RRKM theory which calculates the translational energy distributions of products dissociating from various levels of excitation. Calculating the weighted average over the product yield distribution of the RRKM $P(E_T)$'s gives a result that can be compared to experiment.[31]

In order to do this one must know the dissociation rate constants for levels above the dissociation limit. The technique for obtaining these values from RRKM theory has been discussed many times previously.[32] Briefly, the vibrational frequencies of the critical configuration are adjusted until they reproduce an accurate experimental Arrhenius A-factor. Once the frequencies of the critical configuration have been found it is easy to calculate the rate constant as a function of excitation above the dissociation limit. Because of the insensitivity of RRKM theory to the exact choice of frequencies of the critical configuration within the constraint of the A-factor, rate constants derived in this way are accurate to within 10 percent.

One must also know the absorption cross sections of states in the quasicontinuum (QC) to treat this dynamic problem. In the past this has been modeled as an exponentially decreasing function of the total energy varying typically by a factor of two over the QC, but we have found empirically that for the practical purpose of determining

barrier heights from an estimation of the internal energy distributions which are consistent with experimental translational energy distributions, it makes no difference if one simply lets all of the levels of the QC have the same absorption cross section. The subsequent calculation involves varying the absorption cross section for the states in the QC until the calculated internal energy distribution gives a $P(E_T)$ for simple bond rupture that agrees with the experimental data. If, for a given laser intensity,the absorption cross sections are large, there will be a greater amount of up pumping and on the average molecules will dissociate with a larger translational energy release. Conversely, if the absorption cross sections are small there will be on the average less up-pumping and molecules will dissociate with less energy available to translation. From the comparison of measured translational energies and model calculations, the simple bond rupture channel can be used as a "thermometer" which reflects the internal energy distribution of the dissociating ensemble of molecules.

D.1. CH_3NO_2, Barrier for Isomerization to CH_3ONO.- The estimation of the internal energy distribution is somewhat more complicated when there are competing channels of dissociation. This is shown schematically for CH_3NO_2 in fig. 10. The twenty-five levels of excitation that are shown are all separated by the photon energy. Most of the levels do not have enough energy to dissociate. However, all levels above the barrier height to isomerization do decay

Fig. 10 Schematic Representation of the Model Competition Calculation for the Unimolecular Decomposition of Nitromethane: The yield for the two dissociation pathways as a function of excitation energy is shown. See section D.1..

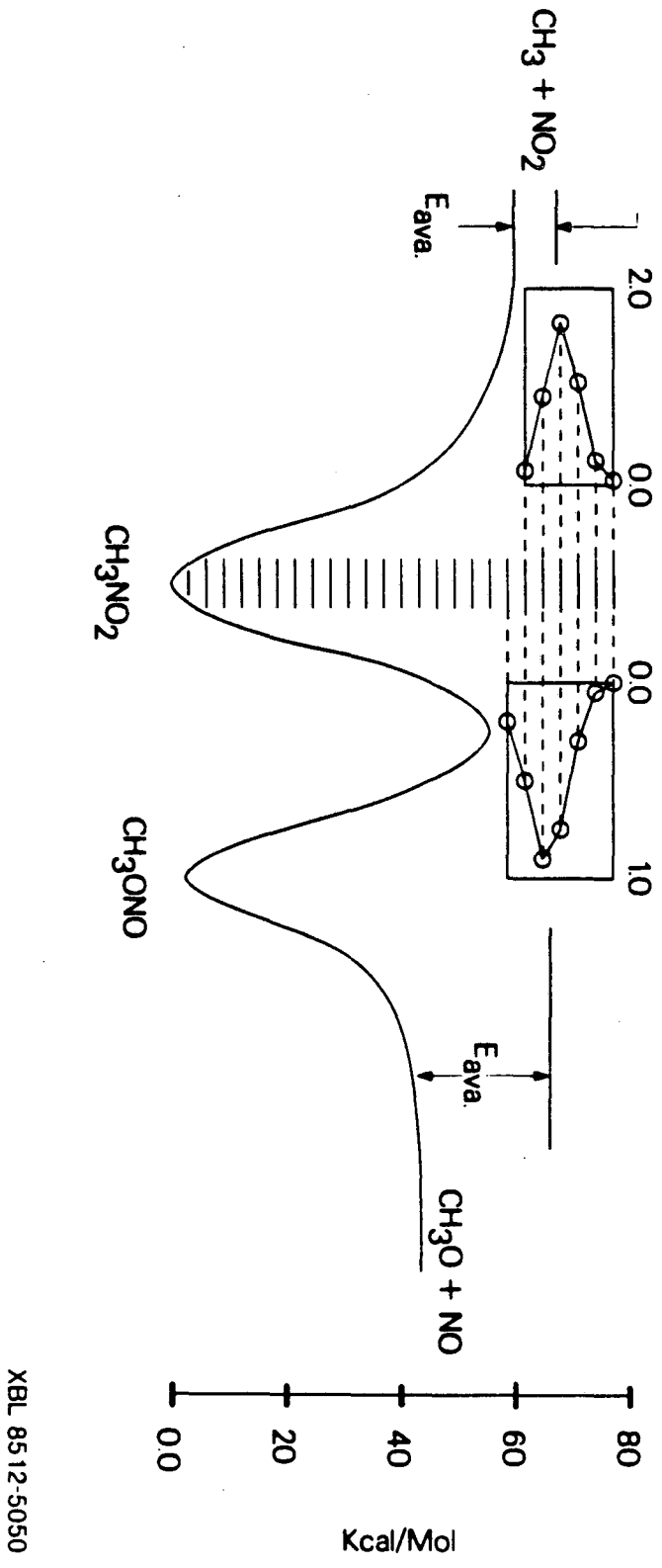

XBL 8512-5050

through one or both of the product channels. The relative yield into the two reaction channels for each level is shown based on analysis similar to what has just been described. In the calculations of the RRKM rate constants, the theoretical Arrhenius A-factor of Dewar et. al.[23] was used for the isomerization reaction and an experimental A-factor of $10^{15.6}$ was used for simple C-N bond rupture.[33] Fitting the data was done by adjusting the absorption cross sections in the QC so that the population distribution of dissociating molecules reproduced the observed translational energy release for reaction I. The results of the calculation of the $P(E_T)$ using RRKM theory is the solid line in fig. 2. Then, by varying the barrier height to isomerization, keeping the A-factor constant, we fit the observed branching ratio for the two reactions. By this analysis the observed branching ratio of reaction II to reaction I of 0.6 led to a barrier height to isomerization of 55.5 kcal/mol. The substantially larger release of translational energy for reaction II compared to reaction I is also in good agreement with that expected from RRKM theory based on the internal energy distribution that the isomerization yield curve in fig. 10 predicts.

From the description so far one might suspect that the inherent error in such an analysis would be too large to obtain any useful results. In fact this is not the case. Although the absorption cross sections for states in the QC can vary by more than a factor of three ($0.08 \times 10^{-19} cm^2$ to $0.3 \times 10^{-19} cm^2$) within the constraints of the observed translational energy release of the simple bond rupture

reaction, this gives rise to only a ± 1.5 kcal/mol uncertainty in the barrier height to isomerization.

The major sources of error in the derivation of the barrier height are the uncertainty associated with the Arrhenius A-factor used for isomerization and the uncertainty in the measured branching ratio due to the low signal to noise ratio in this experiment. Fortunately, the calculation of the barrier height is not very sensitive to error in the A-factor. We found that if the A-factor is off by a factor of 3, it only changes the barrier height by 3 kcal/mol.

There are some questions that still remain concerning the branching ratio measurement. If it is true that 41 percent of the fast contribution to mass 30 is NO^+ this means that the mass spectrum for methoxy radical consists of mass 29 (HCO^+) and mass 30 (H_2CO^+) with the intensity ratio being 1:4 in favor of H_2CO^+. On the basis of the thermodynamics alone it is surprising that H_2CO^+ outweighs HCO^+ by four to one and not the other way around. If the value of .41 were in error, the most drastic effect on the branching ratio would be if all of the fast contribution to the mass 30 TOF spectrum were NO^+. Then the branching ratio would be 1.5 in favor of isomerization. Although this is quite a large change in the branching ratio, the consequent change in the barrier height is only 1.5 kcal/mol, from 55.5 kcal/mol to 54.0 kcal/mol.

There is yet another experimental uncertainty in the translational energy release of the decomposing methylnitrite, symbolized by the cross-hatched area in fig. 3. The branching ratio

of 0.6 is based on the results of the RRKM calculation of the translational energy release shown as the thick line in fig. 3. This is clearly on the slow side of the indicated error bars. If the true translational energy release of the products were given by the fastest edge of the error bars in fig. 3, this would have the effect of raising the relative contribution of reaction II in the c.m. frame. This effect alone would change the branching ratio from 0.6 to 1.2 and would lower the barrier height by another 1.0 kcal/mol.

It should be noted that this is quite a conservative estimation of the error, since it is very unlikely, if RRKM theory accurately reflects the release of translational energy in methylnitrite, that there could possibly be as large a release of translational energy as the fast edge of the error bars in fig. 3 reflects. Using the A-factor for simple bond rupture of methylnitrite of $10^{15.6}$,[34] this large a release of translational energy would imply an average amount of excitation above the dissociation limit of 35 kcal/mol which is clearly unreasonable considering fig 10. If the average level of excitation were 35 kcal/mol above CH_3O + NO, it would be 22 kcal/mol above the threshold for C-N bond rupture. The RRKM lifetime for C-N bond rupture at this degree of excitation is about 30 psec. It would therefore be impossible to pump CH_3NO_2 this high under our experimental conditions which give an average rate of photon absorption of 10^9/sec.

Finally, if all of the experimental uncertainties were to conspire in the most unfortunate way, so that all of the individual

errors added to make the barrier height the lowest it could possibly be, it would change from the reported value of 55.5 kcal/mol to 51.5 kcal/mol. The analysis of the error in the barrier height determination is summarized in table V.

D.2. The Exit Barrier for HONO Elimination from $C_2H_5NO_2$ and 2-$C_3H_7NO_2$.- The best test of the branching ratio matching method for the barrier height determination for isomerization of nitromethane is to apply it to an analogous system where the value of the barrier height is already known. Nitroethane is ideal since the Arrhenius A-factor and activation energy for reaction IV are fairly well known experimentally.[28] The A-factor for reaction III is assumed to be the same as for reaction I. The approach was to use the measured translational energy release distribution for reaction III as a "thermometer" for the internal energy distribution of the dissociating molecules. By varying the absorption cross sections in the QC to reproduce this data (solid line in fig. 5) and adjusting the barrier height for HONO elimination (reaction IV) to match the observed branching ratio, we arrived at a value of 46 ± 1.5 kcal/mol for the barrier height to HONO elimination from $C_2H_5NO_2$.

Fig. 11 shows a schematic representation of this calculation which is similar to the nitromethane calculation. The only difference is that now we cannot use the translational energy distribution of reaction IV to double check the calculation since RRKM theory cannot predict the product energy distribution for molecular elimination

Table V

55.5 kcal/mol MOST PROBABLE VALUE OF BARRIER HEIGHT CONSISTENT WITH AN ARRHENIUS A-FACTOR OF $10^{13.3}$

MAGNITUDE OF ERROR	SOURCE OF UNCERTAINTY
-1.5 kcal/mol	; translational energy release of C-N simple bond rupture reaction in nitromethane
-1.5 kcal/mol	; amount of mass thirty that is NO^+
-1.0 kcal/mol	; translational energy release of N-O simple bond rupture reaction in methylnitrite
+1.5 kcal.mol	;translational energy release of C-N simple bond rupture

51.5 kcal/mol MINIMUM BARRIER HEIGHT CONSISTENT WITH ARRHENIUS A-FACTOR OF $10^{13.3}$

57.0 kcal/mol MAXIMUM BARRIER HEIGHT CONSISTENT WITH ARRHENIUS A-FACTOR OF $10^{13.3}$

Table V: Uncertainty in the Nitromethane Isomerization Barrier Height Determination.

Fig. 11 Schematic Representation of the Model Competition Calculation for the Unimolecular Decomposition of Nitroethane: See caption of fig. 10 and section D.2..

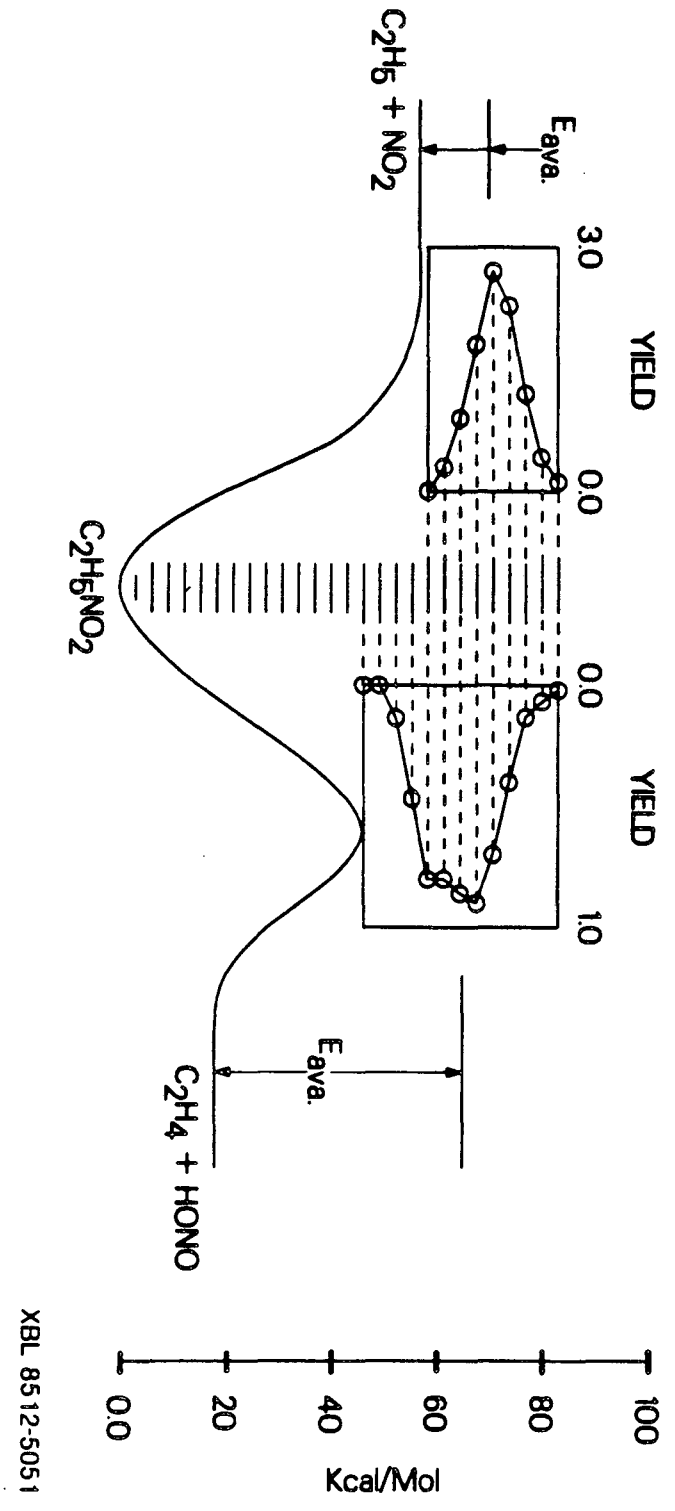

XBL 8512-5051

reactions. One advantage of the large translational energy release in the molecular elimination channel is that we can fully resolve the two proccesses in the TOF spectra and therefore there is much less uncertainty in the measured branching ratio. This reduces the error in the determination of the barrier height of the HONO elimination reaction. Consequently, the major source of error is in the determination of the translational energy release of the simple bond rupture reaction which leads to the stated uncertainty.

In order to compare this to the experimental activation energy, we must make use of equation (3) which relates the activation energy at a specific temperature to the height of the barrier.

$$E_a = \frac{\sum \epsilon_i k_i g_i e^{-\epsilon_i/kT}}{\sum k_i g_i e^{-\epsilon_i/kT}} - \left\{ - \frac{\delta \ln Q}{\delta (1/T)} \right\} \qquad (3)$$

where:

ϵ_i = energy of the i^{th} level

k_i = rate constant for dissociation of the i^{th} level

g_i = degeneracy of the i^{th} level

k = Boltzmann's constant

T = Temperature of pyrolysis experiment

Q = Molecular partition function excluding translation

The density of states as a function of total energy was used to approximate the g_i's above, the k_i's are derived from RRKM theory, and the summation was carried out numerically. The activation energy

obtained is 45 ± 1.5 kcal/mol at 700°K, in excellent agreement with the experimental result of 45 kcal/mol.[28,34] This is the most direct test of our method of determining barrier heights in two channel dissociation systems and leads us to believe it is quite reliable.[35]

Although there is significant scatter in the data, it does appear that the average translational energy release for HONO elimination from 2-nitropropane is slightly less than for nitroethane by about 3-5 kcal/mol. In the abscence of good thermochemical and kinetic data we applied our method of branching ratio matching in order to see if there was any reason to believe that the barrier height to HONO elimination was lower in 2-nitropropane than in nitroethane. Of course, one must make certain assumptions. First of all, in order to get an absolute value for the barrier height, we must know the simple bond rupture endothermicities. From ref. 34, the ΔH_{298}'s of reactions I, III and V are 60.0, 57.7 and 59.7 kcal/mol, respectively. We do expect that the C-N bond energies of the series nitromethane, nitroethane, and 2-nitropropane should decrease, due to the increasing stabilization of the free radical. Indeed, this can be seen in the C-H bond energies of methane, ethane and propane (to form isopropyl radical and H).[36] In that series a stabilization of ~3 kcal/mol is obtained by adding each methyl group. It is immediately apparent that the 59.7 kcal/mol value for 2-nitropropane is suspect since it is nearly as strong as nitromethane. For this reason we have assumed the C-N bond energies in the series to be 59.4, 56.4 and 53.4

kcal/mol respectively. This includes a small (~0.5 kcal/mol) correction from ΔH_{298} to D_o(C-N) and conforms to the expected trend.

The A-factor for the simple bond rupture of nitromethane is well known to be $10^{15.6}$.[34] Since the extra degrees of freedom present in nitroethane and 2-nitropropane are not expected to play an important role in the simple bond rupture reactions of these molecules, it is reasonable to assume that the A factors for reactions I, III, and V are the same.

The A-factor for the HONO elimination from 2-nitropropane was assumed to be a factor of two larger than the recommended value for HONO elimination from nitroethane. This is a simple result of the reaction path degeneracy of the two reactions and can be understood by realizing that there are twice as many H atoms that can undergo transfer to the NO_2 group and subsequent HONO elimination in 2-nitropropane than there are in nitroethane.

The final assumption that has been made in the comparison of 2-nitropropane to nitroethane is that the endothermicities of the HONO elimination channels are the same. Experimentally they differ by two kcal/mol, but the error in these values is large enough to make it impossible to state that they are in fact different. For the purpose of comparison, the assumption of equality is preferred to the experimental values because the difference in experimental endothermicities contradicts the reasonable expectation that the HONO elimination from 2-nitropropane should be slightly less endothermic

than that from nitroethane if, in fact, there were to be any difference at all.[37] The prefered thermochemical and kinetic values, both experimentally determined and assumed, for all of the systems we have studied are summarized in table VI.

The application of the branching ratio matching method is done in exactly the same way as before. This procedure yields a barrier height of 41 kcal/mol, a full 5 kcal/mol lower than in nitroethane. There is one inconsistency in this calculation in that the calculated best fit (solid line of fig. 7) requires the absorption cross sections in the QC to be 1.0×10^{-19} cm^2. This is to be compared to the values for nitromethane and nitroethane of 0.15×10^{-19} cm^2 and 0.20×10^{-19} cm^2, respectively. While it is possible that this is a real effect, if the true value of the absorption cross sections in 2-nitropropane were to be more in line with nitromethane and nitroethane, say 0.25×10^{-19} cm^2, the calculated translational energy release for the simple bond rupture reaction would still agree fairly well with the data as shown in fig. 8 (dashed curve) and the barrier height would then be 43 kcal/mol. This would lead to the same conclusion that the barrier height to HONO elimination is somewhat lower in 2-nitropropane than in nitroethane.[38]

In view of the nitromethane results, one interesting phenomenon in the IRMPD of nitroethane and 2-nitropropane is the absence of evidence for the unimolecular isomerization and formation of alkoxy radicals and NO, for example reaction VII.

Table VI

Parent Molecule	Process	Barrier Height	ΔH_0	Arrhenius A-Factor	Activation Energy
CH_3NO_2	SBR[a]	59.4[b]	59.4[c]	15.6[d]	59[c]
CH_3NO_2	ISO[e]	55.5[f]	2.5[c]	13.3[g]	
CH_3ONO	SBR	41.0[b]	41.0[c]	15.6[d]	
$C_2H_5NO_2$	SBR	56.4	56.4[h]	15.6[i]	56[h]
$C_2H_5NO_2$	CME[j]	46.0[f]	18.0[c]	12.4[d,k]	45[f,k]
$2\text{-}C_3H_7NO_2$	SBR	53.4	53.4[h]	15.6[i]	53[h]
$2\text{-}C_3H_7NO_2$	CME	41.0[f]	18.0[l]	12.7[m]	40[f,n]

a. Simple bond rupture.
b. For SBR reaction no barrier to reverse reaction is assumed.
c. Units are kcal/mol, see ref. 34.
d. Units are logarithmic, see ref. 34.
e. Isomerization.
f. Derived from branching ratio matching analysis (see text).
g. See to ref. 23.
h. Based on 3 kcal/mol stabilization for each added methyl group, see text.
i. Assumed to be the same as for SBR of CH_3NO_2.
j. Concerted molecular elimination, HONO elimination.
k. Recommended experimental value, see ref. 28 and 34.
l. Assumed same as for nitroethane (see text).
m. Assumed to be twice the value of that for nitroethane (see text).
n. Experimental values range between 40 and 45 kcal/mol (see ref. 34 and 38).

Table VI: Pertinent Thermochemical Data.

$$C_2H_5NO_2 \xrightarrow{\ddagger} C_2H_5ONO \xrightarrow{\ddagger} C_2H_5O + NO \qquad \text{(VII)}$$

This can be understood by considering the competition between HONO elimination and isomerization in an analagous way to the calculations represented by fig.'s 10 and 11. We used the known A-factor and barrier height for HONO elimination for reaction IV and the same barrier height and A-factor for the isomerization of nitromethane to characterize reaction VII. Then by using the same absorption cross sections as in the calculation represented by fig. 11, we obtained a branching ratio of more than 10:1 in favour of HONO elimination. This, at first glance, may seem odd since we know that the isomerization channel can compete with simple bond rupture in nitromethane. However, an inspection of fig. 10 reveals that in nitromethane the isomerization channel competes only because it can dissociate from levels below the dissociation limit of the simple bond rupture channel, or at sufficiently low energies that the rate constant for simple bond rupture is quite small. As soon as the system has an internal energy of about 6 kcal/mol above the C-N bond energy, simple bond rupture dominates. In nitroethane, in order for isomerization to be important there must be no other reactions that can dissociate rapidly from the energy levels below or near the energy threshold for simple bond rupture. Since the HONO elimination channel is present this cannot be the case. The same is true in the dissociation of nitropropane and explains the absence of the isomerization channel.

D.3. The Translational Energy Release in Concerted Molecular Elimination Reactions: $C_2H_5NO_2$ and 2-$C_3H_7NO_2$.- For a reaction that goes over a substantial mechanical barrier in the PES, the essential question we must address is what is the nature of the potential energy barrier and to what extent does the potential energy of that barrier appear as product translation. For instance, in the concerted four-center elimination of HCl from 1,1,1-trichloroethane, the transition state is a very distorted configuration, far from the equilibrium structure of the products or the reactant. Consequently, when the electrons rearrange to form products, the potential energy of the barrier will appear mainly as internal energy of the products as the molecules make their way back to their equilibrium configurations, and only a relatively small fraction of the potential energy of the exit barrier appears as translation.[39] On the other hand, in the dissociation of formaldehyde to H_2+CO, the transition state corresponds to a configuration in which one of the hydrogens moves toward the other hydrogen without extending the CO or CH bonds. The formation of the H_2 bond takes place at close proximity to the CO. The potential energy in this case mainly appears as repulsion between H_2 and CO and it is not surprising that as much as 75 percent of the barrier appears as translation.

In the case of nitroethane or 2-nitropropane, the transition state of the reaction at the top of the mechanical barrier in the PES is a five membered ring. With the exception of the transfer of H from C to O, it is not necessary to distort the molecule very far from its

equilibrium bond lengths and angles to reach the five membered ring transition state. This implies that the potential energy barrier is mainly due to repulsion of the closed shell products after the electrons have rearranged to the configuration of the products and not to "strain energy" of the reactant molecule. We recognize that this is similar to CH_2O and are therefore not surprised to see an average release of translational energy of 20 kcal/mol, 70 percent of the 28 kcal/mol exit barrier.

For the case of 2-$C_3H_7NO_2$ we see an average release of translational energy of 15 kcal/mol or 65 percent of the 23 kcal/mol exit barrier. A comparison of the two systems implies that there is more involved here than just a difference in the barrier heights since the fraction of energy appearing as translation is different. Since it is clear that strain energy is relatively unimportant in producing the mechanical barrier in the PES's of these molecules, the variation must arise from the difference in the repulsive interral excitation dynamics as the fragments descend down the barrier.

We have used a "scaled-reduced-mass impulse approximation" to interpret the differences between nitroethane and 2-nitropropane in the translational energy release of the concerted molecular elimination channels. To calculate the relative amounts of translational and internal energy in the products using the standard impulse approximation for the case when C and N are initially only very loosely coupled to the rest of the atoms, one assumes that the impulsive energy release is sufficiently sudden that momentum is

initially balanced between the two repulsive sites, the C and N atoms and all the other atoms are spectators, as shown in equations (4).

$$m_C v_C = m_N v_N$$
$$m_C E_C = m_N E_N \qquad (4)$$

This means that, initially, the total available energy all appears as the kinetic energy of C and N atoms, $E_C + E_N$. The final translational energy release for nitroethane must also balance linear momentum between HONO and C_2H_4 according to equations (5),

$$m_{C_2H_4} v_{C_2H_4} = m_{HONO} v_{HONO}$$
$$m_{C_2H_4} T_{C_2H_4} = m_{HONO} T_{HONO} \qquad (5)$$

and the total final translational energy would be $T_{HONO} + T_{C_2H_4}$. The difference between the total available energy ($E_C + E_N$) and the total translational energy ($T_{HONO} + T_{C_2H_4}$) is the amount of internal excitation due to the relative motion between the C and N atoms and the atoms they are bound to. If one works through this calculation one comes up with 0.4 of the available energy or barrier height appearing as translation. This low value clearly indicates that the infinitely loose limit of this approximation is not realistic. In contrast, the infinitely rigid limit of this approximation would neglect all product vibrational degrees-of-freedom and simply require the balance of linear and angular momentum between HONO and C_2H_4. One would then predict that nearly all of the available energy would appear as translation of the products. Apparently, the true situation lies somewhere in between. A

convenient way to scale the extent of coupling between C and N atoms and the atoms they are bound to is by way of the effective reduced mass in the impulse approximation. One can see that in the infinitely loose limit, the reduced mass of the impulse aproximation is simply the reduced mass of the C,N pair or μ_{min}=6.46. The reduced mass for the infinitely rigid limit would be that of the HONO,C_2H_4 pair or μ_{max}=17.55. There will be an effective reduced mass between these two that predicts the observed amount of translational energy release. In order to reproduce the experimentally observed translational energy release of 0.7 of the exit barrier, it is neccesary to have an effective reduced mass of μ_{eff}=12.5 which is about twice as large as the reduced mass of C and N or 70 percent of the reduced mass of C_2H_4 and HONO. We can define an empirical parameter α by equation (6).

$$\alpha = (\mu_{eff} - \mu_{min})/(\mu_{max} - \mu_{min}) \qquad (6)$$

α is reflective of the deviation from each limit of the approximation. The interesting thing about α is that if one repeats the analysis just descibed for the case of 2-nitropropane, assuming α to be the same in 2-nitropropane as in nitroethane, one arrives at 0.66 of the exit barrier potential energy going into translation, in very good agreement with experiment. To get an idea of the general usefulness of this method consider table VII. For UV photodissociation of alkyl halides the principle mechanism of product internal excitation is also repulsive excitation. By setting α=0.44

Table VII

Reaction	μ_{min}	μ_{max}	α	Theor. E_T/E_a	Obs. E_T/E_a
IRMPD					
$C_2H_5NO_2 \longrightarrow C_2H_4+HONO$[a]	6.46	17.55	.53	0.70	0.71
$C_3H_7NO_2 \longrightarrow C_3H_6+HONO$[a]	6.46	22.18	.53	0.66	0.65
UV Excitation					
$CF_3I \xrightarrow{248\ nm} CF_3+I^*$[b]	10.96	44.71	.44	0.58	0.61
$C_2F_5I \xrightarrow{248\ nm} C_2F_5+I^*$[c]	10.96	61.43	.44	0.54	0.51
$CH_3 \xrightarrow{266\ nm} CH_3+I^*$[d]	10.96	13.42	.44	0.90	0.88
$C_2H_4ClI \xrightarrow{266\ nm} C_2H_4Cl+I^*$[e]	10.96	42.11	.44	0.59	0.58
$C_2F_4BrI \xrightarrow{248\ nm} C_2F_4Br+I^*$[c]	10.96	74.63	.44	0.52	0.48
$C_2F_4BrI \xrightarrow{193\ nm} C_2F_4Br+I^*$[c]	10.96	74.63	.44	0.52	0.37

a. This work.
b. See ref. 41.
c. See ref. 40.
d. See ref. 42.
e. See ref. 43.

Table VII: Scaled Reduced Mass Impulse Approximation.

we were able to obtain very good agreement between the model and the experimental results for 5 different molecules. In addition, it is also clear that the dissociation of C_2F_4BrI at 193 nm is anomalous. This might be due to another mechanism besides direct repulsive excitation as was hypothesized by Krajnovich et. al..[40] Since at 193 nm the excitation is an n(Br)→σ*(C-Br) transition, electronic energy transfer to the C-I bond must precede C-I bond rupture.

E. Conclusions.- The major conclusion of this work is that it is possible to make a quantitative connection between molecular beam IRMPD experiments and classical thermolysis experiments. This is accomplished through the use of RRKM theory and relies on the relationship between the translational energy distribution for simple bond rupture reactions and the internal energy distribution of the ensemble of dissociating molecules. Due to the unambiguous determination of and discrimination between different primary unimolecular decomposition pathways, the molecular beam IRMPD experiments can provide information on the energetics and dynamics of a system where pyrolysis techniques would be mired in an overly complex set of primary and secondary dissociation proccesses. Yet it is also possible to use this technique, where the concept of temperature is meaningless, to predict phenomenological quantities such as activation energies that are normally measured under collisional, thermal conditions.

Specifically, we have been able to observe the isomerization of nitromethane to methylnitrite and make a good estimation of the isomerization barrier height using a branching ratio matching method. We have tested this method by using it to determine the barrier height and activation energy to HONO elimination from nitroethane and find excellent agreement with the known activation energy. We then used the same procedure to determine the barrier height for HONO elimination from 2-nitropropane and have found that there is good reason to believe that this barrier height is 3-5 kcal/mol lower than in nitroethane.

We have also observed very large releases of translational energy in concerted molecular elimination reactions of nitroalkanes which proceed through 5 membered cyclic transition states. We have used a scaled-reduced-mass impulse approximation to interpret the difference in translational energy release between 2-nitropropane and nitroethane. Within a "family" of dissociating molecules we have found that this model can be used to predict the relative translational energy release from one member to another when impulsive internal excitation is the principle mechanism of product internal excitation. In contrast to the mixed nature of the transition state for four center HCl elimination in chlorinated ethanes, we have suggested that the transition state for HONO elimination qualitatively resembles the two closed shell product molecules held at normal bonding distance from one another, i.e. ~1-2 Å, and that this then naturally gives rise to a large fraction of the available energy

appearing as translation. We expect that this will be a general feature of concerted molecular elimination reactions that proceed through a cyclic transition state that can be formed without a great deal of molecular distortion.

REFERENCES

1. N.R. Isenor, M.C. Richardson, Appl. Phys. Lett., 18, 224 (1971)

2. N.R. Isenor, M.C. Richardson, Optics Commun., 3, 360 (1971)

3. V.S. Letokhov, E.A. Ryabov, O.A. Tumanov, Optics Commun., 5, 168 (1972)

4. V.S. Letokhov, E.A. Ryabov, O.A. Tumanov, Sov. Phys. J.E.T.P. (Engl. transl.), 36, 1069 (1973)

5. N.R. Isenor, V. Merchant, R.S. Halworth, M.C. Richardson, Can. J. Phys., 51, 1281 (1973)

6. R.V. Ambartzumian, Yu.A. Gorokov, V.S. Letokhov, G.N. Makarov, J.E.T.P. Lett. (Engl. transl.), 21, 171 (1974)

7. R.V. Ambartzumian, Yu.A. Gorokov, V.S. Letokhov, G.N. Makarov, J.E.T.P. Lett. (Engl. transl.), 43, 22 (1975)

8. J.L. Lyman, R.J. Jensen, J. Rink, C.P. Robinson, S.D. Rockwood, Appl. Phys. Lett., 27, 87 (1975)

9. See for example: N. Bloembergen, E. Yablonovitch, Physics Today, pp. 23-30, May (1978); M.N.R. Ashfold, G. Hancock, Gas Kinetics and Energy Transfer, Royal Soc. (Spec. Per. Rep.), 4, pp. 73-116 (1980); C.D. Cantrell, S.M. Freund, J.L. Lyman, The Laser Handbook, North Holland Pub. Co., M.L. Stitch Ed., pp. 485-576 (1979); P.A. Schultz, Aa.S. Sudbo, D.J. Krajnovich, H.S. Kwok, Y.R. Shen, Y.T. Lee, Ann. Rev. Phys. Chem., 30, 379 (1979)

10. J.D. Rynbrandt, B.S. Rabinovitch, J. Phys. Chem., 75, 2164 (1971)

11. J.P. Maier, A. Seilmeier, A. Laubereau, W. Kaiser, Chem. Phys. Lett., 46, 527 (1977)

12. P.J. Robinson, K.A. Holbrook, Unimolecular Reactions, John Wiley and Sons Pub. Co., London (1972)

13. M.J. Coggiola, P.A. Schultz, Y.T. Lee, Y.R. Shen, Phys. Rev. Lett., 38, 17 (1977)

14. E.R. Grant, M.J. Coggiola, Y.T. Lee, P.A. Schultz, Aa.S. Sudbo, Y.R. Shen, Chem. Phys. Lett., 52, 595 (1977)

15. Aa.S. Sudbo, P.A. Schultz, E.R. Grant, Y.R. Shen, Y.T. Lee, J. Chem. Phys., 68, 1306 (1978)

16. Aa.S. Sudbo, P.A. Schultz, E.R. Grant, Y.R. Shen, Y.T. Lee, J. Chem. Phys., 70, 912 (1979)

17. L.J. Butler, R.J. Buss, R.J. Brudzynski, Y.T. Lee, J. Phys. Chem., 87, 5106 (1983)

18. F. Huisken, D. Krajnovich, Z. Zhang, Y.R. Shen, Y.T. Lee, J. Chem. Phys., 78, 3806 (1983)

19. E.R. Grant, P.A. Schultz, Aa.S. Sudbo, Y.R Shen, Y.T. Lee, Phys. Rev. Lett., 40, 115 (1978)

20. The problem of using RRKM theory to calculate the product energy distributions for reactions with exit barriers has received considerable attention. See for example: R.A. Marcus, J. Chem. Phys., 62, 1372 (1975) and G. Worry, R.A. Marcus, J. Chem. Phys., 67, 162 (1977), however one must always make dynamical assumptions in such theories.

21. A.M. Wodtke, E.J. Hintsa, Y.T. Lee, J. Chem. Phys., 84, 1044 (1986)

22. B.H. Rockney, E.R. Grant, J. Chem. Phys., 79, 708 (1983)

23. M.J.S. Dewar, J.P. Ritchie, J. Alster, J. Org. Chem. 50, 1031 (1985)

24. R.J. Bartlett has performed ab initio calculations placing an upper bound to the barrier height to isomerization in nitromethane at 70 kcal/mol.

25. D.A. Dixon, A. Komornicki, W.P. Kraemer, J. Chem. Phys., 81, 3603 (1984) give heats of formation for H_2COH^+ and HCO^+ of 165.2 and 197.9 kcal/mol respectively. The relative instability H_3CO^+ with respect to H_2COH^+ is estimated to be 80 kcal/mol based on the 107 kcal/mol O-H bond strength in H_2COH^+ and assuming that the C-H bond strength in H_3CO^+ is 27 kcal/mol, the same as in H_2CO^+. This gives an exothermicity for H_2 elimination from H_3CO^+ of 47 kcal/mol.

26. R. Glanzer, J. Troe, Ber. Bunsen. Phys. Chim. 78, 121 (1984).

27. R.E Center, A. Mandl, J. Chem. Phys., 57, 4104 (1972) Atomic polarizabilities can be found in T.M. Miller, B. Bederson, Adv. At. Mol. Phys., 13, 1 (1977). Molecular polarizabilities are assumed to be the sum of the constituent atomic polarizabilities.

28. G.N. Spokes, S.W. Benson, J. Am. Chem. Soc., 89, 6030 (1967)

29. The electron impact ionization mass spectrum of CH_3ONO consists of m/e = 46:30:61 abundances of 1:100:0 at an electron energy of 250 eV. Our electron energy was 200 eV. Atlas of Mass Spectral Data, 1, p. 41, E. Stenhagen, S. Abrahamson, F.W. McLafferty Eds., John Wiley and Sons Pub. Co., New York (1969)

30. S.A Safron, N.D. Weinstein, D.R. Herschbach, J.C. Tully, Chem. Phys. Lett., 12, 564 (1972)

31. This program has been reported earlier: P.A. Schultz, Aa.S. Sudbo, E.R. Grant, Y.R. Shen, Y.T. Lee, J. Chem. Phys., 72, 4985 (1980) and is an extension of previous work by J.L. Lyman, J. Chem. Phys., 67, 1868 (1977) and W. Fuss, Chem. Phys., 36, 135 (1979)

32. D.J. Krajnovich, Ph.D. Thesis, pp. 83-90, University of California, Berkeley (1983)

33. L. Phillips, R. Shaw, Tenth Int. Symp. on Comb., p. 453 (1964) and V. Yashtern, Chemical Kinetics and Chain Reactions, 286, p. 313, U.S.S.R. Acadamy of Sciences, Moscow (1966)

34. S.W. Benson, H.E. O'Neal, Kinetic Data on Gas Phase Unimolecular Reactions, National Standard Reference Data Series, National Bureau of Standards (1970), Library of Congress Card Catalog number 68-67395

35. In fact there is some ambiguity in the pyrolysis experiment. Reference 28 was reevaluated by Benson to give A=12.4 and E_a=45 kcal/mol which we agree with. The original data gave A=11.8 and E_a=43 kcal/mol. If we use A=11.8 we obtain E_a=43 kcal/mol. So our result agrees with either value and cannot distinguish between them. This is because both data give the same rate.

36. See the very accurate theoretical work of C.F. Melius, J.S. Binkley, M.L. Kszykowski, Proc. Combustion Res. Contractors Meeting, May (1984), U.S. Dept. of Energy, Office of Energy Sciences, for calculations of the heats of formation for CH_3, C_2H_5, and 2-C_3H_7.

37. C.F. Melius, J.S. Binkley, M.L. Kszykowski, Proc. Combustion Res. Contractors Meeting, May (1984), U.S. Dept. of Energy, Office of Energy Sciences. Consider the analogous H_2 elimination from ethane and n-propane in view of Melius' calculation of heats of formation for C_2H_6, C_2H_4, C_3H_8 and C_3H_6.

38. This is consistent with what would be expected from the Benson-Bose semi ion pair model. S.W. Benson, G.P. Haugen, J. Am. Chem. Soc. 87, 4036 (1965). It is also consistent with the experimental work of J. Pola, M. Farkacova, P. Kubat, A. Trka, J. Chem. Soc. Far. Trans. I, 80, 1499 (1984).

39. Aa.S. Sudbo, P.A. Schultz, Y.R. Shen, Y.T.Lee, J. Chem. Phys., 69, 2312 (1978)

40. D. Krajnovich, L.J. Butler, Y.T. Lee, J. Chem. Phys., 81, 3031 (1984)

41. G.N.A. Van Veen, Excited Species from Photofragmentation, Ch. 8, Proefschrift, Stichtung voor Fundamenteel Onderzoek der Materie (Foundation for Fundamental Research on Matter), Amsterdam, the Netherlands

42. R.K. Sparks, K. Shobatake, L.R. Carlson, Y.T. Lee, J. Chem. Phys., 75, 3838, (1981)

43. T.K. Minton, P. Felder, R.J. Brudzynski, Y.T. Lee, J. Chem. Phys., 81, 1759 (1984)

APPENDIX: ANALMAX, a Program for Analyzing Secondary Dissociation Data

This appendix is included in this thesis more for historical reasons that anything else. ANALMAX was the first program in our group that could simulate secondary dissociation TOF spectra. It was written in reaction to the observation of secondary photodissociation of C_2H in the UV photolysis of C_2H_2. See chapter III. The secondary decomposition of photoproducts, caused either by the high internal energy that they are commonly formed with or by secondary absorption of a photon, is very common and had been seen many times before the acetylene experiment.[1] In fact, this phenomenon was exploited by Minton et. al. in the photodissociation of dihalogenated ethanes to successfully obtain very accurate C-X bond energies in a whole series of halogenated ethyl radicals.[2]

Unfortunately, one cannot in general obtain very detailed information on the translational energy distribution of the secondary process since the observed TOF is convoluted not only over the velocity distribution of the molecular beam but also over the velocity distribution of the primary photoproducts. This is normally enough to wash out any possible structure in the $P(E_T)$ and I'm sure is the major reason that no one in our group had ever bothered to analyze such data before.

One important exception to this is when the the primary process releases only a small amount of translational energy and a fast, usually He seeded, molecular beam is employed. In this case, the velocity distribution of the primary products may be only slightly different than the molecular beam velocity distribution and information on the secondary event can be gotten with much greater detail. In such a situation it is even possible to analyze tertiary dissociation data and as it turned out, this was totally essential to the understanding of the IRMPD of RDX.[3]

I said this program was the first in our group. In fact, Kroger et. al. had, much to our interest after we had finished all of our programs, written a forward convolution program to analyze secondary dissociation TOF spectra as far back as 1977.[4] As will be seen, ANALMAX is a very inelegant, brute-force approach to the problem and I think it was at least partially his disdain for this that stimulated Gil Nathanson, with the help of Zhao Xinsheng and Tim Minton, to put together a much more efficient algorithm which far surpasses either

ANALMAX or the earlier work of Kroger. So one can see that mediocrity can be the catalyst of great things.

In any case, the analysis of secondary dissociation has not appeared in any Lee group thesis and I believed this appendix might be useful to group members who may be compelled to use one of the secondary dissociation programs that we now have or who might have to construct a similar program in the future, say for reactive scattering. Actually, the brute-force nature of ANALMAX makes it relatively easy to understand and may serve as a better learning tool than Gil's or Xinsheng's programs. However, the advances that they have both accomplished, i.e. the Legendre polynomial averaging technique and the calculation of quantitative secondary decomposition probabilities, should by all means be included in future programs.

In following this explanation it is best to keep in mind that forward convolution is just "mathematese" for experimental simulation. By measuring the instrumental features which give rise to broadening of the data, we can predict the observed TOF spectrum based on an assumed $P(E_T)$. We then vary the $P(E_T)$ until the predicted TOF spectrum matches, as closely as possible, the experimental one. The instrumental features that ANALMAX specifically accounts for are: (1) the molecular beam velocity distribution, (2) the beam angular divergence, (3) the finite size of the detector apertures, (4) the finite length of the electron impact ionizer and (5) the time width of the channels of the multichannel scaler. Although this program does

not explicitly average over the size of the beam/laser interaction region this can be effectively taken into account under (4).

To understand the way in which secondary dissociation is treated, it is essential to first understand primary dissociation. The input section of the program is self explanatory and well commented so this appendix is mainly constrained to the so-called "heart" of the program, which is structured as a set of nested summing do-loops. By the time one gets to the innermost do-loop for the first time, a single lab-frame recoil velocity vector, $\underline{v}$, and a single beam velocity vector, $\underline{v}_b$, have been chosen. By vectorially subtracting $\underline{v}_b$ from $\underline{v}$, the c.m. recoil velocity vector, $\underline{u}$, that connects these two vectors is found. The probability of this particular $\underline{v}_b$ is found in the matrix BPROB(j,k) that was generated in the input section of the program. The probability of the derived $\underline{u}$ depends on two things: the position that it corresponds to in the input $P(E_T)$ and, if β is non-zero, the angle that it makes with the polarization vector of the laser, $\underline{\varepsilon}$. These two probabilities are refered to as EPROB and POLAR in the program and the total probability of this single newton diagram is BPROB(j,k)*EPROB*POLAR.

The summing do-loops 170 and 180 systematically find all newton diagrams that yield this lab frame recoil velocity vector and sum the total probability. Next, the magnitude of $\underline{v}$ is incremented and the entire process is repeated. After the magnitude of $\underline{v}$ has been incremented over the selected range, this entire process is repeated at a slightly different angle and the simulation of the finite

detector acceptance window is accomplished. The results for different angles with the same magnitude of $\underline{v}$ are all summed together to give the total probability at this lab recoil speed coming at the nominal source, detector angle.

The resulting SIGNL(i), where i ranges over the magnitude of $\underline{v}$, is proportional to the lab frame flux as a function of velocity. This is convoluted over the ionizer, modelled with a gaussian electron density, to yield SIGNAL(i). The TOF spectrum is calculated by dividing each TOF channel into ten pieces and calculating the number density, making the correct jacobian transformation, as a function of arrival time along the channel interpolating between points in SIGNAL(i). These ten pieces are then summed to give the total contribution to each channel.

The basic approach of ANALMAX to secondary dissociation is to extend the range of the calculation which simulates the detector aperture so that the probability of primary photodissociation in 3D lab velocity space is derived. A huge matrix SIGNLS(I,J,ITH,JTH) is generated and used like the beam velocity distribution matrix BPROB(j,k) in the primary calculation. Here i ranges over the different reaction channels, j over the magnitude of the lab velocity vectors, and ith and jth range over the in-plane and out-of-plane angle of the lab velocity vector. The program is constructed in such a way that a different primary $P(E_T)$, PESP(i,j), can be used for the calculation of the primary distribution that will decompose since not all primary products will decompose. In addition, because the

calculation takes so long, it is generally a good idea to calculate the secondary TOF with a much coarser grid in velocity space and usually with only a single beam velocity vector. However, one usually wants to retain a fine grid for the primary calculation. This is possible with this program and accounts for the large number of input variables that have the same name as the primary input variables but also have an "s" at the end.

The flag NLABEL is used to pass through the heart of the program up to three times. If NLABEL is 0 the program calculates the primary distribution. If a secondary distribution has been requested, NLABEL is incremented to 1 and the program passes through the heart again, this time using different values for the detector aperture averaging so that SIGNLS(i,j,ith,jth) is generated over a wide angular range. NLABEL is then incremented to 2 and the heart is re-executed as a primary calculation using SIGNLS(i,j,ith,jth) in place of BPROB(j,k). This generates SIGNLSS(i) which is analogous to SIGNL(i) in the primary calculation. Ionizer and scaler channel convoltuion is treated in exactly the same way as before.

In the final section of the program, the different components of the TOF are scaled with respect to one another and the total predicted TOF is normalized to the height of the experimental data. Output is produced in a form that can be used by TELL-A-GRAFF graphics on LBL's Vax, CSA2 or CSA4.

```
      PROGRAM ANALMAX
C     SINGLE PRECISION VERSION OF CMLABUV
C     WITH ENHANCED FLEXIBILTY TO ACCOMADATE
C     SECONDARY DISSOCIATION
C++++++++++++++++++++++++++++++++++++++++++++++++++++++++++++++++++++++++++++++
C++++++++++++++++++++++++++++++++++++++++++++++++++++++++++++++++++++++++++++++
C     THIS SECTION GIVES INSTRUCTIONS FOR THE INPUT SECTION OF THE
C     PROGRAM
C     UNITS ARE THE FOLLOWING
C     MASS - AMU
C     ENERGY - KCAL/MOL
C     VELOCITY - 10,000 CM/SEC
C     TIME - MICROSECONDS
C     DISTANCE - CM
C     ANGLES - DEGREES
C     LINE #  VARIABLES       EXPLANATIONS
C     ++++++  +++++++++       ++++++++++++
C
C     1       TH              NOMINAL DETECTOR ANGLE
C             DIMASS          DETECTED MASS/CHARGE RATIO
C             TADJ            SCALING FACTOR TO ADJUST THE EXACT HEIGHT
C                             OF THE TOTAL CALCULATED TOF TO THE
C                             OBSERVED TOF
C             TPNORM          SCALING FACTOR FOR PRIMARY TOF
C             TSNORM          SCALING FACTOR FOR SECONDARY TOF
C             POL             POLARIZATION ANGLE
C                                     0 IS ALONG BEAM DIRECTION
C                                     POSITIVE ANGLE IS A COUNTER CLOCKWISE
C                                     ROTATION AS VIEWED LOOKING INTO THE
C                                     LASER ON THE ROTATING SOURCE MACINE
C                                     1000 MEANS UNPOLARIZED LIGHT
C             NYSEC           DETERMINES IF SECONDARY DISSOCIATION IS TO BE
C                             CALCULATED
C                             0 - PRIMARY ONLY
C                             1 - PRIMARY AND SECONDARY
C             NDANG           # OF DETECTOR ACCEPTANCE ANGLES TO BE AVER-
C                             AGED OVER
C             ANGRES          ANGULAR RESOLUTION OF DETECTOR
C     2       TITLE           TITLE OF CALCULATION
C     3       WIDTH           DWELL TIME FROM MCS
C             ALFA            ION FLIGHT TIME CONSTANT
C             OFFSET          A DELAY OF THE TRIGGER IS A POSITIVE OFFSET
C             DIST            FLIGHT PATH OF THE MACHINE
C             DL              EFFECTIVE IONIZER LENGTH
C     4       NBCHAN          FIRST CHANNEL IN TOF TO BE ANALYZED
C             NECHAN          LAST CHANNEL IN TOF TO BE ANALYZED
C             NBG1            FIRST CHANNEL USED IN BACKGROUND SUBTRACTION
C             NBG2            LAST CHANNEL USED IN BACKGROUND SUBTRACTION
C     5       NTHBM           # ANGLES TO AVERAGE OVER PRIMARY BEAM
C             NVBM            # VELOCITIES TO AVERAGE OVER PRIMARY BEAM
C     6       VMIN            MINIMUM LAB VELOCITY APPEARING IN TOF
C                             IF SECONDARY DISSOCIATION IS BEING CALCULATED
C                             THIS MUST BE SMALLER THAN THE MINIMUM LAB
C                             VELOCITY DETECTABLE AT ANY ANGLE (0<THETA<360)
C             VINC            VELOCITY INCREMENT TO BE CALCULATED
C             NV              # OF VELOCITIES TO BE CALCULATED
C                             IF DOING SECONDARY DISSOCIATION VMIN+NV*VINC
C                             MUST BE GREATER THAN THE MAXIMUM VELOCITY
C                             DETECTABLE AT ANY ANGLE
C     7       ALPHA           ALPHA FROM KELVIN PROGRAM
```

```
C               SPDRT           SPEED RATIO FROM KELVIN PROGRAM
C               HWIDBM          HALF WIDTH OF PRIMARY BEAM
C       8       NDIST           # OF INPUT PRIMARY P(E)'S
C               NE              # OF ENERGIES IN INPUT P(E)
C                               SHOULD BE THE SAME FOR ALL P(E)'S
C               NER             =0 GIVES AN EVEN GRID FOR THE P(E) (NORMAL)
C                               =1 THEN YOU MUST SPECIFY THE ENERGIES AT WHICH
C                               YOU WANT P(E) VALUES TO APPEAR
C       9(OPTIONAL)NERG(J)      # OF ENERGIES IN EACH DISTRIBUTION
C                               ASSUMING NER WAS SET TO 1
C       9       M1(J)           MASS OF DETECTED NEUTRAL
C       10      M2(J)           MASS OF UNDETECTED NEUTRAL
C       11      RPROB(J)        RELATIVE CONTRIBUTIONS OF J P(E)'S
C       12      EZEROH(J)       MINIMUM ENERGY OF EACH P(E)
C       13      EINCH(J)        ENERGY INCREMENT OF EAC P(E)
C       14      BETA(J)         ANISOTROPY PARAMETER FOR EACH DISTRIBUTION
C       15      NYSECT(J)       1 - YES THERE IS A SECONDARY CALCULATION THAT
C                               USES THIS PRIMARY CHANNEL
C                               0 - NO THERE IS NOT
C       16      NPDISP(J)       1 - YES THIS PRIMARY CHANNEL SHOULD BE
C                               USED AS A COMPONENT OF THE FINAL TOF
C       17      PE(I,J)         INPUT P(E)'S
C       THRU
C       N
C
C
C
C
C       THE FOLLOWING INPUT IS ONLY NECESSARY IF SECONDARY DISSOCIATION IS
C       REQUESTED
C+++++++++++++++++++++++++++++++++++++++++++++++++++++++++++++++++++++++++++++++
C               TPRIME2         SAME, BUT FOR SECONDARY DISSOCIATION
C       N+2     NANGS           # OF ANGLES TO AVERAGE PRIMARY DISTRIBUTION
C                               OVER
C               ANGRS           ANGULAR RANGE OVER WHICH PRIMARY DISTRIBUTION
C                               IS FOUND
C               NTHBMS          #OF BEAM ANGLES TO AVERAGE OVER IN SECOND-
C                               #OF BEAM VELOCITIES TO AVERAGE
C                               OVER IN SECONDARY CALCULATION
C                               CALCULATION
C       N+3     VMINS           MINIMUM VELOCITY APPEARING IN SECONDARY DISS-
C                               OCIATION TOF
C               VINCS           VELOCITY INCREMENT
C               NVS             # VELOCITIES TO BE CALCULATED
C       N+4     VMINP           MIN PRIMARY VELOCITY FOR SEC CALC
C               VINCP           INCREMENT
C               NVP             # OF PRIMARY VELOCITIES
C       N+5     NDISTS          # OF P(E)'S USED TO MODEL SECONDARY
C                               DISSOCIATION
C               NES             # OF ENERGIES IN THESE P(E)'S
C       N+6     M1S(J)          DETECTED NEUTRAL MASS OF SECONDARY PRODUCT
C       N+7     M2S(J)          UNDETECTED NEUTRAL MASS OF SECONDARY PRODUCT
C       N+8     RPROBS(J)       RELATIVE CONTRIBUTIONS OF THGE INPUT P(E)'S
C       N+9     EZEROHS(J)      MINIMUM ENERGIES OF THE DISTRIBUTIONS
C       N+10    EINCHS(J)       ENERGY INCREMENTS OF THE DISTRIBUTIONS
C       N+11    BETAS(J)        ANISOTROPY PARAMETERS OF THE DISTRIBUTIONS
C       N+12    PES(I,J)        INPUT DISTRIBUTIONS FOR SECONDARY DISSOCIATION
C       THRU
C       M
```

```
C       M+1     NDPES(J)        IF 0, THEN PRIMARY P(E) THAT WILL BE USED FOR
C                               SECONDARY CALCULATION IS THE SAME AS THAT USED
C                               FOR THE PRIMARY CALCULATION. THIS IS USEFUL IN
C                               THE CASE OF SECONDARY ABSORPTION OF A PHOTON
C                               SINCE SOME INTERNAL STATES OF THE PRIMARY PRO-
C                               DUCTS MAY ABSORB THE SECOND PHOTON MORE EFFI-
C                               ENTLY THAN OTHERS
C                               IN THIS CASE SET NDPES TO 1 AND INPUT A P(E)
C                               THAT INCLUDES THE PROBABILITY OF SECONDARY
C                               ABSORPTION
C       M+2     PESP(I,J)       THIS IS THE ALTERNATIVE P(E) TO BE USED,
C       THRU                    IT MUST HAVE THE SAME FORMAT AS THE PRIMARY
C       M+K                     P(E), THAT IS THE SAME EZERO, EINC AND NE
C
C+++++++++++++++++++++++++++++++++++++++++++++++++++++++++++++++++++++++++++++
C+++++++++++++++++++++++++++++++++++++++++++++++++++++++++++++++++++++++++++++
C               IN CONSTRUCTING THE P(E)'S FOR ALL THE DIFFERENT
C               PRIMARY AND SECONDARY CALCULATIONS, YOU WILL FIND A
C               SUBSET OF THE INPUT WHICH HAS THE FOLLOWING FORM
C
CCCCCCCCCCCCCCCCCCCCCCCCCCCCCCCCCCCCCCCCCCCCCCCCCCCCCCCCCCCCCCCCCCCCCCCCCCCCC
C               CHANNEL 1       CHANNEL 2       CHANNEL 3
C       M1
C       M2
C       RPROB
C       EZEROH
C       EINCH
C       BETA
C       NYSECT
C       NPDISP
C
C
C       M1S
C       M2S
C       RPROBS
C       EZEROHS
C       EINCHS
C       BETAS
C
C
CCCCCCCCCCCCCCCCCCCCCCCCCCCCCCCCCCCCCCCCCCCCCCCCCCCCCCCCCCCCCCCCCCCCCCCCCCCCC
C
C
C
C       IT IS IMPORTANT THAT THE MOST COMPLICATED CHANNELS BE PUT TO TH
C       THE FARTHEST LEFT SO THAT NDIST IS ALWAYS GREATER THAN OR EQUAL TO
C       NDISTS
C
C
C
C
C       NON EXECUTABLE STATEMENTS
C
C
      implicit real*4 (a-h,o-z)
      real*4 m1(4),m2(4),IPTHS(400),
     *M1S(4),M2S(4),OPTHS(400),IPTH(10),OPTH(10)
      COMMON/IGSZZZ/Z(200)
      DIMENSION NDPES(10)
        DIMENSION NPDISP(10),NYSECT(10),NLABEL(10),AVGSIGTOT(255)
```

```
      DIMENSION ANGLE(8),FG(8),FB(16),BPROB(8,16)
     DIMENSION ANGLEP(8),FGP(8),FBP(8),BPROBP(8,16)
     DIMENSION COSOPTHS(500),SINOPTHS(500),COSIPTHS(500),SINIPTHS(500)
     character*80 title
     dimension GAUSS(11)
     DIMENSION RPROB(10),EINC(10),EINCH(10),
    *EZERO(10),EZEROH(10),ERG(32),
    *PERG(32),PESP(10,300),PE(10,300),
    *EMEAN(10),BETA(10),NERG(10)
     DIMENSION RPROBS(10),EINCS(10),EINCHS(10),EZEROS(10),EZEROHS(10)
     DIMENSION PES(10,300),EMEANS(10),BETAS(10)
     DIMENSION CHAN(255),RAWDAT(255),TOFSIG(255),VEL(255),FLUX(255),
    *ASIG(255),AVGSIG(10,255),TIME(255),AVGSIGC(255)
     DIMENSION AVGSIGS(10,255),
       1VLS(1000),SIGNLSS(10,1000),SIGNALS(10,1000)
     DIMENSION FLUXIS(1000),SIGNLS(100,30,30,5)
     DIMENSION VLP(1000),VL(1000),SIGNL(10,1000)
       1,SIGNAL(10,1000),FLUXI(1000)
     DATA GAUSS/.0088E0,.027E0,.0648E0,.121E0,.1761E0,.1995E0
    * ,.1761E0,.121E0,.0648E0,
    *          .0270E0,.0088E0 /
     data degrad/0.017453293E0/
700  FORMAT (2I5,5F10.4)
702  FORMAT (a80)
704  FORMAT (8F10.4)
706  FORMAT (9I5)
708  FORMAT (2F10.4,I5)
800  FORMAT (1H1,20a4)
802  FORMAT ('0ANGLE =',F5.1,' DEGREES.'/
     '       '0DC BACKGROUND =',F8.1,',     MCS OFFSET =',F5.1,
     '       ' MICROSECONDS,     MCS CHANNEL WIDTH =',F6.1,
     '       ' MICROSECONDS.'/
     '       '0ION MASS =',F6.1,' AMU,     ION FLIGHT TIME =',F4.1,
     '      6H'SQRT(,F5.1,') =',F5.1,' MICROSECONDS.'/
     '       '0TIME-OF-FLIGHT PATH LENGTH =',F5.1,
     '       ' CM,      IONIZER LENGTH =',F5.1,' CM.')
803  FORMAT ('0TIME-OF-FLIGHT DATA SMOOTHED BY',I3,
    '' POINT POLYNOMIAL FILTER.')
804  FORMAT ('0ALPHA =',F5.3,5X,'SPEED RATIO =',F6.3,5X,'HALF W
    '',F5.2,' DEGREES')
805  FORMAT ('0LASER POLARIZATION ANGLE =',F4.1)
806  FORMAT ('0VELOCITY AND ANGULAR DISTRIBUTION OF BEAM')
808  FORMAT (' VELOCITY',20X,'ANGLES')
810  FORMAT (9X,8F8.2)
812  FORMAT(1H ,9F8.4)
814  FORMAT (1H1,10X,'ENERGY DISTRIBUTION(S)')
816  FORMAT (1H0,10X,'RELATIVE WEIGHTS')
817  FORMAT (1H0,10X,'ASYMMETRY PARAMETERS')
818  FORMAT (7X,7(F6.2,10X),F6.2)
819  FORMAT (1H0,10X,'MEAN ENERGIES')
820  FORMAT (1H0,10X,'ENERGIE(S) AND DISTRIBUTION(S)')
821  FORMAT ('0PRIMARY DISSOCIATION INPUT DATA')
822  FORMAT (1H ,8(F5.2,1X,F6.3,4X))
824  FORMAT ('0M1 =',F8.1,3F16.1)
826  FORMAT ('0M2 =',F8.1,3F16.1)
828  FORMAT ('0NORMALIZATIONS, EXPT. ',F8.1,',  THEORY =',F8.1)
830  FORMAT ('1TIME-OF-FLIGHT DISTRIBUTIONS',44X,
    ''VELOCITY FLUX DISTRIBUTIONS'//
    '' CH.',3X,'VELOCITY',11X,'LAB',6X,'CALCULATED',28X,
    ''VELOCITY',7X,'THEORY',6X,'IONIZER',3X,'INTERPOL.'/25X,
```

```
     ''DATA',9X,'TOF',45X,'(NOT AVG.)',3X,'AVERAGED',4X,'AVG. LAB'//)
832   FORMAT (1H ,I3,F10.2,F15.0,1F14.0,F37.2,F15.3,2F12.3)
834   FORMAT (F80.2,F15.3,2F12.3)
836   FORMAT ('1VELOCITY DISTRIBUTIONS'/)
838   FORMAT ('1TIME OF FLIGHT DISTRIBUTIONS'/)
840   FORMAT ('0SECONDARY DISSOCIATION INPUT DATA')
842   FORMAT ('0M1S = ',F8.1,3F16.1)
844   FORMAT ('0M2S = ',F8.1,3F16.1)
846   FORMAT (1H ,20X,'SECONDARY DISSOCIATION DATA')
848   FORMAT (1H ,I3,F10.2,F15.5,F14.5,F37.2,F15.3,2F12.3)
850   FORMAT (6F10.6)
632    FORMAT(1X,F6.2,2X,F10.4)
C
C
C
C       END OF NON EXECUTABLE STATEMENTS
C
C
      NYSEV=0
C
C
C       BEGINNING OF INPUT SECTION
C       REFER TO TOP FOR EXPANATION OF INPUT
C
C
5     READ (5,*) TH,DIMASS,TADJ,TPNORM,TSNORM,
     *POL,NYSEC,NDANG,ANGRES
      IF (NDANG.EQ.1) GO TO 6
      DANGINC = ANGRES/(NDANG-1)
C
C
C       IPTH AND OPTH ARE IN PLANE AND OUT OF PLANE ANGLES OF THE DETECTOR
C       USED IN THE AVERAGING OVER THE DETECTOR APERTURE
C
C
6     IF (NDANG.EQ.1) IPTH(1) = 0.
      IF (NDANG.EQ.1) OPTH(1) = 0.
      IF (NDANG.EQ.1) GO TO 12
      DO 10 ITH=1,30
      IPTH(ITH) = 0.0E0
      OPTH(ITH) = 0.0E0
 10    CONTINUE
      DO 11 ITH=1,NDANG
      IPTH(ITH) = -.5E0*ANGRES + (ITH-1)*DANGINC
      OPTH(ITH) = IPTH(ITH)
 11   CONTINUE
C
C
C
 12   COSPOL=COS(POL*degrad)
      SINPOL=SIN(POL*degrad)
20    READ (5,702) TITLE
      WRITE (6,800) TITLE
      WRITE (6,805) POL
        READ (5,*) WIDTH,ALFA,OFFSET,DIST,DL
      READ (5,*) NBCHAN,NECHAN,NACHAN,
     *             NBG1,NBG2
        MINCH = NBCHAN
      MINCH=MINCH-NBCHAN+1
      IF (NBG1.EQ.0) NBG1=231
```

```
      IF (NBG2.EQ.0) NBG2=250
35    NCHAN=NECHAN-NBCHAN+1
C
C
C       THE TOF DATA IS READ IN AT THIS POIN
C
C
      DO 40 I=1,255
      RAWDAT(I)=0.0E0
40    TOFSIG(I)=0.0E0
      READ (7,*) (ASIG(I),I=1,255)
      DO 45 I=1,255
45    RAWDAT(I)=RAWDAT(I)+ASIG(I)
      SUM=0.0E0
C
C
C       THIS LOOP SUBTRACTS THE BACKGROUND FROM THE TOF
C
C
      DO 50 I=NBG1,NBG2
50    SUM=SUM+RAWDAT(I)
      DC=SUM/(NBG2-NBG1+1)
      DO 55 I=1,NCHAN
      J=I+NBCHAN-1
55    TOFSIG(I)=RAWDAT(J)-DC
C
C
C
C       THIS LOOP CALCULATES THE VELOCITY AND THE FLUX
C       OF OF EACH CHANNEL IN THE TOF SPECTRUM,
C       THIS IS USED IN THE HARD COPY OUTPUT
C
C
      TION=ALFA*SQRT(DIMASS)
      DO 60 I=1,NCHAN
      IF (I.GE.MINCH) GO TO 58
      VEL(I)=0.0E0
      FLUX(I)=0.0E0
      GO TO 60
58    VEL(I)=DIST*100.0E0/(((I+NBCHAN-1.5E0)*WIDTH)+OFFSET-TION)
      FLUX(I)=TOFSIG(I)/VEL(I)
60    CONTINUE
C
C
C
C       THIS LOOP FINDS THE MAXIMUM CHANNEL OF
C       THE FLUX VERSION OF THE TOF
C
C
      IF (NACHAN.EQ.0) NACHAN=1
      TEMP=FLUX(1)
      N=1
      DO 65 I=2,NCHAN
      IF (FLUX(I).LT.TEMP) GO TO 65
      TEMP=FLUX(I)
      N=I
65    CONTINUE
C
C
C       HAVING FOUND THE MAXIMUM THIS LOOP USES THE NEAREST FEW
```

```
C       CHANNELS TO THE MAXIMUM, HOW MANY IS DETERMINED BY NACHAN,
C       TO NORMALIZE THE TOF SPECTRUM SCALING IT TO TPNORM
C
C
      TEMP=0.0E0
      DO 70 I=1,NACHAN
      J=N-NACHAN/2+I-1
70    TEMP=TEMP+FLUX(J)
      TEMP=TEMP/NACHAN
      DO 75 I=1,NCHAN
75    FLUX(I)=FLUX(I)*TPNORM/TEMP
C
C
C
      WRITE (6,802) TH,DC,OFFSET,WIDTH,DIMASS,ALFA,DIMASS,TION,DIST,DL
      READ (5,*) NTHBM,NVBM
      READ (5,*) VMIN,VINC,NV
      READ (5,*) ALPHA,SPDRT,HWIDBM
      WRITE (6,804) ALPHA,SPDRT,HWIDBM
C
C
C       THIS NEXT SECTION IS CONCERNED WITH CALCULATING
C       THE BEAM INTENSITY AS A FUNCTION OF VELOCITY AND
C       ANGLE OF DIVERGENCE. THIS INFORMATION IS CONTAINED
C       IN THE MATRIX  BPROB(I,J). ONE INDEX REFERS TO
C       BEAM VELOCITY AND THE OTHER REFERS TO DIVERGENCE ANGLE
C
C
C
C       THIS LOOP CONSTRUCTS FB(I) WHICH IS THE VELOCITY PART
C       OF BPROB
C
C
      VPK=SPDRT*(1.0E0+SQRT(1.0E0+4.E0/SPDRT**2))/2.E0
      FNORM=EXP((VPK-SPDRT)**2)/(VPK*VPK)
      BVINC=3.33/FLOAT(NVBM+1)
      NH=NVBM/2+1
      BVMIN=ALPHA*(VPK-FLOAT(NVBM/2)*BVINC)
      DO 80 J=1,NTHBM
      ANGLE(J)=(J-1)*2.*HWIDBM/NTHBM
C
C
C       FG(J) IS THE ANGULAR PART OF BPROB
C
C
80    FG(J)=2.-ANGLE(J)/HWIDBM
      DO 85 I=1,NVBM
      R=VPK+FLOAT(I-NH)*BVINC
      FB(I)=FNORM*R*R*EXP(-(SPDRT-R)**2)
      DO 85 J=1,NTHBM
C
C
C
C       BPROB IS CONSTRUCTED HERE
C
C
85    BPROB(J,I)=FG(J)*FB(I)
C
C
C       BVINC IS THE VELOCITY INCREMENT USED IN THE AVERAGING
```

```
C       OVER THE BEAM
C
C
      BVINC=ALPHA*BVINC
C
C
      WRITE (6,806)
      WRITE (6,808)
      WRITE (6,810) (ANGLE(I),I=1,NTHBM)
      BV=BVMIN
      DO 90 J=1,NVBM
      WRITE (6,812) BV,(BPROB(I,J),I=1,NTHBM)
90    BV=BV+BVINC
      READ (5,*) NDIST,NE,NER
      NDISTSAV=NDIST
      IF (NER.NE.0) READ (5,*) (NERG(J),J=1,NDIST)
C NERG- NUMBER OF EXPLICIT POINTS AT WHICH USER WILL INPUT TRANSLA-
C TIONAL ENERGIES (ERG) AND PROBABILITIES (PERG). THE PROGRAM WILL
C INTERPOLATE THE PE GRID FROM THESE DATA. IF NERG=0, THE PE GRID IS
C READ IN AS USUAL.
      READ (5,*) (M1(J),J=1,NDIST)
      READ (5,*) (M2(J),J=1,NDIST)
      READ (5,*) (RPROB(J),J=1,NDIST)
      READ (5,*) (EZEROH(J),J=1,NDIST)
      READ (5,*) (EINCH(J),J=1,NDIST)
      READ (5,*) (BETA(J),J=1,NDIST)
        READ (5,*) (NYSECT(J), J=1,NDIST)
        READ (5,*) (NPDISP(J), J=1,NDIST)
        DO 1002  I=1,NDIST
        IF (NYSECT(I).EQ.1.AND.NPDISP(I).EQ.1) NLABEL(I) = 1
        IF (NYSECT(I).EQ.0.AND.NPDISP(I).EQ.1) NLABEL(I) = 0
        IF (NYSECT(I).EQ.1.AND.NPDISP(I).EQ.0) NLABEL(I) = -1
 1002   CONTINUE
      DO 95 J=1,NDIST
      IF (NER.EQ.0.OR.NERG(J).EQ.0) GO TO 91
      READ (5,*) (ERG(K),K=1,NERG(J))
      READ (5,*) (PERG(K),K=1,NERG(J))
      E=EZEROH(J)
      DO 94 I=1,NE
      DO 93 K=1,NERG(J)
      IF (ERG(K).LE.E) GO TO 93
      PE(J,I)=PERG(K-1)+(PERG(K)-PERG(K-1))*(E-ERG(K-1))/
     *(ERG(K)-ERG(K-1))
      GO TO 92
93    CONTINUE
      IF (NDPES(J).EQ.1) PESP(J,I) = 0.
      PE(J,I)=0.0E0
92    E=E+EINCH(J)
94    CONTINUE
      GO TO 95
91    READ (5,*) (PE(J,I),I=1,NE)
95    CONTINUE
      IF (NYSEC.EQ.0) GO TO 102
C
C
C
C       THE FOLLOWING SECTION IS THE INPUT FOR SECONDARY DISSOCIATION
C       CALCULATIONS. IF NYSEC IS ZERO, THEN THIS IS NOT DONE
C       IF NYSEC IS ONE, THEN YOU HAVE REQUESTED SECONDARY
C       DISSOCIATION CALCULATION, AND INPUT SHOULD BE MODIFIED
```

```
C
C
C
      READ (5,*) DIMASSS
      TIONS = ALFA*SQRT(DIMASSS)!ION FLIGHT TIME
      READ (5,*) NANGS,ANGRS,NTHBMS,NVBMS
C
C
C
C       #ANGLES,ANGULAR RANGE,#OF BEAM ANGLES
C       AND # OF BEAM VELOCITIES OVER WHICH PRIMARY
C       DISSOCIATION SHOULD BE CALCULATED IN ORDER TO GENERATE AN INPUT
C       "BEAM" FOR SECONDARY DISSOCIATION AVERAGING
C
C
C
C
C       OPTHS AND IPTHS ARE THE IN PLANE AND OUT
C       OF PLANE ANGLES AT WHICH PRIMARY DISSOCIATION
C       WILL BE CALCULATED FOR THE PURPOSE OF
C       CALCULATING THE SECONDARY DISSOCIATION
C
C
C
      DO 5050 I=1,400  !INITIALIZE VARIABLES
      OPTHS(I) = 0.0E0
      IPTHS(I) = 0.0E0
5050  CONTINUE
        ANGINCS = ANGRS/(NANGS-1)
      DO 14 I=1,NANGS
      IPTHS(I) = -.5E0*ANGRS + (I-1)*ANGINCS
      OPTHS(I) = IPTHS(I)
 14   CONTINUE
C
C
C       SINCE THE SECONDARY CALCULATION
C       IS SO EXTENSIVE OFTEN YOU WILL WANT TO
C       RETAIN MORE BEAM AVERAGING FOR THE PRIMARY
C       CALCULATION THAN FOR THE SECONDARY
C       CALCULATION, THIS SECTION CALCULATES BPROBP(I,J)
C       WHICH IS ANALAGOUS TO BPROB(I,J) WHICH WILL BE USED
C        FOR THE SECONDARY CALCULATION INSTEAD OF BPROB(I,J)
C
C
      BVINCP = 3.33/FLOAT(NVBMS + 1)
      NHP = NVBMS/2 + 1
      BVMINP = ALPHA*(VPK - FLOAT(NVBMS/2)*BVINCP)
      DO 81 J=1,NTHBMS
      ANGLEP(J) = (J-1)*2.E0*HWIDBM/NTHBMS
81    FGP(J) = 2. - ANGLEP(J)/HWIDBM
      DO 86 I=1,NVBMS
      R = VPK + FLOAT(I-NHP)*BVINCP
      FBP(I) = FNORM*R*R*(-(SPDRT-R)**2)
      DO 86 J=1,NTHBMS
86    BPROBP(J,I) = FGP(J)*FBP(I)
      BVINCP = BVINCP*ALPHA
C
C
C
C
```

```
      READ (5,*) VMINS,VINCS,NVS ! MIN LAB VELOCITY, # LAB VELOCITIES,
C       AND LAB VELOCITY INCREMENT FOR SEC. DISS. CALCULATION
      READ (5,*) VMINP,VINCP,NVP
      V = VMINS
      DO 15 I=1,NVS
      VLS(I) = V
      V = V + VINCS
 15   CONTINUE
      VMAXS = VLS(NVS)
      READ (5,*) NDISTS, NES ! #P(E)'S USED FOR SEC. DISS, # OF ENERGIES
C       IN THE P(E)'S
      READ (5,*) (M1S(J),J=1,NDISTS) !DETECTED NEUTRAL MASSES FOR EACH P(E)
      READ (5,*) (M2S(J),J=1,NDISTS) !UNDETECTED  "       "    "    "   "
      READ (5,*) (RPROBS(J),J=1,NDISTS) !RELATIVE WEIGHTS OF EACH P(E)
      READ (5,*) (EZEROHS(J),J=1,NDISTS) !INITIAL ENERGIES IN P(E)'S
      READ (5,*) (EINCHS(J),J=1,NDISTS) !ENERGY INCREMENTS FOR EACH P(E)
      READ (5,*) (BETAS(J),J=1,NDISTS) !ANISOTROPY PARAMETERS FOR P(E)'S
      DO 16 J=1,NDISTS
          READ (5,*) (PES(J,I),I=1,NES) !P(E)'S FOR SECONDARY DISSOCIATION
 16   CONTINUE
      READ (5,*) (NDPES(I), I=1,NDISTS)
C
C
C       THIS LOOP READS IN THE ALTERNATIVE PRIMARY P(E)'S FOR
C       THE SECONDARY CALCULATIONS THAT THESE HAVER BEEN
C       REQUESTED FOR
C
C
        DO 1007 J=1,NDISTS
      IF (NDPES(J).NE.1) GO TO 1007
      READ (5,*) (PESP(J,I),I=1,NE)
 1007   CONTINUE
C
C
C
C
C       THIS LOOP INTEGRATES THE P(E)'S AND NORMALIZES
C       THEM TO THEIR AREA
C
C
 102  DO 97 J=1,NDIST
      PESUM=0.0E0
      PESUMP=0.
      DO 96 I=2,NE
      PESUM=PESUM+EINCH(J)*(PE(J,I)+PE(J,I-1))/2.E0
        IF (NDPES(J).EQ.1) THEN
        PESUMP=PESUMP+EINCH(J)*(PESP(J,I)+PESP(J,I-1))/2.
        END IF
 96   CONTINUE
      DO 97 I=1,NE
      PE(J,I)=PE(J,I)/PESUM
      IF (NDPES(J).EQ.0) GO TO 97
      PESP(J,I)=PESP(J,I)/PESUMP
 97   CONTINUE
C
C
C
C       THIS LOOP CALCULATES THE MEAN KINETIC ENERGY RELEASE
C       OF THE GIVEN P(E)
C
```

```
C
      DO 99 I=1,NDIST
      EMEAN(I)=0.0E0
      ENERG=EZEROH(I)+EINCH(I)/2.
      DO 98 J=2,NE
      EMEAN(I)=EMEAN(I)+ENERG*EINCH(I)*(PE(I,J)+PE(I,J-1))/2.
98    ENERG=ENERG+EINCH(I)
99    CONTINUE
C
C
C
C       THIS SECTION SCALES THE P(E) IN A FUNNY WAY SO THAT
C       THE RELATIVE ENERGY CAN BE QUICKLY CALCULATED FROM THE VELOCITY
C       OF ONE OF THE FRAGMENTS
C
C
      DO 100 J=1,NDIST
      EZERO(J)=EZEROH(J)*837.*M2(J)/(M1(J)*(M1(J)+M2(J)))
 100    EINC(J)=EINCH(J)*837.*M2(J)/(M1(J)*(M1(J)+M2(J)))
      IF (NYSEC.EQ.0)GO TO 101
C
C
C
C       THIS SECTION MANIPULATES THE INPUT DATA FOR SECONDARY
C       DISSOCIATION BEFORE IT CAN BE USED BY THE MAIN PART
C       OF THE PROGRAM
C
C
      DO 5000 J=1,NDISTS !NORMALIZE THE P(E) TO THE AREA
      PESUMS = 0.0E0
      DO 17 I=2,NES
 17   PESUMS = PESUMS + EINCHS(J)*(PES(J,I) + PES(J,I-1))/2.E0
      DO 5000 I=1,NES
5000  PES(J,I) = PES(J,I)/PESUMS
C
C
C       IT IS NECESSARY TO CALCULATE ALL OF THE SINES
C       AND COSINES THAT WILL BE USED IN THE SECONDARY CALCULATION
C       IN ADVANCE SO THAT THEY ARE CALCULATED ONLY ONCE
C       THIS SPEEDS UP THE INNERMOST LOOPS OF THE CALCULATION
C
C
      DO 5020 KTHS=1,NANGS
      COSOPTHS(KTHS)=COS(OPTHS(KTHS)*DEGRAD)
5020  SINOPTHS(KTHS)=SIN(OPTHS(KTHS)*DEGRAD)
      DO 5030 I=1,NANGS
      COSIPTHS(I)=COS(IPTHS(I)*DEGRAD)
5030  SINIPTHS(I)=SIN(IPTHS(I)*DEGRAD)
C
C
C
      DO 18 I=1,NDISTS ! CALCULATE AVERAGES OF P(E)'S
      EMEAN(I) = 0.0E0
      ENERG = EZEROHS(I) + EINCHS(I)/2.E0
      DO 19 J=2,NES
      EMEAN(I) = EMEAN(I) + ENERG*EINCHS(I)*(PES(I,J) + PES(I,J-1))/2.E0
 19   ENERG = ENERG + EINCHS(I)
 18   CONTINUE
      DO 21 J=1,NDISTS ! CONVERT P(E) TO U1**2 SPACE
      EZEROS(J) = EZEROHS(J)*837.*M2S(J)/(M1S(J)*(M1S(J) + M2S(J)))
```

```
21    EINCS(J) = EINCHS(J)*837.*M2S(J)/(M1S(J)*(M1S(J) + M2S(J)))
      WRITE (6,821)
      WRITE (6,821)
      WRITE (6,821)
C
C
C
C
 101  WRITE (6,814)
      WRITE (6,816)
      WRITE (6,818) (RPROB(J),J=1,NDIST)
      WRITE (6,819)
      WRITE (6,818) (EMEAN(J),J=1,NDIST)
      WRITE (6,817)
      WRITE (6,818) (BETA(J),J=1,NDIST)
      WRITE (6,820)
      DO 105 I=1,NE
 105  WRITE (6,822) (EZEROH(J)+EINCH(J)*(I-1),PE(J,I),J=1,NDIST)
      WRITE (6,824) (M1(J),J=1,NDIST)
      WRITE (6,826) (M2(J),J=1,NDIST)
      WRITE (6,828) TPNORM,TSNORM
      IF (NYSEC.EQ.0) GO TO 208
C
C
C
C
      WRITE (6,840)
      WRITE (6,840)
      WRITE (6,840)
      WRITE (6,814)
      WRITE (6,816)
      WRITE (6,818) (RPROBS(J),J=1,NDISTS)
      WRITE (6,819)
      WRITE (6,818) (EMEANS(J),J=1,NDISTS)
      WRITE (6,817)
      WRITE (6,818) (BETAS(J),J=1,NDISTS)
      WRITE (6,820)
      DO 498 I=1,NES
498   WRITE (6,822) (EZEROHS(J) + EINCHS(J)*(I-1),PES(J,I), J=1,NDISTS)
      WRITE (6,842) (M1S(J),J=1,NDISTS)
      WRITE (6,844) (M2S(J),J=1,NDISTS)
C
C
C
C       HEART OF PROGRAM (WHAT AN INFORMATIVE COMMENT)
C       THIS IS WHERE THE ACTUAL NUMBER CRUNCHING TAKES
C       PLACE
C
C
208   CONTINUE
      TYPE *, 'INPUT SUCCESSFUL'
      V=VMIN
      DO 110 I=1,NV
      VL(I)=V
 110  V=V+VINC
      VMAX=VL(NV)
      IF (NYSEC.EQ.0) GO TO 5204
      VP = VMINP
      DO 5203 I=1,NVP
      VLP(I) = VP
```

```
5203  VP = VP + VINCP
      VMAXP = VLP(NVP)
C
C
C
5204  DO 112 I=1,NV
      SIGNL(10,I) = 0.0E0
      SIGNAL(10,I) = 0.0E0
      DO 112 J=1,NDIST
      SIGNL(J,I)=0.0E0
 112  SIGNAL(J,I)=0.0E0
      DO 115 I=1,NCHAN
 115  AVGSIG(10,I)=0.0E0
C
C
C
      IF (NYSEC.EQ.0) GO TO 207
      DO 122 I=1,NVS
      SIGNLSS(10,I)=0.0E0
 122  SIGNALS(10,I)=0.0E0
      DO 124 I=1,NCHAN
 124  AVGSIGS(10,I)=0.0E0
C
C
C
C        THIS IS THE HEART OF THE PROGRAM
CCCCCCCCCCCCCCCCCCCCCCCCCCCCCCCCCCCCCCCCCCCCCCCCCCCC
C        THIS PARAGRAPH IS A DESCRIPTION OF THE COORDINATE SYSTEM USED IN DER-
C        IVING THE FORMULAE NECESSARY TO THE EXECUTION OF THE PROGRAM.
C        1)IT IS A CARTESIAN (X,Y,Z) COORDINATE SYSTEM
C        2)THE NOMINAL BEAM DIRECTION IS THE X DIRECTION
C        3)THE X,Y PLANE IS THE PLANE DEFINED BY THE NOMINAL DIRECTIONS
C        OF THE MOLECULAR BEAM AND THE DETECTOR DIRECTION. THE Z AXIS IS DEFINED
C        WITHIN THIS RIGHT HANDED COORDINATE SYSTEM AS ALONG THE LASER PROPOGA-
C        TION DIRECTION, HOWEVER IT IS ANTI PARALLEL TO THE LASER
CCCCCCCCCCCCCCCCCCCCCCCCCCCCCCCCCCCCCCCCCCCCCCCCCCCC
C        THE PROGRAM FUNCTIONS IN THE FOLLOWING WAY FOR PRIMARY DISSOCIATION.
C        THERE IS A SERIES OF NESTED DO LOOPS WHICH ACCOMPLISH THE FOLLOWING:
C        1)AN INPUT P(E) IS CHOSEN : LOOP 210
C        2)AN IN PLANE ANGLE OF ACCEPTANCE TO THE DETECTOR IS CHOSEN : LOOP 211
C        3)AN OUT OF PLANE ANGLE OF ACCEPT. "  "      "     "   "    : LOOP 212
C        4)A LAB SPEED IS CHOSEN : LOOP 190
C        5)A BEAM DIVERGENCE ANGLE IS CHOSEN : LOOP 180
C        6)A BEAM AZIMUTHAL ANGLE IS CHOSEN : LOOP 180
C        7)A BEAM SPEED IS CHOSEN : LOOP 170
C        8)FROM THE SPECIFIED VB AND V VECTORS A U VECTOR IS CALCULATED
C        THAT IS THE C.M. RECOIL VELOCITY VECTOR
C        9)THE PROBABILITY THAT THIS CHOICE OF BEAM VECTOR(BASED ON BEAM PROFILE
C        THAT WAS CALCULATED EARLIER USING TH ARRAY BPROB(BTH,KVB))
C        AND RECOIL C.M.VECTOR(BASED ON P(E) AND POLARIZATION CALCULATION)
C        IS GOING TO OCCUR IS CALCULATED.
C        JACOBIAN IS TAKEN INTO CONSIDERATION.
C        10)BEAM VELOCITY IS INCREMENTED AND LOOP OUT OF 170
C        11)BEAM ANGLES ARE INCREMENTED AND LOOP OUT OF 180
C        12)THE SUM OF ALL THE PROBABILITIES CALCULATED SO FAR IS THE CONTRIBU-
C        TION AT THIS LAB VELOCITY VECTOR.
C        THE LAB VELOCITY  VECTOR IS INCREMENTED OVER THE REGION OF INTEREST
C        IN THIS CASE, ITS MAGNITUDE IS INCREMENTED FROM VMIN TO VL(NVS) IN
C        INCREMENTS OF VINC,THE ANGLES ARE INCREMENTED OVER THE VIEWING REGION
C        OF THE DETECTOR.
```

```
C       FINALLY, THE RESULT AT EACH LAB SPEED
C       IS AVERAGED OVER THE IONIZER (MODELED AS A GAUSSIAN
C       ELECTRON DENSITY DISTRIBUTION) AND IS CONVERTED FROM I(V) TO N(T)
CCCCCCCCCCCCCCCCCCCCCCCCCCCCCCCCCCCCCCCCCCCCCCCCCCCCCCCCCCCCCCCCCCCCCCC
CCCCCCCCCCCCCCCCCCCCCCCCCCCCCCCCCCCCCCCCCCCCCCCCCCCCCCCCCCCCCCCCCCCCCCC
C       THE PROGRAM FUNCTIONS IN THE FOLLOWING WAYFOR SECONDARY DISSOCIATION.
C       IN THIS CASE NYSEC IS SET TO ONE. THIS TELLS THE PROGRAM TO ESSENTIALLY
C       EXTEND THE ANGULAR RANGE OVER WHICH THE AVERAGING OF THE DETECTOR APER-
C       TURE IS DONE. THIS PROCESS GENERATES THE ARRAY SIGNLS(I,J,KTHS,KPHS)
C       WHERE:
C               I       RANGES OVER THE P(E)'S
C               J       RANGES OVER SPEEDS OF LAB RECOIL VELOCITY
C               KTHS    RANGES OVER THE IN PLANE ANGLES OF THE LAB RECOIL
C                       VECTORS
C               KPHS    RANGES OVER THE OUT OF PLANE ANGLES
C       SIGNLS IS AN  I(V)
C
C       AFTER THIS IS DONE NYSEC IS INCREMENTED TO 2 AND THIS TELLS THE PROGRAM
C       1)TO USE SIGNLS AS A BEAM PROFILE ARRAY
C       2)TO CALCULATE THE SECONDARY DISSOCIATION TOF ESSENTIALLY USING THE
C       PRIMARY DISSOCIATON FLUX MAP AS THE NEW BEAM.
C
C
C       LOOP 210 RANGES OVER THE COLUMNS OF THE DISSOCIATION
C       MAP
C
C
207     DO 210 I=1,NDIST! INPUT P(E)'S
C
C
C       FLAGS ARE SET TO HANDLE SECONDARY CALCULATION
C
C
        IF (NLABEL(I).EQ.1.OR.NLABEL(I).EQ.-1) THEN
        NYSEV = 1
        NYSEC = 0
        END IF
C
C
C       THIS IS THE CASE WHERE ONLY PRIMARY IS CALCULATED
C
C
        IF (NLABEL(I).EQ.0) NYSEC = 0
C
C
C
C       WHETHER OR NOT SECONDARY IS CALCULATED THE FIRST RUN THROUGH
C       THE PROGRAM ASSUMES ONLY THE PRIMARY TOF IS TO BE CALCULATED
C       THIS IS DENOTED BY SETTING THE FLAG NYSEC = 0, NYSEV
C       HOLDS THE ORIGINAL VALUE OF NYSEC
C
C
C       NYSEC IS INCREMENTED AFTER THE FIRST PASS THROUGH AND THE
C       RANGE OF NDANG IS ALTERED TO GENERATE A CALCULATION
C       AT ALL ANGLES IN THREE DIMENSIONAL SPACE WHERE PRIMARY
C       PRODUCT IS SCATTERED
C
C
209   IF (NYSEC.EQ.1) NDANGSAV=NDANG
C
```

```
C
C       AFTER NYSEC =1 GENERATES THE PROBABILITY MAP FOR THE
C       "MOLECULAR BEAM" GIVEN BY THE PRIMARY DISSOCIATION
C       THE PROGRAM IS RUN THROUGH AGAIN AS IF YOU WERE CALCULATING A
C       PRIMARY DISSOCIATION BUT THE AVERAGING PARAMETERS FOR SECONDARY
C       DISSOCIATION ARE USED AND THE PROBABILITY MAP IS USED
C
C
C
C
      IF (NYSEC.EQ.2) NDANG=NDANGSAV
C
C
C
      IF (NYSEC.EQ.1) NDANG = NANGS
C
C
C
      DO 211 ITH=1,NDANG ! IN PLANE DETECTOR APERTURE ANGLE
      THD = TH - IPTH(ITH)
      IF (NYSEC.EQ.1) THEN
      COSIPTH=COSIPTHS(ITH)
      SINIPTH=SINIPTHS(ITH)
      ELSE
      COSIPTH = COS(THD*DEGRAD)
      SINIPTH = SIN(THD*DEGRAD)
      END IF
C
C
C       NOTE THAT COSIPTH AND SINIPTH HAVE DIFERRENT MEANING DEPENDING
C       ON WHETHER NYSEC = 0 OR 1
C
C
6300  DO 212 JTH=1,NDANG ! OUT OF PLANE DETECTOR ANGLE
      THD = OPTH(JTH)
      IF (NYSEC.EQ.1) THEN
      COSOPTH=COSOPTHS(JTH)
      SINOPTH=SINOPTHS(JTH)
      ELSE
      COSOPTH = COS(THD*DEGRAD)
      SINOPTH = SIN(THD*DEGRAD)
      END IF
5200  NVSAV = NV
      IF (NYSEC.EQ.1) NV=NVP
      IF (NYSEC.EQ.2) NV = NVS
      DO 190 J=1,NV ! DETECTED LAB VELOCITIES
      SIG = 0.0E0
C
C
C
      IF (NYSEC.EQ.2) GO TO 195 ! IF YOU ARE CALCULATING SECONDARY DISSOCIA-
C       TION IT IS NECESSARY TO USE SLIGHTLY DIFFERENT FORMULAE, DUE TO THE
C       DEFINITION OF THE ANGLES, BTH,PH,IPTHS,OPTHS
C
C
C
      IF (NYSEC.EQ.1) NTHBM=NTHBMS
      DO 180 KTH=1,NTHBM !ANGULAR DEFINITION OF BEAM
      IF (NYSEC.EQ.1) THEN
      COSBTH=COS(ANGLEP(KTH)*DEGRAD)
```

```
      SINBTH=SIN(ANGLEP(KTH)*DEGRAD)
      ELSE
      COSBTH = COS(ANGLE(KTH)*DEGRAD)
      SINBTH = SIN(ANGLE(KTH)*DEGRAD)
      END IF
5201  KPHM = MAX0(1,4*(KTH-1))!THIS CHOOSES THE # OF AZIMUTHAL ANGLES TO BE
C       AVERAGED OVER
      DO 180 KPH=1,KPHM ! AZIMUTHAL ANGLE OF BEAM
      COSPH = COS(6.283185*(KPH-1)/KPHM) !6.283185 = 2PI
      SINPH = SIN(6.283185*(KPH-1)/KPHM)
      IF (NYSEC.EQ.1) THEN
      BV= BVMINP
      NVBM=NVBMS
      BVINC=BVINCP
      ELSE
      BV = BVMIN
      END IF
5202  DO 170 KVB=1,NVBM ! SPEED OF BEAM
      COSDTH = COSBTH*COSOPTH*COSIPTH + SINBTH*COSPH*COSOPTH*SINIPTH +
     *SINBTH*SINPH*SINOPTH !COSDTH IS THE COS OF THE ANGLE BETWEEN THE
C
C
C       CHOSEN BEAM VEL. VECTOR AND THE CHOSEN DETECTED LAB VEL. VECTOR
C       THE CENTER-OF-MASS RECOIL SPEED IS CALCULATED FROM THE LAW
C       OF COSINES.
C
C
      IF (NYSEC.EQ.1) THEN
      USQ = VLP(J)*VLP(J) + BV*BV - 2.E0*VLP(J)*BV*COSDTH
      ELSE
      USQ = VL(J)*VL(J) + BV*BV -2.0E0*VL(J)*BV*COSDTH ! U**2
      END IF
C
C
C
C       THE NEXT FEW LINES ARE THE PROCESS OF LOOKING UP THE PROBABILITY
C       ON THE CHOSEN P(E)
C
C
C
5205  COOR = (USQ - EZERO(I))/EINC(I)
      IF (COOR.LT.0.0E0) GO TO 170
      INDX = INT(COOR) + 1
      IF (INDX.GE.NE) GO TO 170
      TMP = INDX-COOR
      IF (NYSEC.EQ.1.AND.NDPES(I).EQ.1) THEN
      EPROB = PESP(I,INDX)*TMP+PESP(I,INDX)*(1.-TMP)
      ELSE
      EPROB = (PE(I,INDX)*TMP + PE(I,INDX + 1)*(1.0E0 - TMP))*RPROB(I)
      END IF
C
C
C
C       SO FAR ONLY THE MAGNITUDE OF THE C.M.RECOIL VECTOR HAS BEEN SPECIFIED
C       IT IS NOW TIME TO CALCULATE THE COMPONENTS AND HENCE THE DIRECTION
C
C
C
      IF (NYSEC.EQ.1) THEN
      UX=VLP(J)*COSOPTH*COSIPTH-BV*COSBTH
```

```
      UY=BV*SINBTH*COSPH-VLP(J)*COSOPTH*SINIPTH
      ELSE
      UX = VL(J)*COSOPTH*COSIPTH - BV*COSBTH ! X COMPONENT OF U
      UY = BV*SINBTH*COSPH - VL(J)*COSOPTH*SINIPTH ! Y COMPONENT OF U
      END IF
5206  IF (POL.EQ.1000) GO TO 171 ! POL = 1000 MEANS THAT THE YOU HAVE CHOSEN
C       THE LIGHT TO BE UNPOLARIZED
      COSTHV = (UX*COSPOL + UY*SINPOL)/SQRT(USQ) ! COSTHV IS THE COS OF THE
C       ANGLE BETWEEN U VECTOR AND THE POLARIZATION VECTOR OF THE LIGHT
      POLAR = (1.0E0 + BETA(I)*(1.5D0*COSTHV*COSTHV - 0.5E0))/12.5663706
C       POLAR IS THE PROBABILITY FACTOR DUE TO POLARIZATION
C       12.5663706 IS 4*PI
 172  EPROB = EPROB*POLAR
      GO TO 173
C
C
C
C       THIS IS WHERE THE CORRECT EXPRESSION FOR THE UNPOLARIZED CASE IS
C
C
C
 171  UXT=UX/SQRT(USQ)
      UYT=UY/SQRT(USQ)
      THVMIN=ACOS(UXT**2+UYT**2)
      POLAR=((3.141592654-2.0E0*THVMIN)*(1.0E0+BETA(I)/4.0E0)
     *-3.0E0*BETA(I)/4.0E0*SIN(2.0E0*THVMIN))/12.56637062
      GO TO 172
C
C
 173  S = M1(I)/M2(I)*EPROB*VL(J)*VL(J)/SQRT(USQ)*BPROB(KTH,KVB) ! THIS LINE
C
C
C
C       IS THE JACOBIAN FOR CONVERTING I(E) IN C.M. TO I(V) IN LAB
C
C
C
      IF (ANGLE(KTH).NE.0.) S=S*2.E0*SINBTH/(ANGLE(KTH)*DEGRAD)
C
C
C
C       THIS LAST LINE IS NECESSARY TO CORRECT THE WAY IN WHICH THE AZIMUTHAL
C       AVERAGING OVER THE BEAM VELOCITY VECTORS IS DONE. IF YOU LOOK AT THE
C       WAY IN WHICH KPHM IS DEFINED YOU WILL SEE THAT THIS GENERATES A PRO-
C       BABILITY FACTOR PROPORTIONAL TO BTH. IN ACTUALITY THE PROBABILITY FAC-
C       TOR SHOULD BE PROPORTIONAL TO THE
C       CIRCUMFERENCE OF THE CIRCLE SCRIBED OUT
C       BY THE AZIMUTHAL ANGLE, OR, EQUIVALENTLY IT SHOULD BE PROPORTIONAL TO
C       THE RADIUS OF THAT SAME CIRCLE WHICH IS PROPORTIONAL TO THE SINBTH.
C       THIS WOULD IMPLY PICKING A NON INTEGER VALUE OF THE # OF AZIMUTHAL ANG-
C       LES TO BE AVERAGED OVER WHICH OF COURSE IS IMPOSSIBLE
C       THIS THEREFOR SUGGESTS THAT A CORRECTION TERM BE USED (SINBTH/BTH)
C
C
      SIG = SIG + S
 170  BV = BV + BVINC
C
C       THIS ENDS AVERAGING OVER BEAM VELOCITIES
C
C
```

```
 180  CONTINUE
C
C       THIS ENDS AVERAGING OVER BEAM ANGLES
C
C
C       IF NYSEC = 0 THE TOF IS CALCULATED
C       AT 181
      IF (NYSEC.EQ.0) GO TO 181
C
C
C       IF NYSEC =1 THE PROBABILITY MAP IS GENERATED
C
C
      SIGNLS(J,JTH,ITH,I) = SIG*VL(J)*VL(J)
C
C
C       MULTIPLYING BY VL(J)**2 IS NECESSARY BECAUSE THE DENSITY OF POINTS
C       THAT ARE BEING SAMPLED IS INVERSLY PROPORTIONAL TO VL(J)**2
C
C
      SIGNLS(J,JTH,ITH,5) = SIGNLS(J,JTH,ITH,5) + SIGNLS(J,JTH,ITH,I)
      GO TO 190
C
C
 181  SIGNL(I,J) = SIGNL(I,J) + SIG
      SIGNL(10,J) = SIGNL(10,J) + SIGNL(I,J)
      GO TO 190
C
C
C       THE FOLLOWING SECTION IS THE CALCULATION OF THE SECONDARY DISSOCIATION
C       TOF, THE LOOPS BEGINNING AT 195 ARE REACHED ONLY IF NYSEC = 2
C       THE VELOCITY FLUX MAP OF THE PRIMARY DISSOCIATION PROCESS IS NOW
C       USED AS AN INPUT BEAM.
C       IN THIS SECTION THE LETTER S HAS BEEN ADDED TO THE END OF THE VARIABLE
C       NAMES IN ORDER TO STRESS THE ANALOGY WITH OTHER PARTS OF THE PROGRAM
C
C
 195  SIGS = 0.0E0
      DO 196 KTHS=1,NANGS ! IN PLANE ANGLE OF BEAM
      DO 196 KPHS=1,NANGS! OUT OF PLANE ANGLE
      DO 197 JV=1,NVP ! SPEED OF NEW BEAM
      COSDTHS = COSOPTHS(KPHS)*COSIPTHS(KTHS)*COSOPTH*COSIPTH
     *          + COSOPTHS(KPHS)*SINIPTHS(KTHS)*COSOPTH*
     *SINIPTH + SINOPTHS(KPHS)*SINOPTH
      USQS = VLS(J)*VLS(J)+VLP(JV)*VLP(JV)-2.E0*VLS(J)*VLP(JV)*COSDTHS
      COORS = (USQS - EZEROS(I))/EINCS(I)
      IF (COORS.LT.0.0E0) GO TO 197
      INDXS = INT(COORS) + 1
      IF (INDXS.GE.NES) GO TO 197
      TMPS = INDXS - COORS
      EPROBS = (PES(I,INDXS)*TMPS +
     *PES(I,INDXS + 1)*(1.0E0 - TMPS))*RPROBS(I)
      IF (EPROBS.EQ.0.0E0) GO TO 197
      UXS = VLS(J)*COSOPTH*COSIPTH - VLP(JV)*
     *COSOPTHS(KPHS)*COSIPTHS(KTHS)
      UYS=VLP(JV)*COSOPTHS(KPHS)*SINIPTHS(KTHS)-VLS(J)*COSOPTH*SINIPTH
C       IF (POL.EQ.1000.) GO TO 198
      COSTHVS = (UXS*COSPOL + UYS*SINPOL)/SQRT(USQS)
      POLARS = (1.0E0 + BETAS(I)*
     *(1.5E0*COSTHVS*COSTHVS - 0.5E0))/12.5663706
```

```
194   EPROBS = EPROBS*POLARS
      GO TO 199
198   UXST=UXS/SQRT(USQS)
      UYST=UYS/SQRT(USQS)
      THVMINS=ACOS(UXST**2+UYST**2)
      POLARS=((3.141592654-3.0E0*THVMINS)*(1.0E0+BETAS(I)/4.0E0)
     *-3.0E0*BETAS(I)/4.0E0*SIN(2.0E0*THVMINS))/12.56637062
      GO TO 194
199   SS = M1S(I)/M2S(I)*EPROBS*VLS(J)*VLS(J)/
     *SQRT(USQS)*SIGNLS(JV,KPHS,KTHS,I)
      SINBTHS = SQRT(SINOPTHS(KPHS)**2 + COSOPTHS(KPHS)**2*
     *SINIPTHS(KTHS)**2)
      IF (SINBTHS.NE.0) SS = SS*2.E0*SINBTHS/ASIN(SINBTHS)
      SIGS = SIGS + SS
197   CONTINUE
196   CONTINUE
      SIGNLSS(I,J) = SIGNLSS(I,J) + SIGS
      SIGNLSS(10,J) = SIGNLSS(10,J) + SIGNLSS(I,J)
190   CONTINUE
212   CONTINUE
211   CONTINUE
      IF (NYSEC.EQ.1.OR.NYSEC.EQ.2) NYSEC = NYSEC + 1
      IF (NYSEC.EQ.2) GO TO 209
C
C
C       WE HAVE NOW GENERATED THE FOLLOWING ARRAYS
C               SIGNL(I,J)      I(V) PRIMARY PROCESS FOR EACH P(E)
C               SIGNL(10,J)     SUM OF ALL PRIMARY I(V)'S FOR EACH P(E)
C               SIGNLSS(I,J)    I(V) SECONDARY PROCESS FOR EACH P(E)
C               SIGNLSS(10,J)   SUM OF ALL SECONDARY I(V)'S FOR EACH P(E)
C       THE NEXT STEP IS TO AVERAGE THEM OVER THE IONIZER LENGHTH.
C       THIS IS DONE BY ASSUMING THAT THE ELECTRON DENSITY FUNCTION ALONG
C       TH AXIS OF THEE IONIZERIS A GAUSSIAN.
C
C
      IF (NYSEC.EQ.3) GO TO 402
C
C
C       IONIZER AVERAGING OF SIGNL(I,J)
C
C
      NV = NVSAV
      DO 400 J=1,NV
      SIG = 0.0E0
      DO 401 J1=-5,5,1
      VPRIME = VL(J)/(1 + J1*DL/DIST/4)
      IF (VPRIME.GT.VMAX.OR.VPRIME.LT.VMIN) GO TO 401
      JV = INT((VPRIME-VMIN)/VINC) + 1
      IF (JV.GE.NV) JV = NV - 1
      VLESS = VMIN + (JV-1)*VINC
      SIGADD = GAUSS(J1+6)*(SIGNL(I,JV) + (SIGNL(I,JV+1) - SIGNL(I,JV))*
     *(VPRIME-VLESS)/VINC)
      SIG = SIG + SIGADD
401   CONTINUE
      SIGNAL(I,J) = SIG
400   SIGNAL(10,J) = SIGNAL(10,J) + SIGNAL(I,J)
C
C
C       IONIZER AVERAGING FOR SIGNLSS(I,J)
C
```

```
C
402   IF (NYSEC.NE.3) GO TO 415
      DO 410 J=1,NVS
      SIGS = 0.0E0
      DO 411 J1=-5,5,1
      VPRIME = VLS(J)/(1 + J1*DL/DIST/4.)
      IF (VPRIME.GT.VMAXS.OR.VPRIME.LT.VMINS) GO TO 411
      JV = INT((VPRIME-VMINS)/VINCS) + 1
      IF (JV.GE.NVS) JV = NVS - 1
      VLESS = VMINS + (JV-1)*VINCS
      SIGADD = GAUSS(J1+6)*(SIGNLSS(I,JV) + (SIGNLSS(I,JV+1)-
     *SIGNLSS(I,JV))*(VPRIME-VLESS)/VINCS)
      SIGS = SIGS + SIGADD
411   CONTINUE
      SIGNALS(I,J) = SIGS
410   SIGNALS(10,J) = SIGNALS(10,J) + SIGNALS(I,J)
      IF (NYSEC.EQ.3) GO TO 422
C
C
C       THE NEXT STEP IS TO CALCULATE THE TOF SPECTRUM AND AVERAGE IT
C       OVER EACH OF THE MCS CHANNELS USED IN THE EXPERIMENT
C       CALCULATE THE TOF FOR SIGNAL(I,J)
C
C
415   DO 420 J=1,NCHAN
      SIG = 0.0E0
      DO 421 J1=0,9
      VPRIME = DIST*100.E0/(((J+NBCHAN+.1E0*J1-1.95E0)*
     *WIDTH)+OFFSET-TION)
      IF (VPRIME.GE.VMAX.OR.VPRIME.LE.VMIN) GO TO 421
      JV = INT((VPRIME-VMIN)/VINC) + 1
      IF (JV.GE.NV) JV = NV-1
      VLESS = VMIN + (JV-1)*VINC
      SIG = SIG + .1E0*(SIGNAL(I,JV)+(SIGNAL(I,JV+1)-SIGNAL(I,JV))*
     *(VPRIME-VLESS)/VINC)
421   CONTINUE
      AVGSIG(I,J) = SIG*VEL(J) !CONVERTS JACOBIAN TO CORRECT FORM
420   AVGSIG(10,J) = AVGSIG(10,J) + AVGSIG(I,J)
C
C
C       CALCULATE THE TOF OF SIGNALS(I,J)
C
C
422   IF (NYSEC.NE.3) GO TO 432
      DO 430 J=1,NCHAN
      SIGS = 0.0E0
      DO 431 J1=0,9
      VPRIME = DIST*100.E0/(((J+NBCHAN+.1E0*J1-1.95E0)*
     *WIDTH)+OFFSET-TIONS)
      IF (VPRIME.GE.VMAXS.OR.VPRIME.LE.VMINS) GO TO 431
      JV = INT((VPRIME-VMINS)/VINCS) + 1
      IF (JV.GE.NVS) JV = NVS-1
      VLESS = VMINS + (JV-1)*VINCS
      SIGS = SIGS + .1E0*(SIGNALS(I,JV)+(SIGNALS(I,JV+1)-
     *SIGNALS(I,JV))*(VPRIME-VLESS)/VINCS)
431   CONTINUE
      AVGSIGS(I,J) = SIGS*VEL(J)
      AVGSIGS(10,J) = AVGSIGS(10,J) + AVGSIGS(I,J)
430   CONTINUE
432   IF (NYSEC.EQ.3) NYSEV = 0
```

```
      IF (NYSEV.EQ.1) NYSEC = 1
      IF (NYSEC.EQ.1) GO TO 209
210   CONTINUE
C
C
CCCCCCCCCCCCCCCCCCCCCCCCCCCCCCCCCCCCCCCCCCCCCCCCCCCCCCCCCCCCCCCCCC
C       THIS IS THE END OF THE HEART OF THE PROGRAM
CCCCCCCCCCCCCCCCCCCCCCCCCCCCCCCCCCCCCCCCCCCCCCCCCCCCCCCCCCCCCCCCCC
C
C
C       NORMALIZE THE VELOCITY AND TOF DISTRIBUTIONS
C
C
C
C       THIS SECTION FINDS THE MAX OF THE TOF DATA
C
C
      TEMP = TOFSIG(1)
      K = 1
      DO 225 I=2,NCHAN
      IF (TOFSIG(I).LT.TEMP) GO TO 225
      TEMP = TOFSIG(I)
      K = I
225   CONTINUE
      TEMP = 0.0E0
      NACHAM = NACHAN
      IF (NACHAN.EQ.0) NACHAM = 1
      DO 230 I=1,NACHAM
      L = K - NACHAM/2 + I - 1
230   TEMP = TEMP + TOFSIG(L)
C
C       TOFMAX IS THE AVERAGED MAXIMUM OF THE TOF DATA
C
        TOFMAX = TEMP/NACHAM
C
C
C       THE TOTAL OF ALL PRIMARY CHANNELS IS SCALED TO
C       THE TOF DATA, THIS ENSURES THAT ALL SEPARATE PRIMARY
C       CHANNELS WILL HAVE THE CORRECT PROPORTION TO ONE
C       ANOTHER
C
C
      TEMP = AVGSIG(10,1)
      DO 235 J=2,NCHAN
235   IF (AVGSIG(10,J).GT.TEMP) TEMP = AVGSIG(10,J)
      DO 240 J=1,NCHAN
      IF (TEMP.EQ.0) GO TO 240
      AVGSIG(10,J) = AVGSIG(10,J)*TOFMAX/TEMP
      DO 240 I1=1,NDISTSAV
      AVGSIG(I1,J)=AVGSIG(I1,J)*TOFMAX/TEMP
240   CONTINUE
C
C
C
C       THE SAME IS DONE WITH ALL THE SECONDARY CHANNELS
C
C
        IF (NYSEV.EQ.0) GO TO 526
        TYPE *, NYSEV
      TEMP = AVGSIGS(10,1)
```

```
      DO 520 J=2,NCHAN
520   IF (AVGSIGS(10,J).GT.TEMP) TEMP = AVGSIGS(10,J)
      DO 525 J=1,NCHAN
      AVGSIGS(10,J) = AVGSIGS(10,J)*TOFMAX/TEMP
      DO 525 I=1,NDISTS
      AVGSIGS(I,J) = AVGSIGS(I,J)*TOFMAX/TEMP
525   CONTINUE
526     CONTINUE
C
C
C
C       THIS LOOP DECIDES WHICH CHANNELS ARE TO BE ADDED TO
C       GIVE THE TOTAL TOF
C
C
        DO 529 I=1,NCHAN
529     AVGSIGTOT(I) = 0.0
        DO 530 I=1,NDIST
        DO 530 J=1,NCHAN
        IF (NPDISP(I).EQ.1) THEN
C
C
C       TPNORM SCALES THE PRIMARY DATA
C
        AVGSIGTOT(J) = AVGSIGTOT(J) + TPNORM*AVGSIG(I,J)
C
C
        END IF
        IF (NYSECT(I).EQ.1) THEN
C
C
C       TSNORM SCALES THE SECONDARY DATA
C
C
        AVGSIGTOT(J) = AVGSIGTOT(J) + TSNORM*AVGSIGS(I,J)
C
C
        END IF
530     CONTINUE
        TEMP = AVGSIGTOT(1)
        DO 535 I=2,NCHAN
535     IF (TEMP.LT.AVGSIGTOT(I)) TEMP = AVGSIGTOT(I)
C
C       THIS LOOP NORMALIZES THE CALCULATED DATA TO
C       THE OBSERVED TOF
C
C
        DO 540 I=1,NCHAN
        AVGSIGTOT(I) = AVGSIGTOT(I)*TADJ*TOFMAX/TEMP
        DO 540 J=1,NDIST
        AVGSIG(J,I) = AVGSIG(J,I)*TADJ*TOFMAX/TEMP
        IF (NYSECT(J).EQ.1) THEN
        AVGSIGS(J,I) = AVGSIGS(J,I)*TADJ*TOFMAX/TEMP
        END IF
540     CONTINUE
C
C
C
C
C
```

```
C
C
C
C       THIS LOOP CREATES THE PART OF THE TELL-A-GRAFF
C       FILE THAT PLOTS THE OBSERVED TOF
C
C
320      WRITE(8,*) ' INPUT DATA. '
      WRITE(8,*) ' "OBSERVED TOF" '
      DO 600 I=MINCH,NCHAN
      NCH=I+NBCHAN-1
      FT=NCH*WIDTH+offset
      WRITE(8,*) FT,TOFSIG(I)
600   CONTINUE
C
C
C       THIS LOOP MAKES THE PART OF THE TELL-A-GRAFF
C       FILE THAT WILL PLOT AVGSIGTOT
C
C
C
        WRITE (8,*) '"TOTAL CALCULATED TOF"'
        DO 610 I=1,NCHAN
        NCH = I + NBCHAN - 1
        FT = NCH*WIDTH + OFFSET
610     WRITE (8,*) FT,AVGSIGTOT(I)
C
C
        DO 621 J=1,NDIST
        IF (NPDISP(J).EQ.0.AND.NYSECT(J).EQ.0) GO TO 621
        IF (NPDISP(J).EQ.1) GO TO 615
        IF (NPDISP(J).EQ.0.AND.NYSECT(J).EQ.1) GO TO 617
615   WRITE(8,*) '"CALCULATED PRIMARY TOF" '
        DO 620 I=1,NCHAN
      NCH=I+NBCHAN-1
      FT=NCH*WIDTH+offset
       WRITE(8,*) FT,AVGSIG(J,I)
620   CONTINUE
        IF (NYSECT(J).EQ.1) GO TO 617
        GO TO 621
617     WRITE (8,*) '"CALCULATED SECONDARY TOF"'
        DO 618 I=1,NCHAN
        NCH = I + NBCHAN - 1
        FT = NCH*WIDTH + OFFSET
618     WRITE (8,*) FT, AVGSIGS(J,I)
621     CONTINUE
      WRITE (8,*) 'END OF DATA.'
C
C
C
C       THIS IS THE SECTION THAT WRITES THE P(E) TO A FILE
C       THAT CAN BE USED BY TELL-A-GRAFF.
C
C
        WRITE (9,*) ' INPUT DATA.'
        WRITE (9,*) '"P(E) #1,PRIMARY"'
        DO 7000 I=1,NE
        ENERG = (I - 1)*EINCH(1) + EZEROH(1)
7000    WRITE (9,*) ENERG, PE(1,I)
        WRITE (9,*) '"P(E) #2,PRIMARY"'
```

```
      DO 7100 I=1,NE
      ENERG = (I - 1)*EINCH(2) + EZEROH(2)
7100  WRITE (9,*) energ, PE(2,I)
C
C
      IF (NYSEC.EQ.0) GO TO 999
      WRITE (9,*) '"P(E) #1,SECONDARY"'
      DO 7200 I=1,NES
      ENERG = (I - 1)*EINCHS(1) + EZEROHS(1)
7200  WRITE (9,*) ENERG, PES(1,I)
      WRITE (9,*) '"P(E) #2,SECONDARY"'
      DO 7300 I=1,NES
      ENERG = (I - 1)*EINCHS(2) + EZEROHS(2)
7300  WRITE (9,*) ENERG, PES(2,I)
999   WRITE (9,*) 'END OF DATA.'
      stop
      end
```

REFERENCES

1. (a) J.W. Hepburn, D.J. Trevor, J.E. Pollard, D.A. Shirley, Y.T. Lee, J. Chem. Phys., 76, 4287 (1982); (b) L.J. Butler, D.J. Krajnovich, Y.T. Lee, J. Chem. Phys., 79, 1708 (1983)

2. T.K. Minton, Ph.D. Thesis, University of California, (1986)

3. X.S. Zhao, E.J. Hintsa, Y.T. Lee, (to be published)

4. P.M. Kroger, S.J. Riley, J. Chem. Phys., 67, 4483 (1977)

This report was done with support from the Department of Energy. Any conclusions or opinions expressed in this report represent solely those of the author(s) and not necessarily those of The Regents of the University of California, the Lawrence Berkeley Laboratory or the Department of Energy.

Reference to a company or product name does not imply approval or recommendation of the product by the University of California or the U.S. Department of Energy to the exclusion of others that may be suitable.

LAWRENCE BERKELEY LABORATORY
TECHNICAL INFORMATION DEPARTMENT
UNIVERSITY OF CALIFORNIA
BERKELEY, CALIFORNIA 94720